

UNIVERSITY OF MARIBOR
FACULTY OF MECHANICAL ENGINEERING

Doctoral dissertation

**SYNTHESIS OF GOLD NANOPARTICLES WITH
A MODIFIED ULTRASONIC SPRAY PYROLYSIS**

May, 2016

Peter MAJERIČ



University of Maribor

Faculty of Mechanical Engineering

Doctoral dissertation

**SYNTHESIS OF GOLD NANOPARTICLES WITH
A MODIFIED ULTRASONIC SPRAY PYROLYSIS**

Doktorska disertacija

**SINTEZA NANODELCEV ZLATA Z
MODIFICIRANO ULTRAZVOČNO RAZPRŠILNO
PIROLIZO**

May, 2016

Author: Peter MAJERIČ

Mentor: Doc. Dr. Rebeka Rudolf

Comentor: Prof. Dr. Ing. Dr. h.c. Bernd Friedrich

ACKNOWLEDGMENT

I would like to thank my Mentor Dr. Rebeka Rudolf sincerely for her efforts in management and assistance in carrying out the research work, without which this dissertation could not be written. Thank you for the discussions, expert advice, ideas and criticisms, the outcome of which was the completion of this Doctorate.

I thank my Co-Mentor Prof. Dr. Ing. Dr. H.C. Bernd Friedrich for his consent to the use of the equipment for the experimental work done at the IME Institute, RWTH Aachen, and for the professional discussions and ideas.

I thank Priv. Doc. Dr.-Ing. Srečko Stopić and Dr.-Ing. Jelena Bogović for their support at the IME institute, and for the help and advice given when working with the USP devices.

I thank Dr. Darja Jenko and the Institute IMT Ljubljana for nanoparticle analysis with Transmission Electron Microscopy.

I would also like to express gratitude for the investigations, which contributed to the completion of this work: KI Ljubljana, VMA Belgrade and Zlatarna Celje d.d.

I am grateful to my colleagues at the Institute of Materials Technology, FS UM and the IME Institute, RWTH Aachen for their support and assistance, without which carrying out the work would certainly have been much more costly and time-consuming.

I also thank the agency ARRS, for the co-financing of my Doctoral Dissertation and the Public Fund for Human Resources Development and Scholarships RS, which has co-funded the research work.

I would also like to thank my parents and family for their support during my studies and the course of the Doctoral Thesis.

TABLE OF CONTENTS

1	INTRODUCTION	- 1 -
1.1	Doctoral Thesis	- 4 -
1.2	Terminology.....	- 4 -
2	AuNPs.....	- 5 -
2.1	Properties and applications	- 5 -
2.2	Surface Plasmon Resonance	- 7 -
2.3	Stabilization and functionalization of AuNPs	- 10 -
2.4	Production of nanoparticles and AuNPs.....	- 12 -
3	METHODS OF AuNP PRODUCTION	- 13 -
3.1	Bottom-up production of AuNPs	- 14 -
3.2	Top-down production of AuNPs.....	- 16 -
4	ULTRASONIC SPRAY PYROLYSIS OF AuNPs	- 18 -
4.1	Evaporation.....	- 20 -
4.2	Thermal decomposition and hydrogen reduction	- 21 -
4.3	Densification.....	- 23 -
4.4	Formation mechanisms with USP.....	- 24 -
4.4.1	Droplet-To-Particle mechanism	- 25 -
4.4.2	Theoretical calculations for evaporation of solution droplet with the DTP mechanism.....	- 26 -
4.4.3	Gas-To-Particle mechanism	- 29 -
5	SYNTHESIS OF AuNPs WITH THE CONVENTIONAL USP	- 32 -
5.1	Parameter selection	- 33 -
5.2	Experiments with conventional USP	- 34 -
6	SYNTHESIS OF AuNPs WITH THE MODIFIED USP.....	- 37 -
6.1	Parameter selection	- 38 -
6.1.1	Concentration of Au in the starting solution	- 38 -
6.1.2	Ultrasound frequency	- 39 -

6.1.3	Evaporation zone temperature	- 40 -
6.1.4	Reaction zone temperature	- 40 -
6.1.5	Gas flow.....	- 41 -
6.1.6	Collection medium	- 42 -
6.1.7	Summary of selected parameters.....	- 42 -
6.2	Characterization of AuNPs	- 45 -
6.2.1	TEM.....	- 45 -
6.2.2	DLS, zeta potential and ICP-OES	- 45 -
7	RESULTS AND DISCUSSION.....	- 46 -
7.1	AuNPs obtained with conventional USP	- 46 -
7.1.1	AuNPs appearing in the ultrasonic generator chamber	- 49 -
7.2	AuNPs obtained with modified USP	- 51 -
7.2.1	Influence of Au concentration in precursor solution.....	- 51 -
7.2.2	Influence of evaporation zone temperature	- 54 -
7.2.3	Influence of reaction zone temperature	- 56 -
7.2.4	Influence of Au concentration in precursor solution and temperature of evaporation zone – evaporation parameters obtained from calculations.....	- 58 -
7.2.5	Influence of gas flow	- 65 -
7.3	Electron diffraction	- 71 -
7.4	Concentrations of synthesized AuNPs.....	- 75 -
7.4.1	AuNP deposition on tube walls during synthesis and USP efficiency	- 76 -
7.5	Zeta potential of synthesized AuNPs.....	- 78 -
8	SETTING UP A MODEL OF AuNP FORMATION.....	- 80 -
8.1	Formation of AuNPs	- 80 -
8.2	Model of AuNP formation with the modified USP	- 82 -
9	CONCLUSIONS.....	- 84 -
9.1	Future work.....	- 85 -
10	LITERATURE.....	- 86 -

**APPENDIX: THEORETICAL CALCULATIONS FOR EVAPORATION OF
SOLUTION DROPLET..... - 92 -**

SINTEZA NANODELCEV ZLATA Z MODIFICIRANO ULTRAZVOČNO RAZPRŠILNO PIROLIZO

Ključne besede: modificirana ultrazvočna razpršilna piroliza, nanodelci zlata, mehanizmi nastanka, karakterizacija

UDK klasifikacija: 669.21.091:[544.57:66.092-97](043.3)

POVZETEK

Doktorsko delo predstavlja študije, eksperimentalno delo, tehnike karakterizacije, rezultate in analize, s katerimi je povezana sinteza čistih, okroglih, neaglomeriranih nanodelcev zlata (AuNPs) z velikostjo okoli 50 nm. Takšni AuNPs se zaradi dobrih fizikalnih in kemijskih lastnosti, ter zaradi optične lastnosti imenovane površinska plazemska resonanca, lahko uporabijo za biomedicinsko slikanje kot diagnostično orodje. Možno jih je tudi konjugirati s peptidi, z zdravili in drugimi molekulami s čimer dobimo funkcionalizirane AuNPs, uporabne pri terapiji rakavih in drugih obolenj.

V uvodnem delu doktorske disertacije je podana hipoteza, da je z modifikacijo naprave ultrazvočne razpršilne pirolize (USP) možno bolje nadzorovati velikosti in oblike nastalih AuNPs. Modifikacija predstavlja ločitev ogrevalnega območja za izhlapevanje kapljic aerosola od reaktorske peči ter uvedbo reducirnega plina neposredno v reaktorsko peč. V teh okvirih je teoretično opisano, da so na ta način zagotovljeni pogoji, kjer je možno identificirati mehanizme procesov, ki so osnova za postavitve novega modela nastanka AuNPs pri USP. Temu sledi opis lastnosti in možnosti za uporabo AuNPs.

V nadaljevanju so predstavljene različne proizvodne metode nanodelcev, ki jih ločimo na »bottom-up« (od spodaj navzgor) in na »top-down« (od zgoraj navzdol). Trenutno so te metode primerne za izdelavo majhnih količin nanodelcev z velikimi odstopanji v velikostih in oblikah od ene do druge serije. Dobre možnosti za odpravo teh tehnoloških problemov in bolj nadzorovano sintezo nanodelcev ima »top-down« USP metoda, ki spada med t.i. pirolize.. Piroliza je postopek kemične razgradnje različnih spojin pri povišanih temperaturah. Edinstvenost USP je v tem, da z ultrazvokom razpršimo raztopino z želenim materialom v kapljice, ki jih nato izpostavimo povišani temperaturi, tako da se s pirolizo material iz kapljice kemijsko razgradi in na ta način dobimo nanodelce čistih elementov ali spojin. Glavni elementi konvencionalne USP naprave so: ultrazvočni generator, reaktorska peč in sistem za zbiranje nanodelcev. USP ima preprosto postavitve posameznih elementov in omogoča spreminjanje njihove konfiguracije. Pri tem je zagotovljen kontinuiran potek sinteze

nanodelcev s kontroliranimi velikostmi in oblikami ter možnost sinteze nanodelcev visoke čistosti iz različnih materialov. Trenutno je slabost USP metode nizek izkoristek zaradi izgub materiala na posameznih konstrukcijskih elementih laboratorijske naprave. V primeru AuNPs se le-ti nalagajo na stene kvarčne cevi SiO_2 zaradi fizične adsorpcije in nastanka šibkih van der Waalsovih vezi zlata s kisikovimi atomi iz kristalne strukture kvarčnih cevi. Iz literature je poznano, da je velikost ustvarjenih AuNPs pri USP odvisna od frekvence ultrazvoka, ki določa velikosti kapljic aerosola, in koncentracije raztopljenega zlata v kapljicah.

V prvem delu raziskav so prikazani rezultati sinteze AuNPs s konvencionalno USP. Za izhodno surovino smo izbrali tetrakloroaurično kislino $\text{HAuCl}_4(\text{s})$, ki smo jo raztopili v vodi. $\text{HAuCl}_4(\text{s})$ je bila izbrana zaradi cenovne dostopnosti in kemične obstojnosti. To raztopino smo v komori z ultrazvokom razpršili v kapljice, ki jih je nosilni plin N_2 prenesel v reakcijsko peč. V tej peči so potekale stopnje sinteze: izhlapevanje in krčenje kapljice začetne raztopine (HAuCl_4 v vodi), toplotna dekompozicija HAuCl_4 v AuCl_3 , redukcija AuCl_3 s plinom H_2 in zgoščevanje v končne oblike AuNPs. Navedene stopnje sinteze pri konvencionalnem USP potekajo hkrati. Pri manjših premerih kapljic aerosola nastanejo nanodelci bistveno prej kot pri večjih kapljicah. To se zgodi zaradi trkov in koagulacije kapljic, ko v različnih stopnjah sinteze sintetiziramo nanodelce različnih velikosti in oblik, kar je neugodno za izdelavo ciljanih velikosti in enotnih oblik AuNPs. Karakterizacija nastalih AuNPs je odkrila, da so nanodelci okrogli, nepravilnih, trikotnih in cilindričnih oblik z velikostmi do 300 nm, pri čemer smo identificirali visoko stopnjo aglomeracije. Izdelani AuNPs prav tako niso imeli ustrezne kemijske sestave, saj so imeli veliko nečistoč (Co, Cr, Fe, Si ...).

Ker s konvencionalnim USP nismo dosegli cilja, smo pristopili k podrobnejšim študijam, ki so pokazale, da je oblika sintetiziranih AuNPs odvisna od hitrosti izhlapevanja kapljice in hitrosti difuzije ionov $[\text{AuCl}_4]^-$ in H^+ v kapljici. Nadzorovanje obeh pri sintezi nanodelcev z USP je odvisno od več dejavnikov: koncentracije začetne raztopine, velikosti kapljic, števila kapljic in relativne vlažnosti v sistemu, hitrosti prenašanja kapljic v peč z nosilnim plinom, tlak v sistemu, dimenzije prenašalnih cevi, temperatura v reakcijski peči. Za nastavitve ustreznih parametrov (koncentracija začetne raztopine, pretok plina, temperatura peči) pri sintezi AuNPs je bilo potrebno poznavanje lastnosti začetne raztopine, kot sta gostota in površinska napetost, ter lastnosti raztopljenega $[\text{AuCl}_4]^-$, difuzije ionov v raztopini in rast AuNPs. Na podlagi teoretičnega razumevanja smo za nadaljnji študij in obravnavo izbrali vplivne parametre za sintezo z USP: ultrazvočna frekvenca, koncentracija zlata v začetni raztopini, pretok nosilnega in reakcijskega plina, temperatura reakcijske peči. Z visokofrekvenčnim ultrazvokom (0,5–3 MHz) se namreč ustvarijo kapljice v porazdelitvi

velikosti od 1 do 15 mikronov. Koncentracija raztopljenega zlata (0,5 g/l–5,0 g/l Au) v začetni raztopini določa, koliko materiala vsebuje vsaka kapljica, da ta po izhlapitvi in sušenju tvori nanodelce različnih velikosti, od premera nekaj 10 nm pri 0,5 g/l Au do premera več kot 100 nm pri 5,0 g/l Au v začetni raztopini. Pretok nosilnega plina določa čas zadrževanja kapljice oziroma nanodelca v reakcijski peči, kjer se izvedejo reakcije za nastanek nanodelcev. Temperatura reakcijske peči pa določa hitrost izhlapevanja kapljic in reakcij.

Za dosego cilja doktorskega dela na podlagi te študije smo postavili hipotezo, da lahko izdelamo ciljne AuNPs z modificiranim USP, kjer je cona izhlapevanja kapljic ločena od reakcijske peči, reducirni plin pa je uveden neposredno v reakcijsko peč. Tako smo lahko nadzorovali izhlapevanje kapljic in kemijske reakcije, ki so v takšni konstrukciji potekale bolj stabilno, s ciljem sintetizirati zelene velikosti okroglih AuNPs. Mehanizmi nastanka AuNPs iz raztopine s HAuCl_4 pri USP s takšno konstrukcijo še niso popolnoma pojasnjeni v literaturi. Za doseganje AuNPs z visoko stopnjo čistostjo (99,99 m.% Au) smo morali umestiti USP napravo še v primerno čistem prostoru (na inštitutu IME, RWTH Aachen), uvesti čiščenje elementov USP naprave s kislinami HNO_3 in HCl ter zamenjati nekatere konstrukcijske elemente USP naprave z materiali (teflon, kvarčno steklo), ki ne reagirajo s HAuCl_4 .

Za potrditev hipoteze smo z eksperimenti na modificirani USP preučevali vplivne parametre USP-sinteze: koncentracijo Au v začetni raztopini, temperature v coni izhlapevanja kapljic in v reakcijski peči ter pretok plinov N_2 in H_2 . S pomočjo tehnik karakterizacij (TEM, DLS, ICP) na nastalih AuNPs smo določili velikost, obliko, kemijsko sestavo in stopnjo aglomeracije. Mikrostruktura in elektronska difrakcija AuNPs je pokazala, da imajo polikristalno strukturo, brez izrazito usmerjenih zrn. AuNPs rastejo anizotropno na ravninah z najnižjo energijo ($a_{\{111\}} < a_{\{100\}} < a_{\{110\}}$), zaradi hitre kinetike heterogene rasti pa imajo veliko koncentracijo kristalnih mej in dvojčkov. Ugotovili smo, da pri USP-sintezi hkrati potekata dva mehanizma nastanka nanodelcev (»kapljica-v-delec«, DTP in »plin-v-delec«, GTP). Z DTP nastajajo nanodelci iz tekoče oziroma trdne faze, z izhlapevanjem in krčenjem kapljice aerosola, dokler se AuCl_3 v njej ne prenasiči in precipitira. Z DTP nastajajo veliki nanodelci – do 300 nm. Z GTP pa pri izhlapevanju kapljice hkrati izhlapeva AuCl_3 tudi v kapljici. Iz te plinske faze pa nato s trki in prenasičenjem molekul nastanejo nove kali za rast AuNps s kondenzacijo plinske faze na njihovo površino. Z GTP nastajajo majhni nanodelci – do 50 nm. Kadar potekata oba mehanizma hkrati, dobimo neugodno bimodalno velikostno porazdelitev AuNPs. Pomembna ugotovitev je tudi ta, da imata največji vpliv na nastanek različnih velikosti in oblik AuNPs koncentracija Au v začetni raztopini ter pretok plinov N_2 in H_2 . Povečevanje koncentracije Au v začetni raztopini (od 0,5 do 5,0 g/l) vodi do

prevladujočega vpliva DTP-mehanizma, kar posledično povzroči nastanek večjih AuNPs (<300 nm). Pri povečevanju pretokov nosilnega in reducirnega plin ($N_2 \geq 3,0$ l/min., $H_2 \geq 1,5$ l/min.) pa postane prevladujoči GTP mehanizem, ki daje pogoje za nastanek manjših AuNPs (10 – 50 nm).

Na osnovi študij, opravljenega eksperimentalnega dela in rezultatov karakterizacije smo postavili model nastanka AuNPs, ki pojasnjuje, kako lahko pri USP-sintezi s spreminjanjem koncentracije Au v začetni raztopini in pretokov plinov vplivamo na DTP in GTP mehanizma nastanka v korist GTP. S ciljno izbranimi parametri (0,5 g/l Au, 4,5 l/min N_2 , 2,0 l/min H_2) smo ustvarili pogoje za nastanek AuNPs z GTP-mehanizmom. Pri tem so nastali okrogli AuNPs z ozko velikostno porazdelitvijo (68 % nanodelcev velikosti $37,0 \pm 5,5$ nm). Model smo preverili z nizom eksperimentov na modificirani napravi USP na inštitutu IME, RWTH Aachen, na katerem smo uspeli sintetizirati ciljne AuNPs. Tako smo potrdili pravilnost postavljenega modela in hipotezo, da lahko z modificiranim USP izdelamo AuNPs ciljnih lastnosti.

GOLD NANOPARTICLE SYNTHESIS WITH A MODIFIED ULTRASONIC SPRAY PYROLYSIS

Key words: modified Ultrasonic Spray Pyrolysis, gold nanoparticles, formation mechanism, separate evaporation

ABSTRACT

This Doctoral Dissertation presents the studies, experimental work, characterization techniques, results and analyses of synthesis of very pure, spherical, unagglomerated gold nanoparticles (AuNPs), with sizes around 50 nm. In the first part of the research, the AuNPs were synthesized with conventional Ultrasonic Spray Pyrolysis (USP). For the raw material, tetrachloroauric acid $\text{HAuCl}_4(\text{s})$ was dissolved in water. This precursor solution was then sprayed into droplets with ultrasound, and a carrier gas N_2 then transported the droplets into a reaction furnace. In this furnace the AuNP synthesis stages took place: Droplet evaporation, thermal decomposition, reduction with H_2 gas and densification. The resulting AuNPs had diverse shapes in sizes up to 300 nm, with a high degree of agglomeration. Because the aim was not achieved with the conventional USP, a hypothesis was proposed where the targeted AuNPs could be synthesized with a modified USP. With this modification, the droplet evaporation zone is separated from the reaction furnace and the reduction gas is introduced directly into the reaction furnace. To confirm this hypothesis we have carried out experiments in order to determine the influential parameters of USP synthesis: The concentration of Au in the precursor solution, evaporation zone temperature, reaction furnace temperature and gas flows of N_2 and H_2 . Characterization of the obtained AuNPs has shown that 2 formation mechanisms take place in USP synthesis (Droplet-to-Particle, DTP and Gas-to-Particle, GTP). With DTP, nanoparticles up to 300 nm are formed, while smaller nanoparticles up to 50 nm are formed with GTP. When both mechanisms occur simultaneously, we obtain a bimodal size distribution of AuNPs. Based on these findings, we have set up an AuNP formation model, explaining how one can control the DTP and GTP mechanisms in USP by changing the most influential parameters, the concentration of Au in the precursor solution and the gas flows. Based on this model, parameter values were selected (0.5 g/l Au, 4.5 l/min N_2 , 2.0 l/min H_2) to establish conditions where the AuNPs are formed only by the GTP mechanism. This has yielded spherical AuNPs in a narrow size distribution (37.0 ± 5.5 nm). Targeted AuNPs were thus synthesized, confirming the model and the hypothesis of AuNP synthesis with USP.

SYMBOLS USED

r	μm	Droplet radius
d	μm	Droplet diameter
T_d	K	Droplet temperature
T_∞	K	Environment temperature
Y_{vap}	/	Mass fraction of vapor on the droplet surface
$Y_{vap,\infty}$	/	Mass fraction of vapor in the environment
\dot{m}_{vap}	kg/s	Vapor mass flow
\dot{q}_{liq}	J/s	Thermal flow inside the droplet
\dot{q}_{vap}	J/s	Thermal flow on the droplet surface
β_d or β_r	/	Coefficient of evaporation for the “diameter-“ or the “radius square law”
t	S	Droplet residence time
ΔG	J	Gibbs free energy
p_∞	bar	Vapor pressure in the environment
α_c	/	Ratio of collisions and coalescence
γ	N/m	Precursor solution surface tension
ρ_{sol}	g/cm^3	Density of precursor solution
f	Hz	Ultrasound frequency
D_{Au}	nm	Calculated diameter of gold nanoparticles
C_{sol}	g/l	Concentration of Au in precursor solution
M_{Au}	g/mol	Molar mass of gold
ρ_{Au}	g/cm^3	Density of gold
M_{sol}	g/mol	Molar mass of precursor solution
η	/	Efficiency

ABBREVIATIONS USED

AuNP	Gold nanoparticle
SPR	Surface Plasmon Resonance
USP	Ultrasonic Spray Pyrolysis
DTP	Droplet-to-Particle
GTP	Gas-to-Particle
UV-Vis	Ultraviolet–visible spectroscopy
PEG	Polyethylene Glycol
DI	Deionized
TGA	Thermogravimetric Analysis
TEM	Transmission Electron Microscopy
EDS	Energy-dispersive X-ray spectroscopy
ED	Electron Diffraction
ICP-OES	Optical Emission Spectrometry with Inductively Coupled Plasma
DLS	Dynamic Light Scattering
SD	Standard Deviation

1 INTRODUCTION

Nanotechnology is a branch of science and engineering focused on materials with at least one dimension below 100 nm. Nanomaterials (nanoparticles, nanotubes, nanopyramids,...) have different properties compared to materials with ordinary dimensions. Their altered physical and chemical properties come from a large surface-to-volume ratio and a high surface activity. Because of this, they are useful in various fields (electronics, chemistry, biotechnology, medicine) [1].

Especially interesting are gold nanoparticles (AuNPs), as they have an additional property, called Surface Plasmon Resonance (SPR) [2]. This causes the oscillation of conduction electrons on the surface of the nanoparticles, stimulated by incident light. AuNPs have good physical, chemical and optical properties because of the Plasmon Resonance [3]–[5]. Usually, AuNPs are biologically unreactive and, as such, are suitable for biomedical imaging and therapy [6], [7]. Such AuNPs can be conjugated and functionalized with peptides, medicine and can be used for diagnosis and cancer treatment [8]–[10].

Different production methods for nanoparticles are known; they are divided into bottom-up and top-down approaches. Bottom-up examples include sol-gel, chemical vapour deposition, flame spray synthesis, various pyrolysis and atomic or molecular condensation [11]–[14]. Top-down methods include laser ablation, nanolithography and high-energy milling [15], [16]. Currently, these methods are suitable for production of small quantities of nanoparticles with major variations in shapes and sizes of the nanoparticles from the production of different batches. A bottom-up method, called Ultrasonic Spray Pyrolysis – USP, has good potential for removing these technological issues, for a more controlled nanoparticle synthesis [13], [17]. Pyrolysis in general is a process of chemical decomposition of various compounds at elevated temperatures. With the USP method, we introduce ultrasound additionally for dispersing a precursor solution with our desired material into droplets. These droplets are then exposed to high temperature, such that the material inside the droplet is decomposed chemically via pyrolysis and nanoparticles of pure elements are obtained. The advantage of the USP method is the simplicity of setting up individual process segments and changing their configuration, continuous nanoparticle synthesis and the possibility of synthesizing pure nanoparticles from various materials. The disadvantage is the low efficiency of the method when using an un-optimized USP device used for laboratory

purposes (currently around 10%), due to losses of the dissolved material on the construction elements of the USP device.

The main elements of the standard USP device are the ultrasonic generator, the reactor furnace and a system for nanoparticle collection. There are various raw materials which can be used for preparing precursor solutions for AuNP synthesis (compounds containing Au: AuBr₃, HAu(NO₃)₄, Au(O₂CCH₃)₃). In our case, tetrachlorauric acid HAuCl₄(s) was selected, due to its price, availability and chemical stability, as shown in our previous research with USP synthesis. The precursor solution was prepared by dissolving HAuCl₄ in water [18], [19].

The aim of the Doctoral Dissertation was the synthesis of spherical AuNPs with a narrow size distribution around 50 nm (70% of all AuNPs), with a high content of Au (at least 99.99 wt.% Au).

From literature it is known [13], [17], [18], [20] that the sizes of the synthesized AuNPs depend on the ultrasound frequency, which determines the sizes of the aerosol droplets, and the concentration of the dissolved Au in the droplets. Due to vibrations of the ultrasound below the solution surface, the kinetic energy of the solution's molecules is increased rapidly. This causes small droplets to overcome surface tension and break away from it. With a high-frequency ultrasound (0,5-3 MHz), droplets are created in a size distribution from 1 to 15 micrometers [21].

By using low concentrations of dissolved gold (0,5 g/l – 5.0 g/l Au) in the precursor solution, each droplet contains such an amount of material that, after evaporation and drying, the following particle sizes are formed: i) with diameters of a few 10 nm at 0,5 g/l Au and ii) with diameters of more than 100 nm at 5.0 g/l Au in the precursor solution.

Droplets of the starting solution are transported into the furnace with a carrier gas. Inside the furnace, the AuNPs are formed according to the following synthesis stages:

1. Evaporation and droplet shrinkage (HAuCl₄ with water)
2. Thermal decomposition of HAuCl₄ into AuCl₃
3. Reduction of AuCl₃ with hydrogen and the formation of Au
4. Densification

The listed synthesis stages are taking place at the same time with the conventional USP. With smaller diameters of the aerosol droplets ($2r > 1\mu\text{m}$), nanoparticles are formed much sooner than with larger droplets ($2r < 10\mu\text{m}$). Therefore, nanoparticles of different sizes and shapes can be synthesized, due to droplet collisions and coagulation. This is not suitable for synthesizing the targeted AuNPs.

With the conventional USP, we have synthesized AuNPs with sizes from 10 to 300 nm, with different shapes, from spherical, irregular, triangular and cylindrical [18]. Such AuNPs were not suitable.

More detailed studies [13], [17], [20], [22] have shown, that the shapes of the synthesized AuNPs depend on the rate of droplet evaporation and the rate of ion diffusion $[\text{AuCl}_4]^-$ and H^+ inside the droplet. These rates with USP synthesis depend on several factors: Precursor solution concentration, droplet sizes, number of droplets and relative humidity in the system, velocity of droplet transportation into the furnace with the carrier gas, pressure in the system, dimensions of the transport pipes, and temperature inside the furnace. For setting up suitable parameters (precursor solution concentration, gas flow, furnace temperature), information is needed for the starting solution properties, such as density and surface tension, and characteristics of the dissolved $[\text{AuCl}_4]^-$, ion diffusion inside the solution and AuNP growth.

Based on the presented studies, the objective of the Doctoral Thesis was setting up a modified USP device for the synthesis of AuNPs. With this modification, we have separated the droplet evaporation from the rest of the synthesis stages and introduced the reduction gas directly into the reaction furnace. In this way, we could control the evaporation and chemical reactions in order to achieve the desired sizes of spherical AuNPs. We presumed, that a separate evaporation stage would allow for a more optimal material diffusion inside the droplet ($[\text{AuCl}_4]^-$ and H^+) and would result in the synthesis of spherical AuNPs. The mechanisms of AuNP synthesis from HAuCl_4 by USP with such a design are not yet clarified in the literature.

Several experiments were performed with the modified USP, with different selected influential parameters. The synthesized AuNPs were characterized with various characterization techniques for identification of their sizes, shapes, chemical composition and degree of agglomeration. Based on these results, we have surmised the influence of individual parameters on the AuNP formation mechanisms. We have found out, that the AuNPs are formed from droplets and from the gas phase. This means that they are formed from a combination of DTP (Droplet-To-Particle) and GTP (Gas-To-Particle) formation mechanisms. The next finding was that the parameters with the most influence on formation were the Au concentration in the precursor solution and N_2 and H_2 gas flows. Based on these findings, we have set up a formation model, which explains how we can change these two parameters and achieve dominance of the GTP mechanism in the system. In this way we can obtain the

desired AuNPs. The model was confirmed with synthesis of the targeted, spherical AuNPs with a size distribution around 50 nm.

1.1 Doctoral Thesis

With the modification of the USP process, the synthesis of nanoparticles, their sizes and shapes can be understood and controlled comprehensively. The modification represents separating the evaporation from the reaction zone (thermal decomposition, chemical reduction and densification) and introducing the reduction gas directly into the reaction zone. In this way, it is possible to identify the process mechanisms, which are the basis for setting up a formation prediction model for AuNPs.

1.2 Terminology

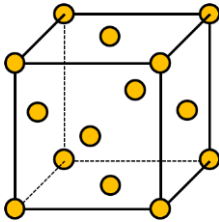
The term “particle” used in this text can be interpreted as all particles, regardless of their size, while the term “nanoparticle” is used for particles which have one dimension below 100 nm. “Nanoparticle” is used where the dimensions of the particle are considered important.

2 AuNPs

2.1 Properties and applications

Gold as a noble metal has a resistance to corrosion and is used mostly in many engineering applications (contacts in microelectronics), medicine (dental alloys, implants) and also in jewellery and currency. It is a soft, ductile material (tensile strength of 120 MPa), with a face centered cubic crystal structure (Table 2.1). It has been a valuable precious metal for a long time in human history due to its rarity, specific colour and its unreactiveness to other elements. When broken into nanoparticles, Au becomes highly useful for a wide range of processes, including general nanotechnology, electronics manufacturing and the synthesizing of different functional materials.

Table 2.1: General information for Au [23]

Atomic number	79
Standard atomic weight	196.97
Density	19.32 g/cm ³ (20°C)
Melting point	1064.43°C
Boiling point	3080°C
Electronic configuration	1s ² 2s ² 2p ⁶ 3s ² 3p ⁶ 3d ¹⁰ 4s ² 4p ⁶ 4d ¹⁰ 4f ¹⁴ 5s ² 5p ⁶ 5d ¹⁰ 6s ¹
Ionic radius	0.85 Å (Au ³⁺)
Crystal form	Face centered cubic: 

AuNPs have good physical, chemical and optical properties because of their high surface to volume ratio and SPR, inherent for noble metal nanoparticles [3]–[5]. The nanoparticles' surface determines their physical properties such as stability and solubility, which can also make them very useful for catalysis. Because of SPR, they have excellent light scattering abilities. SPR is dependant on their size, shapes and agglomeration. Changing these properties changes the SPR effect and their usefulness in various applications. Usually, AuNPs are also biologically unreactive and as such are suitable for a wide range of biomedical applications [6], [7]. Such AuNPs can be conjugated and functionalized with peptides and can be used for diagnosis and cancer treatment [8]–[10], [24]–[27].

Currently, commercially available AuNPs are available in sizes ranging from 1 nm up to gold particles with 8 μm . Different shapes are possible, such as spherical, sub-octahedral, octahedral, decahedral, icosahedral, multiple twined, irregular shapes, tetrahedral, nanotriangles, nanoprisms, hexagonal platelets and nanorods [28]. The main current markets for AuNPs are in biomedicine, in tissue or tumour imaging, drug delivery, photothermal therapy and immunochromatographic identification of pathogens in clinical specimens. They can also be utilised as gas sensors (solvent suspensions in gas detection), decorative coatings, and conductive thin film substrate coatings for flexible electronics, for catalysis, glucose biosensors, chemical sensors, DNA detection, electronic inks, fluorescent probes and fuel cell additives.

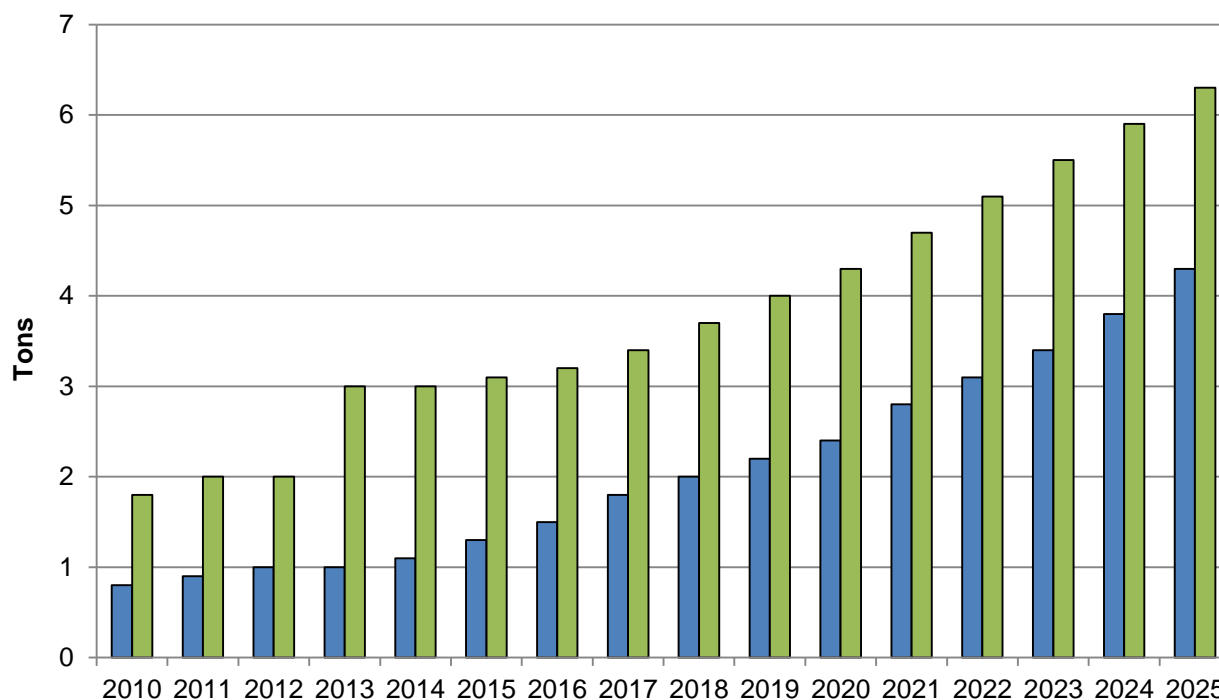


Figure 2.1: Global market for gold nanoparticles, 2010-2025, tons/year, conservative/optimistic estimates (Conservative estimate (Blue), optimistic (Green)), adapted from [28]

The potential benefits of AuNPs used in medicine attract considerable attention in the scientific community [29]–[34]. The exploitation of SPR, ease of surface functionalization and biocompatibility that AuNPs inherit can aid the current methods for diagnosis and treatment substantially [7], [8], [35]. Pre-clinical proofs of concept for treatments using nanoparticles have already been established [36]. In our separate research for the application of the AuNPs in medicine, it has been shown that sizes around 50 nm, with a high purity (99.99 wt.%) are nominal for best results regarding cytotoxicity and biocompatibility [26].

2.2 Surface Plasmon Resonance

SPR causes the oscillation of conduction electrons on the surface of the nanoparticles, stimulated by the electromagnetic field of incident light. AuNPs, along with silver and copper, are the most common nanoparticles used to obtain the surface plasmon effect [37]. SPR enhances all the radiative and nonradiative properties of the nanoparticles [7], such as absorption and scattering. Strongly absorbed light is also transformed rapidly into heat.

The oscillations of conduction electrons around the surface of the particle causes differences of the charges in the atomic structure and creates a dipole oscillation in the direction of the electrical field of incident light (Figure 2.2). The collective oscillations of conduction electrons, or conversely, the oscillations of plasma, are called a plasmon.

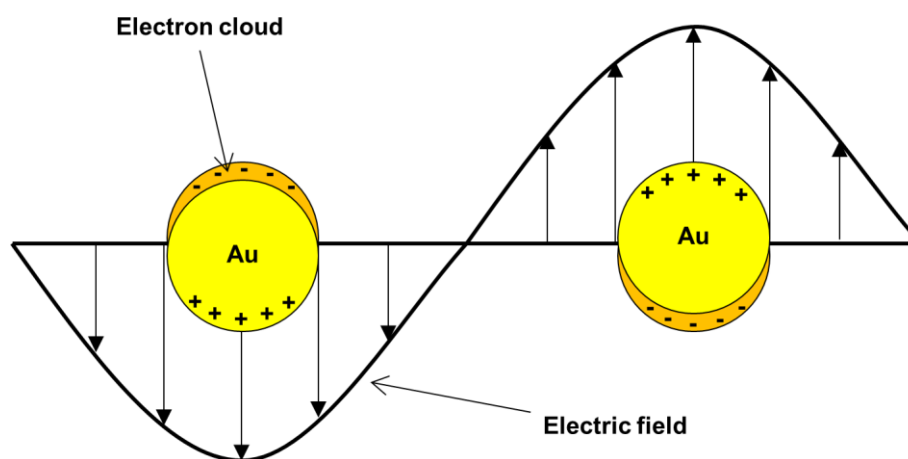


Figure 2.2: Oscillating electrons on the surface of a spherical AuNP

The amplitude of the oscillations reaches a maximum at a certain frequency, called Surface Plasmon Resonance – SPR. The oscillation frequency is determined by four factors: The density of the electrons, the effective electron mass, and the shape and size of the charge distribution [38]. SPR causes a strong absorption of incident light and can be measured with a UV-Vis absorption spectrometer. The intensity of the resonance band and wavelength are dependant upon factors, that effect the density of the electron charge on the surface of the particle, such as metal type, size of the particle, shape, structure, composition and dielectric properties of the surrounding medium (this was described theoretically by Mie [4]).

Due to strong scattering and absorption of light in the green area of the light spectrum, suspensions of spherical AuNPs have a red colour under normal light (the SPR wavelength of AuNPs is around 520 nm, depending on their size and shape, Figure 2.3). When the sizes and shapes of the nanoparticles change, the observed colour also changes. The suspensions of silver nanoparticles have a yellow appearance, due to plasmon resonance in the blue area of the spectrum (SPR wavelength of around 400 nm). The intensities of scattering and absorption in noble metals are up to 40x greater than with other non-plasmonic metals. The brightness and tunability of optical properties of plasmonic nanoparticles is the

reason for their usefulness in numerous applications, from molecule detection, to materials for solar power generation, to discovering and destroying cancer cells.

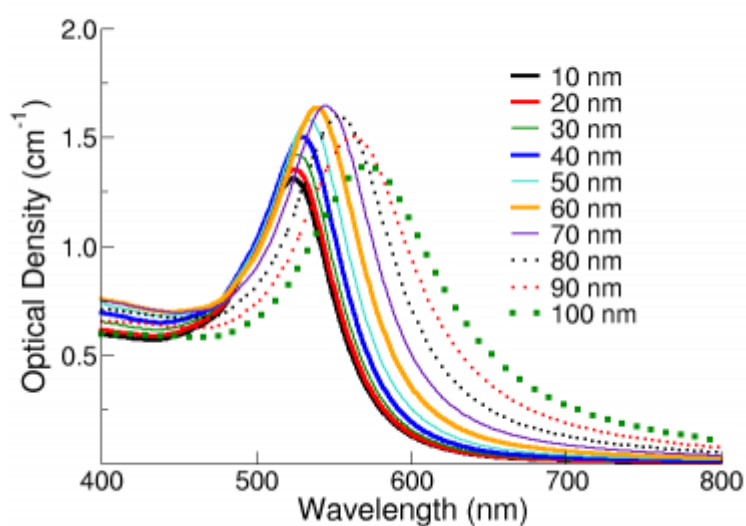


Figure 2.3: Demonstration of SPR: Suspensions appear in different shades of red colour with different sizes of spherical AuNPs, with the SPR extinction spectra (sum of absorption and scattering of visible light), from [39]

Mie [4] originally calculated the Surface Plasmon Resonance by solving Maxwell's equations for small spheres interacting with an electromagnetic field. Modern methods are also using the discrete dipole approximation to calculate the SPR absorption for other shapes [38], [40]. Calculation of the longitudinal plasmon resonance for gold nanorods generates an increase in the intensity and wavelength maximum as the aspect ratio (length divided by width) increases. Thus, the plasmon resonance can be tuned across the visible region by changing the aspect ratio. An increase in the intensity of the Surface Plasmon Resonance absorption leads to the enhancement of the electric field [40].

The optical properties of AuNPs are also sensitive to the presence of other plasmonic materials. When several of these nanoparticles are close together (in the proximity of one nanoparticle diameter or less), the surface plasmons combine and the conduction electrons on both nanoparticles oscillate collectively. Thus, the electrons assume the lowest energy state, which results in a red-shift of the resonance wavelength into longer wavelengths (lower energy) [39]. This effect causes different colours of suspensions with nanoparticle aggregates (Figure 2.3).

2.3 Stabilization and functionalization of AuNPs

The properties of AuNPs in suspensions change when agglomerates are formed. For this reason, the AuNP agglomeration should be prevented with stabilization, for taking full advantage of their properties. Stabilizing AuNPs depends on the application of the nanoparticles and can be very challenging due to the strong influence of a number of factors. The surface of nanoparticles is dynamic and is influenced strongly by the local environment. There are two ways of AuNP stabilization: Charge (electrostatic) stabilization and sterical stabilization (Figure 2.4). With charge stabilization, the surface charge of the nanoparticles prevents agglomeration. The stability of charge stabilized particles can be measured with zeta potential (Figure 2.5). Nanoparticles with a zeta potential greater than 20 mV (positive charge) or less than -20 mV (negative charge) are considered to have enough electrostatic repulsion to remain stable. However, the zeta potential is highly dependent on the presence of other molecules or contaminants in the solution. With sterically stabilized nanoparticles, molecules are bound to the gold surface by physisorption or by extremely stable thiol-gold bonds. The molecules present a double layer of charge, preventing agglomeration. There are several molecules with which AuNPs can be stabilized; the most common are Sodium Citrate (also used as a reducing agent in many synthesis methods) and Polyethylene Glycol (PEG), as the nanoparticles are intended for use in biological applications. Citrate associates weakly with the nanoparticle surface and is often used because the weakly bound capping agent provides long term stability and is displaced readily by a range of other molecules [41]. Other commonly used molecules for functionalization, intended for biomedical use, are based on any one or a combination of the groups such as oligo- or polyethylene glycol (PEG), bovine serum albumin, oligo or polypeptides, oligonucleotides, antisense or sense RNA molecules, antibodies, cell surface receptors and other similar molecules [42].

As Sodium Citrate is a very common stabilization agent, its stability is well documented. Reports indicate that AuNPs stabilized with Sodium Citrate are stable for at least 6 months if stored at 4°C away from light [39].

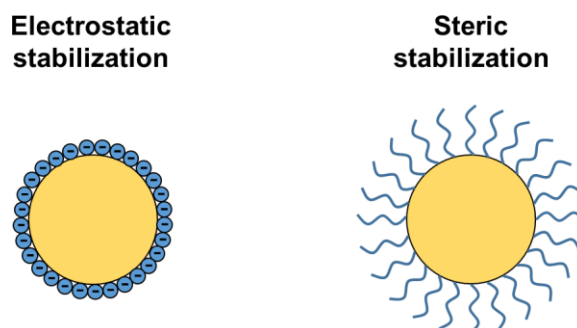


Figure 2.4: Electrostatic and steric particle stabilization

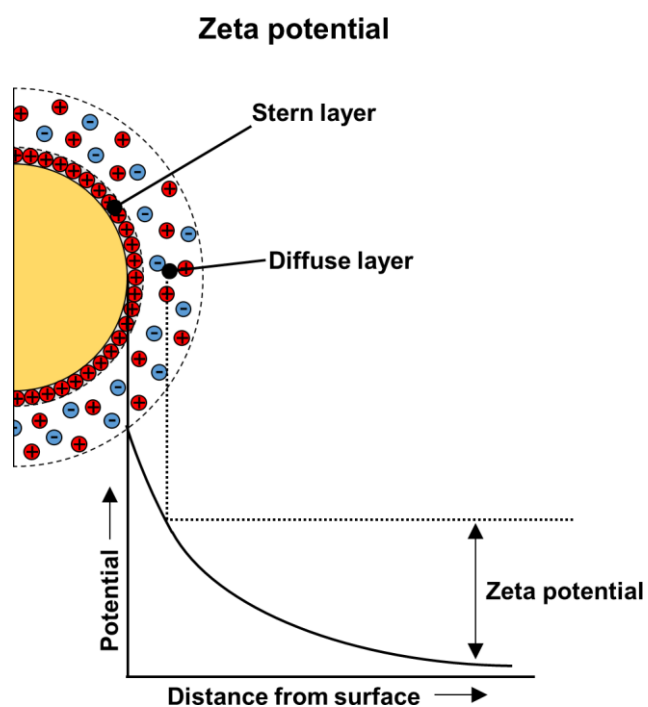


Figure 2.5: Zeta potential of a particle in suspension

2.4 Production of nanoparticles and AuNPs

Currently there is a need for a scaled up production of nanoparticles, able to take up the increasing quantities of nanoparticles required for advanced applications. Technologies for generating nanoparticle powders and suspensions have been existent for several decades [43] and are continuing to be improved upon, while novel approaches are also being studied [11], [44], mostly because the former methods produce large batch-to-batch variations in the AuNPs` properties. One potentially reliable method for the synthesis of AuNPs is the USP [18]. This process is considered to be relatively cost-effective and easily scalable from the laboratory to an industrial level. Several different types of nanoparticles can be produced with this process, as was shown for Au [18], Ag [45], TiO₂ [46], etc. Furthermore, by the modifications to the process, several different structure types can also be produced, such as solid or hollow nanoparticles, core-shell and ball-in-ball structures, etc.[13], [47]–[50].

3 METHODS OF AuNP PRODUCTION

Different production methods for nanoparticles are known and they are commonly divided into bottom-up and top-down approaches. With bottom-up, the AuNPs are formed from atomic or molecular components, while top-down produces nanoparticles from bulk materials. Bottom-up examples include sol-gel, chemical vapour deposition, flame spray synthesis, various pyrolysis and atomic or molecular condensation [11]–[14]. Top-down methods include laser ablation, nanolithography and high-energy milling [15], [16]. Currently, these methods are suitable for production of small quantities of nanoparticles with major variations in shapes and sizes of the nanoparticles from production of different batches. USP is a bottom-up method, which has good potential for removing these technological issues, for a more controlled nanoparticle synthesis [13], [17].

Another classification for nanoparticle synthesis is based on the physical state from which the nanoparticles are formed: From the gas, liquid or solid state. Depending on the type of precursor and material synthesized, USP can be categorized in all three, as nanoparticles can be formed from the gas or the liquid/solid state.

As the physical and chemical properties of AuNPs are determined by their size, shape, purity and surface structure (stability and zeta potential) and although there are several methods for producing AuNPs, controlling their synthesis with a uniform size and morphology still remains a challenge. Several studies have been devoted to accomplish this [37], [51]–[55]. Generally, the synthesis of AuNPs involves the Sodium Citrate reduction method, phase transfer method, templating method, seed-mediated method or chemical radiation. Synthesis via aerosol routes like spray pyrolysis enables production of various nanoscaled materials, including gold. It is relatively simple, flexible and can also be used for film processing. Control of nanoparticle morphology, particle size distribution and particle composition can be achieved with careful selection and modification of the process parameters [13], [56].

3.1 Bottom-up production of AuNPs

The simplest method for AuNP synthesis was found by Turkevich et al. in 1951 [41]. It was improved by Frens two decades later [57]. This method is used for the production of fairly monodispersed spherical AuNPs in sizes of around 10-20 nm, suspended in water. Larger sizes can be produced, although the monodispersity and spherical shapes are then lost. The procedure involves the reaction of small quantities of hot chloroauric acid with small quantities of a solution of Sodium Citrate. The citrate acts as a reducing and stabilizing (capping) agent.

A method for synthesis of AuNPs in organic mediums was investigated by Brust and Schiffrin [58]. Tetrachloroauric acid is reacted with tetraoctylammonium bromide (TOAB) in toluene (acts as an anti-coagulant) and sodium borohydride (acts as a reduction agent). In this manner, AuNPs in sizes of 5-6 nm can be synthesized.

With sonolysis, ultrasound promotes reactions of an aqueous solution of HAuCl_4 with a stabilizer, such as sodium dodecyl sulfate. The method produces AuNPs of a wide size distribution with irregular shapes. Ultrasonic power and different concentration of stabilizer change the properties of the synthesized AuNPs [59].

Sol-gel is a chemical nanoparticle production method, where monomers from a precursor are converted into a colloidal solution (sol) and then formed gradually into a three-dimensional solid network (gel). Typical precursors are metal alkoxides and chlorides, exposed to hydrolysis and condensation in order to form colloid solutions. Sol-gel is a cheap, low-temperature method, which has good control over the chemical composition of the final products. It is used for processing and production of ceramics, or for production of thin films of metallic oxides [60].

Other methods include coprecipitation, microemulsions, hydrothermal/solvothermal syntheses, flame pyrolysis, etc. Recent advances in nanostructured materials have been led by the development of new synthetic methods that provide control over size, morphology, and nano/microstructure [61]. Most production methods are still in development as prototypes or on a lab scale, and only a few of them have been introduced onto the industrial scale of nanoparticle production.

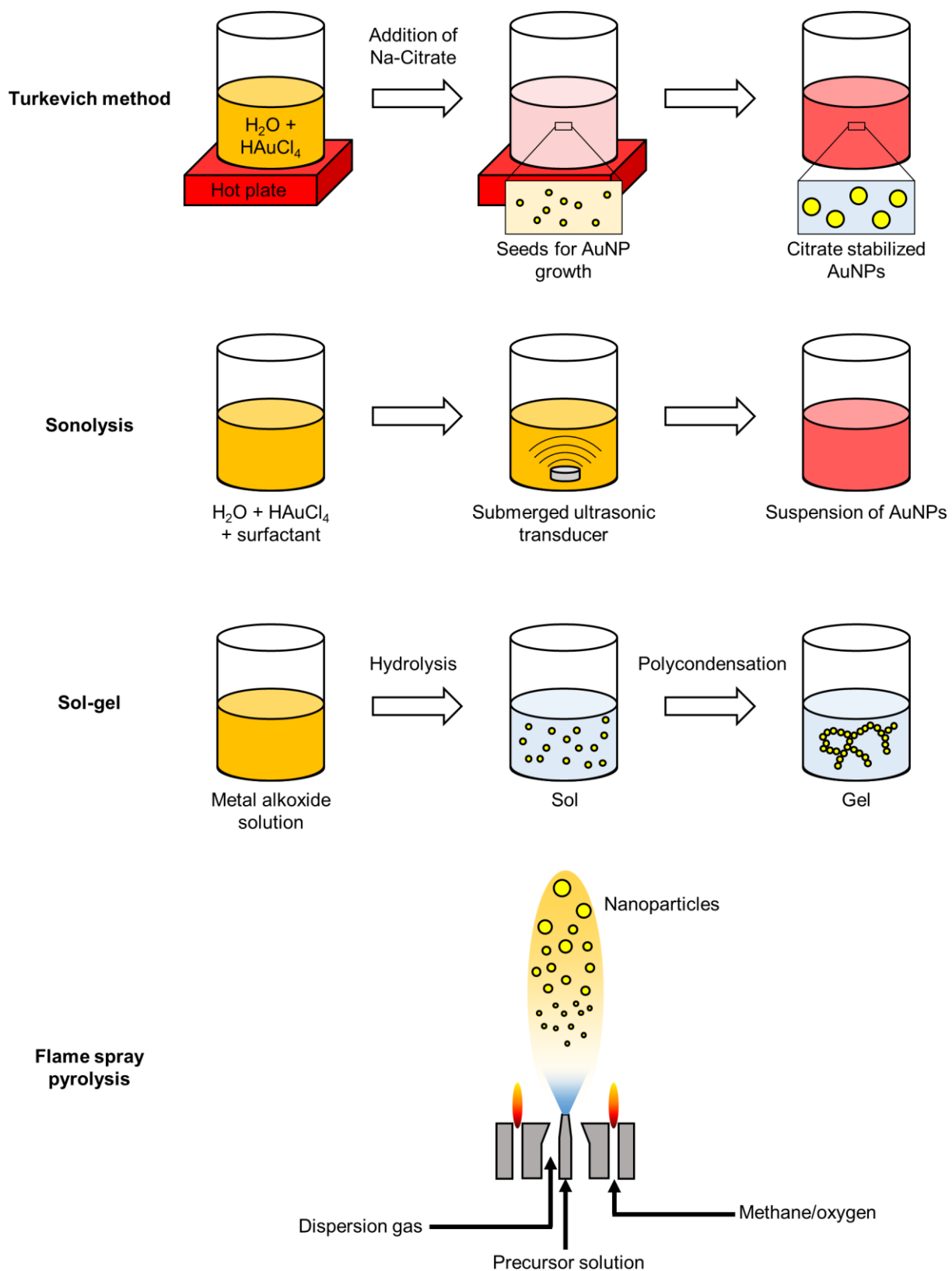


Figure 3.1: Simplified illustration of some bottom-up methods for AuNP production

3.2 Top-down production of AuNPs

With laser ablation, a pulsed laser beam is focused on a target in a solvent. The laser energy is absorbed and the target material is vaporized. It then condenses in the solvent, forming nanoparticles. The use of ultra-short pulses enables the application of volatile organic solvents or monomers. An advantage of laser ablation is that laser-generated AuNPs have a positive surface charge, which is not the case with chemical routes. The charge causes an electrostatic stabilization of the nanoparticles without the need for additional stabilizing agents [62].

In condensation with inert gas, the metal (gold) is first vaporized in a vacuum chamber and then supercooled with inert gas. The supercooled vapour condenses into AuNPs, which are then transported onto a substrate by the inert gas, or are studied in-situ [63].

Sputter deposition and thermal evaporation act on the same principle as laser ablation, where atoms, clusters, or fragments of metals are first ejected from the bulk material and then captured in a medium for re-condensation of the vapours into nanoparticles [64].

High-energy ball milling is a process where a powder mixture of the material is placed in the ball mill. During the high-energy milling process, the powder particles are subjected to high energy impacts in order to refine the powders. Surface and interface contamination of the produced nanoparticles by the milling tools is a major concern in this type of production method [65].

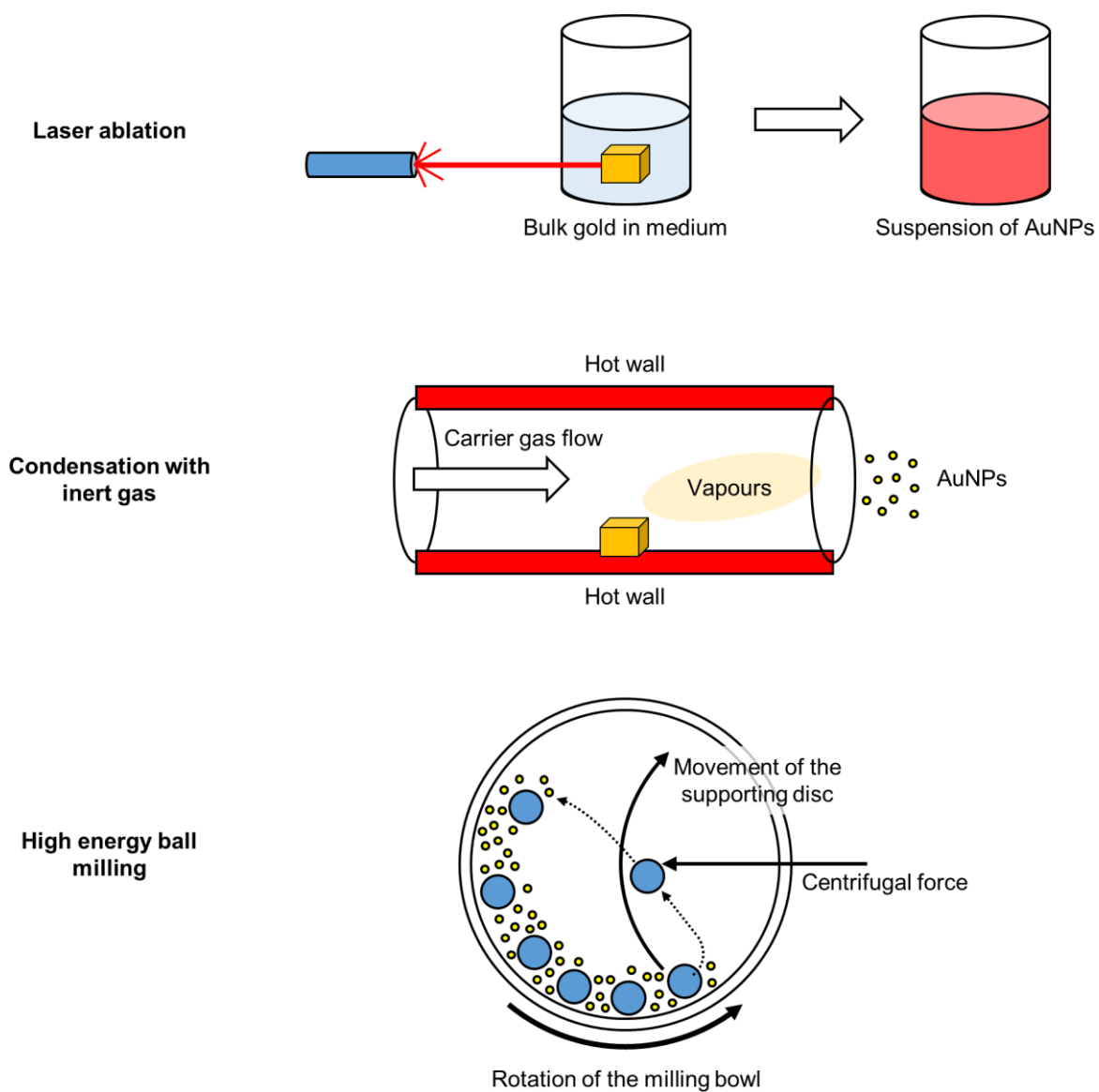


Figure 3.2: Simplified illustration of some top-down methods for AuNP production

4 ULTRASONIC SPRAY PYROLYSIS OF AuNPs

Pyrolysis is a process of chemical decomposition of various compounds at elevated temperatures. Spray pyrolysis involves the decomposition of aerosols (solid or liquid particles, suspended in gas), generated by a nebulizer. The nebulizer can be pneumatic, ultrasonic, or electrostatic, although ultrasonic nebulizers are the most efficient, affordable and have a low droplet velocity. As such, they are used commonly in spray pyrolysis processes. With the ultrasound, the precursor solution with a dissolved material is dispersed into droplets. These droplets are then exposed to high temperature, such that the material inside the droplet is decomposed chemically via pyrolysis and nanoparticles of pure elements are obtained. The advantage of the USP method is the simplicity of setting up individual process segments and changing their configuration, continuous nanoparticle synthesis and the possibility of synthesizing pure nanoparticles from various materials. The disadvantage is the low efficiency of the un-optimized method (currently around 10%) due to losses of the dissolved material on the construction elements of the USP device.

The main elements of the standard USP device are the ultrasonic generator, the reactor furnace and a system for nanoparticle collection (Figure 4.1). The selected raw material for preparing precursor solutions for AuNP synthesis was tetrachlororaucic acid $\text{HAuCl}_4(\text{s})$. The precursor solution was prepared by dissolving HAuCl_4 in deionized (DI) water (ion states: $[\text{AuCl}_4]^- + \text{H}^+ + \text{H}_2\text{O}$) [18], [19].

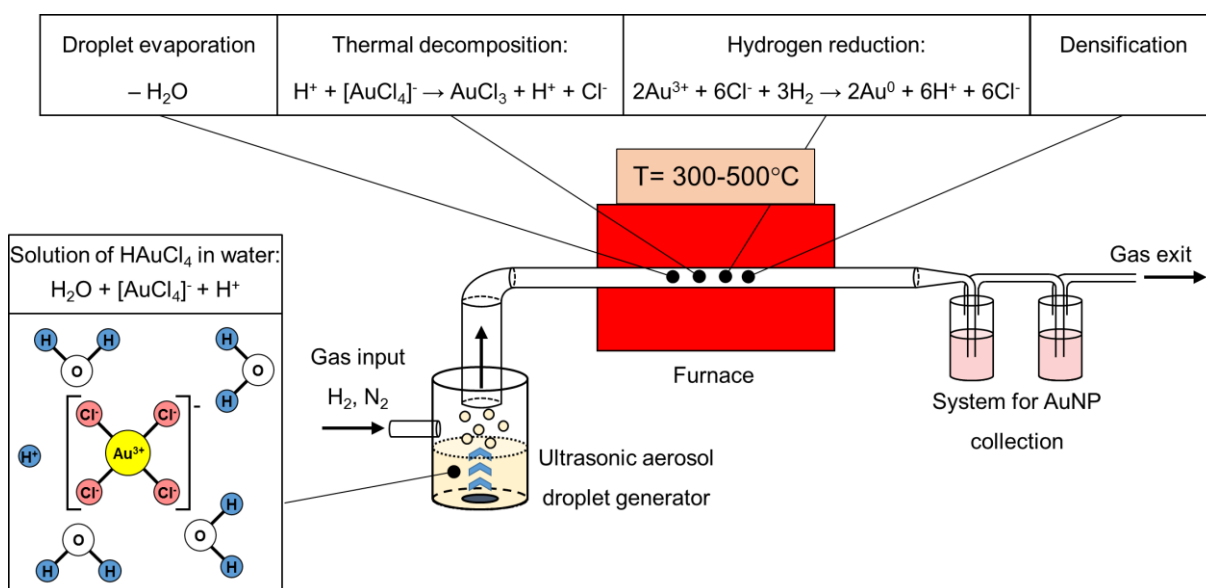


Figure 4.1: AuNP synthesis with the conventional USP

The sizes of the synthesized AuNPs depend on the ultrasound frequency [13], [17], [20], which determines the sizes of the aerosol droplets, and the concentration of the dissolved Au in the precursor solution droplets¹. Due to vibrations of the ultrasound below the solution surface, the kinetic energy of the solution molecules increases rapidly. This causes small droplets to overcome surface tension and break away from it. This effect, known as nebulization (Figure 4.2), produces micron sized aerosol droplets, which act as individual chemical reactors, when subjected to thermal treatment [61], [67]. Droplets in a size distribution from 1 to 15 micrometers are created with a high-frequency ultrasound (0,5-3 MHz) [21].

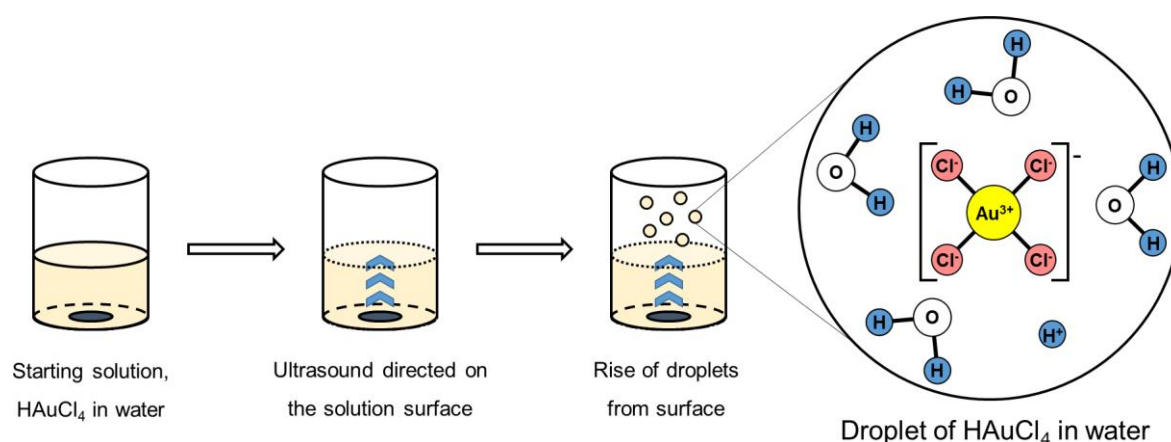


Figure 4.2: Aerosol droplet formation from starting solution with ultrasound (Assumption: the ion states inside the aerosol droplets are the same as in the starting solution [18])

Droplets of the precursor solution ($[\text{AuCl}_4]^- + \text{H}^+ + \text{H}_2\text{O}$) are transported into the furnace with a carrier gas. Inside the furnace, the AuNPs are formed according to the following synthesis stages (Figure 4.1):

1. Evaporation and droplet shrinkage (Au^{3+})
2. Thermal decomposition of HAuCl_4 into AuCl_3
3. Reduction of AuCl_3 with hydrogen and formation of pure Au ($\text{Au}^{3+} \rightarrow \text{Au}^0$)
4. Densification (Au^0)

¹ Au represents around 48-52% of weight in tetrachlorauric acid HAuCl₄ [66]. As the chemical composition of the precursor in the solution changes from HAuCl₄ to pure Au, the concentration of only Au instead of HAuCl₄ is used as a parameter. This concentration of Au is an indicator of final pure AuNP sizes.

The listed synthesis stages are taking place at the same time with the conventional USP (Figure 4.1).

Depending on the physical state from which nanoparticles are formed with USP, there are two main routes described in literature [13], [68], [69]:

- Droplet-To-Particle (DTP)
- Gas-To-Particle (GTP)

These formation mechanisms can both occur during synthesis with USP and are explained in more detail in the following Chapters.

4.1 Evaporation

Studies [13], [17], [20], [22] have shown, that the shapes of the synthesized AuNPs depend on the rate of droplet evaporation and the rate of ion diffusion $[AuCl_4]^-$ and H^+ inside the droplet. These rates depend on several factors with USP synthesis: Starting solution concentration, droplet sizes, number of droplets and relative humidity in the system, velocity of droplet transportation into the furnace with the carrier gas, pressure in the system, dimensions of the transport pipes, and temperature inside the furnace.

Droplet evaporation begins before entering the heating zone, as the formed aerosol droplets are a few micrometers in diameter. The droplet evaporation depends upon several parameters: Droplet radius (r), droplet temperature (T_d), environment temperature (T_∞), mass fraction of vapour on the droplet surface (Y_{vap}). Once the droplet temperature and environment temperature are the same ($T_d = T_\infty$) and the vapour pressure on the surface is the same as the pressure in the environment ($Y_{vap,\infty}$), evaporation will not occur. Evaporation will begin in the case of $Y_{vap} > Y_{vap,\infty}$, where the mass flow will appear (\dot{m}_{vap}), as material is leaving the droplet surface. The internal energy of the droplet is being used up for evaporation. The result is a thermal flow (\dot{q}_{liq}) from the droplet centre to its surface and a thermal flow from the environment to the droplet surface (\dot{q}_{vap}). The result is a temperature gradient inside the droplet and a reduction of temperature T_d , as shown in Figure 4.3.b).

As the temperature of the environment is greater than that of the droplet T_d , the droplet begins to heat up (\dot{q}_{liq} is directed from the surface to the droplet centre) and \dot{m}_{vap} is increased as shown in Figure 4.3.a). The result of increased mass flow is the flow \dot{q}_{vap} , which is now

being used up for the latent heat required for evaporation. At the same time, the thermal flow from the droplet on the boundary layer is lowering \dot{q}_{vap} on the droplet surface, keeping the temperature of the droplet somewhat below T_∞ .

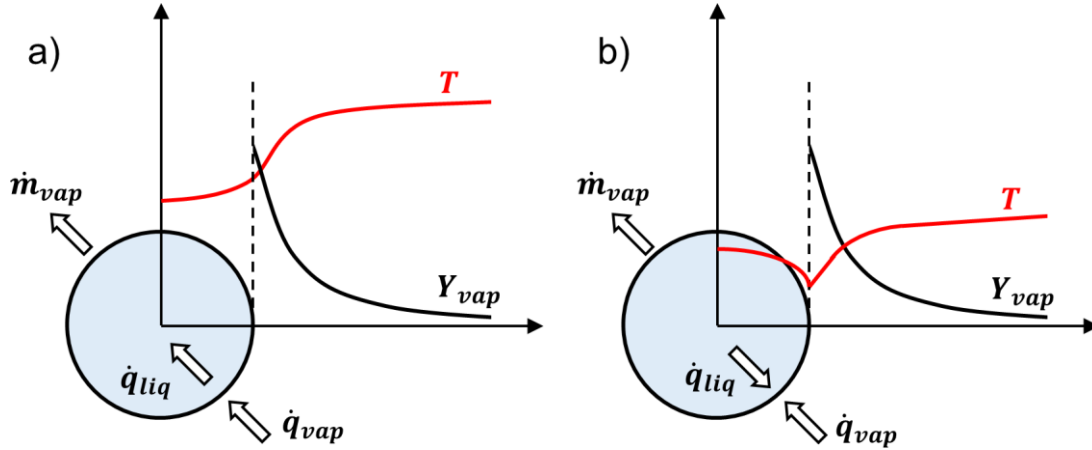


Figure 4.3: Aerosol droplet evaporation conditions (temperature, mass and heat flows and vapour pressure); a) At high environment temperatures; b) At low environment temperatures

At this stage, all the heat on the surface is being used up for evaporation. In this case, the droplet is being evaporated with a linear decrease of the square of its diameter (d^2 , or radius r^2):

$$\frac{dd^2}{dt} = -\beta_d \quad \text{or} \quad \frac{dr^2}{dt} = -\beta_r \quad (4.1)$$

This expression is known as the »diameter square law« (d^2 -Law) or »radius square law«. This is a simple model for describing evaporation of the droplet, where $-\beta_d$ or $-\beta_r$ is the coefficient of evaporation, depending upon the liquid properties and environment conditions [70].

4.2 Thermal decomposition and hydrogen reduction

Before formation of the final AuNPs, the precursor needs to undergo a chemical transformation. In our case, the precursor (HAuCl_4) is first decomposed thermally and then reduced with hydrogen gas, to produce AuNPs. The thermochemical calculations for these reactions are presented in this Chapter.

The thermochemical calculations are based on a ThermoGravimetric Analysis (TGA) used for explaining the decomposition of HAuCl_4 (Figure 4.4, [71]). Thermal decomposition begins at about 77°C . The appearance of the first weight loss below 120°C is caused by water evaporation and the decomposition of HAuCl_4 into AuCl_3 (dimers of AuCl_3 are formed: Au_2Cl_6 [72]). This correlates to the loss of weight between 260°C and 750°C (75 %), which is close to the weight of AuCl_3 (77 %). The subsequent decomposition began at 750°C and did not stop at 900°C . This indicates that HAuCl_4 was not reduced to gold only by thermal treatment below 900°C in a neutral atmosphere.

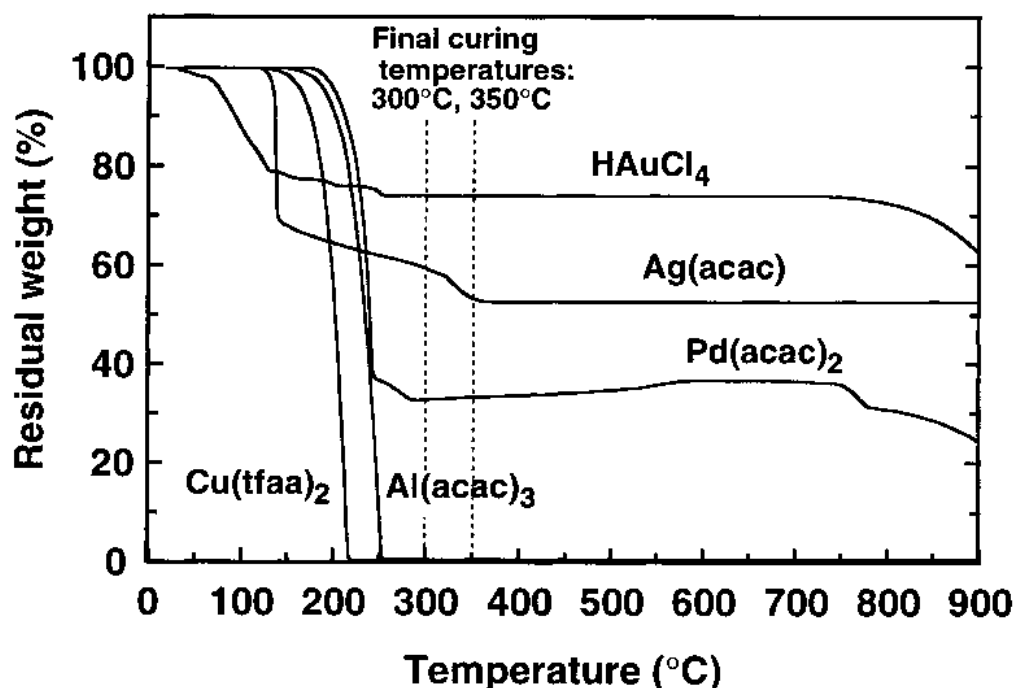


Figure 4.4: TGA of gold chloride HAuCl_4 and some metallic polyimides, from [71]

The gold formation from HAuCl_4 takes place in two steps [18]:



For the formation of AuNPs from HAuCl_4 , a thermal decomposition of HAuCl_4 must be performed, producing Au_2Cl_6 and HCl , followed by a hydrogen reduction of Au_2Cl_6 , to form particles of Au. As the reduction of HAuCl_4 into pure gold in a neutral atmosphere does not occur below 900°C , this means that using a hydrogen atmosphere, or a hydrogen/nitrogen atmosphere reduces the required temperature for the creation of gold nanoparticles considerably.

By increasing the temperature of the reaction from 100°C up to 1000°C, the Gibbs free energy, ΔG changes from 213 to -130 kJ for thermal decomposition of HAuCl_4 and from -570 to -958 kJ for hydrogen reduction [18], [73] (Figure 4.5). The free energy for hydrogen reduction is always negative, meaning this reaction happens with a high probability. The free energy of the thermal decomposition does not reach negative values until 600°C, suggesting a low probability of the reaction occurring until then. However, the theoretical temperature for decomposition of HAuCl_4 is 258°C.

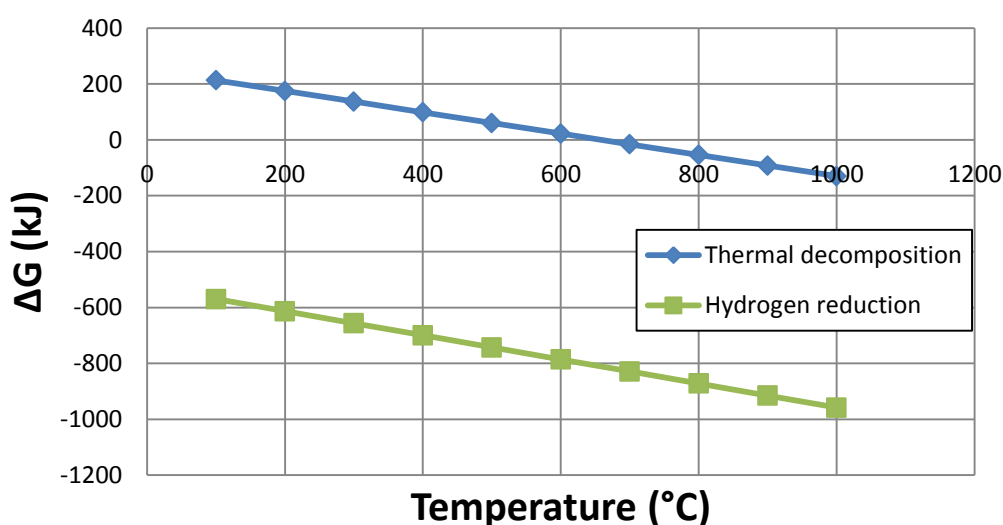


Figure 4.5: Gibbs free energy for thermal decomposition and hydrogen reduction, adapted from [18], [73]

4.3 Densification

When the dried nanoparticles of gold chloride react with hydrogen, new, differently orientated grains of Au are formed, which are then combined with diffusion across their boundaries. The process can be considered analogous to sintering of materials. A simple schematic of densification of porous nanoparticles is presented in Figure 4.6.

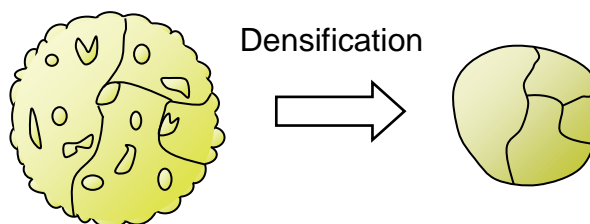


Figure 4.6: Simple representation of densification of porous nanoparticles into solid final nanoparticles

Densification takes place at the atomic level and reduces the particles' surface energy. Because of the high number of surface atoms, inherent in nanoparticles, the surface energy is increased. This enhances the process of densification further, when lower energies are being attained. The driving mechanism for densification are surface diffusion and diffusion over the grain boundaries [74], [75]. Because of their sizes and the large proportion of surface atoms, the thermodynamic properties of nanoparticles (of a few 10 nm) are very different than those of their bulk materials [76]. Figure 4.7 shows the melting point temperature for AuNPs dependent on the sizes of nanoparticles. It is seen that the higher ratio of surface atoms reduces the melting point greatly [76]–[78]. This means that very small AuNPs (below 10 nm) already reach the melting point in our USP system, resulting in the formation of solid, spherical AuNPs, because of achieving lower surface energies during their formation.

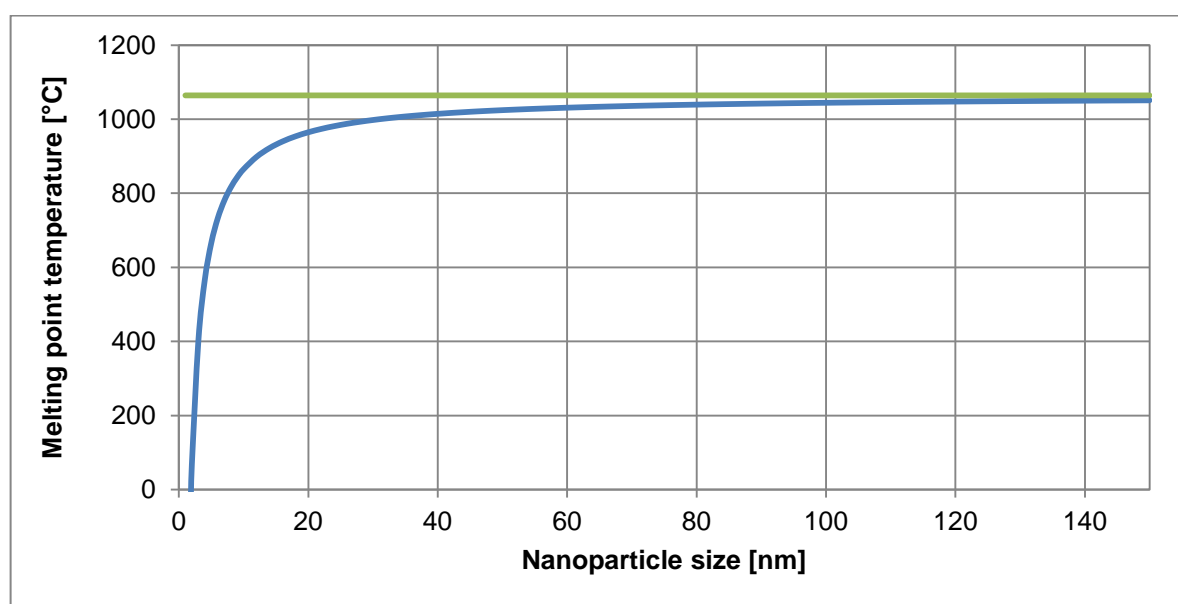


Figure 4.7: Melting point temperature of AuNPs as a function of nanoparticle size [76]

4.4 Formation mechanisms with USP

In USP, the AuNPs can be formed from different physical states, depending on the precursor used and its volatility (ease of vaporization). The two main mechanisms described in literature, DTP and GTP [13], [68], [69], are explained in the following Chapters.

4.4.1 Droplet-To-Particle mechanism

The liquid-to-solid and solid-to-solid conversion processes with USP can be described with the DTP mechanism. This mechanism in general consists of the formation of droplets, transportation of these droplets into a heating zone, evaporation of the solvent and thermal conversion of the solute into the final AuNPs.

As the droplet with dissolved material is being evaporated it shrinks and, simultaneously, increases the mass fraction of the solute inside the droplet. The solute can begin to precipitate before uniform saturation across the droplet is reached because the solute diffusion is slower than the evaporation of the solvent. As the solid material is being precipitated on the droplet surface due to supersaturation, the liquid can become trapped in the centre. It then begins to evaporate through the newly formed surface crust (Figure 4.8). This slows down the evaporation rate.

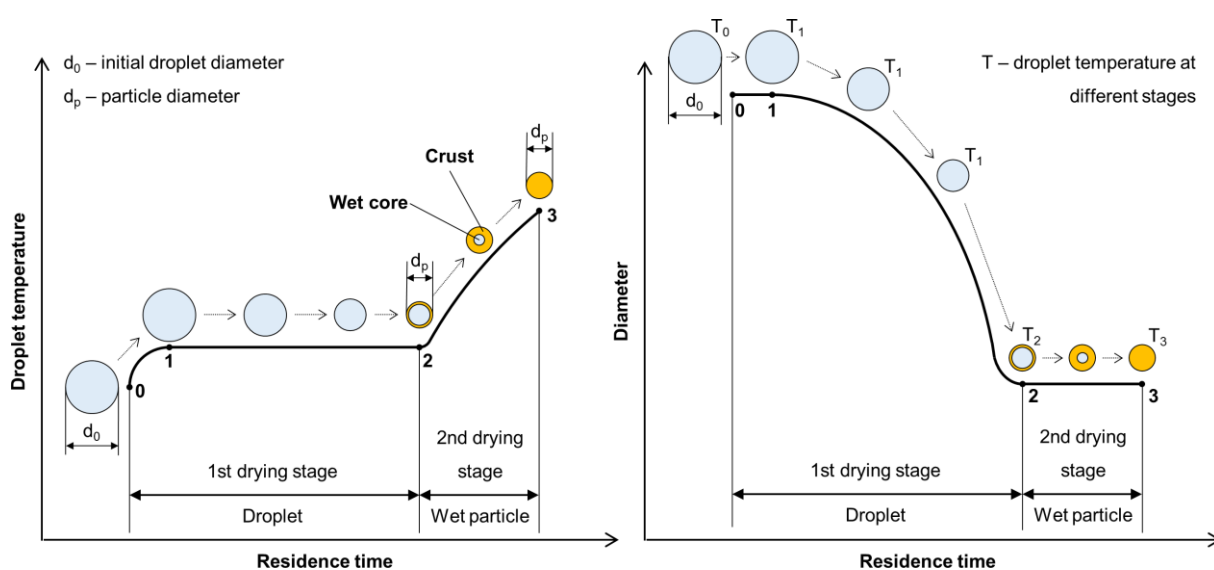


Figure 4.8: Evaporation of aerosol droplet and drying of the precipitated solute², adapted from [79]

Solute precipitation in droplets has not been described by any theory in a quantitative manner. For a given solute, the supersaturation required for precipitation must be measured [13], [80] and is a function of the exact composition of the solution (impurities act as precipitation sites). Because the rate of nucleation determines particle morphology, the

² Residence time is the amount of time the droplet/particle spends in the heating zone

evaporation determines particle morphology (evaporation depends on a number of factors, such as surrounding vapour pressure and temperature, p_∞ and T_∞).

Intraparticle reactions, such as thermal decomposition, also occur in the aerosol before and after solvent evaporation and can influence particle morphology. These were studied with thermogravimetric analysis, differential thermal analysis and differential scanning calorimetry [13]. The precursor characteristics determine whether hollow or porous particles are formed. Whether a precursor melts or not before reacting has a very distinct difference on the final particle morphology. The volume fraction of the solute also influences the formation of porous or hollow particles, as does a high reduction of volume because of reactions.

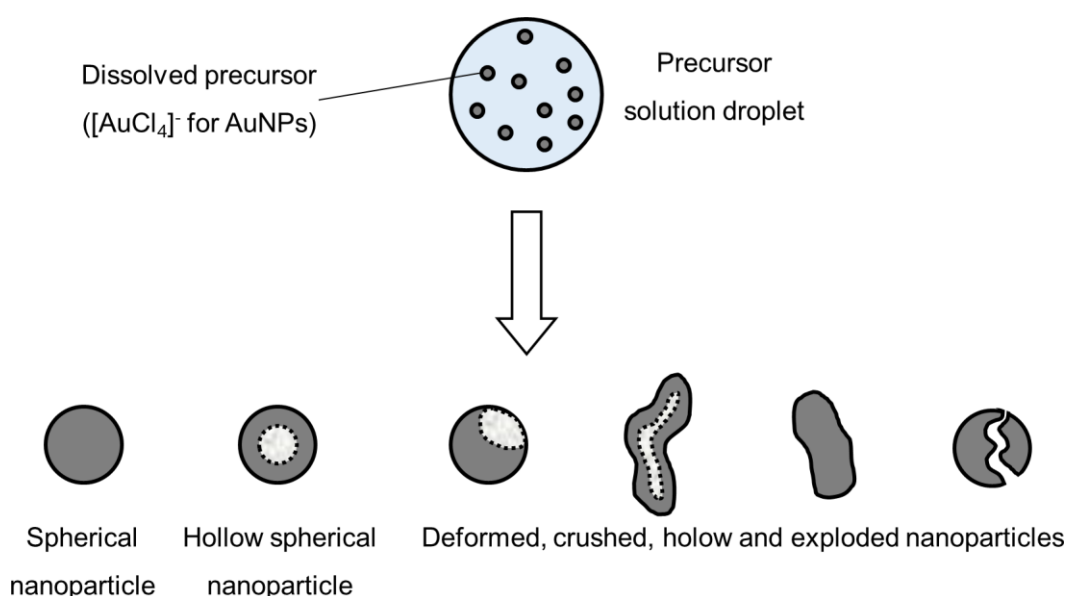


Figure 4.9: Types of nanoparticles that can be synthesized from an aerosol droplet, depending on the parameter conditions, adapted from [70]

4.4.2 Theoretical calculations for evaporation of solution droplet with the DTP mechanism

For the theoretical calculations of solution droplet evaporation, an analytical model with a system of five differential equations was used [13], [20]. In the calculations, some assumptions were made:

- Natural and forced convection was ignored.
- The gas state physical properties were considered constant.
- The faster reaction rates of the gas state were ignored (because of density differences, the liquid state reacts much slower to the temperature and concentration changes).
- No thermal radiation effects, heat flow due to concentration gradients and mass flow due to temperature gradients were considered.

The evaporation was thus estimated with the following equations:

Aerosol droplet residence time (amount of time the droplet spends in the heating zone), dependant on the position in the furnace:

$$\frac{dt}{dx} = \frac{0,06\pi R^2}{Q} \left(\frac{T_0}{T}\right) \frac{(1 - y_w)}{(1 - y_w^0)} \quad (4.4)$$

Change of droplet diameter:

$$\frac{dd_p}{dx} = \left(\frac{dd_p}{dt}\right) \left(\frac{dt}{dx}\right) = \frac{4D_v m_1}{\rho_p d_p} (n - n_s) \left(\frac{dt}{dx}\right) \quad (4.5)$$

Concentration of water vapour in the furnace:

$$\frac{dn}{dx} = \left(\frac{dn}{dt}\right) \left(\frac{dt}{dx}\right) = \left[-2\pi d_p D_v N_0 (n - n_s) - \frac{2K_m (n - n_w)}{R} \right] \left(\frac{dt}{dx}\right) \quad (4.6)$$

Change of droplet temperature:

$$\frac{dT_s}{dx} = \left(\frac{dT_s}{dt}\right) \left(\frac{dt}{dx}\right) = \frac{1}{C_p d_p} \left[3H_L \frac{dd_p}{dt} + \frac{6h_s}{\rho_p} (T - T_s) \right] \left(\frac{dt}{dx}\right) \quad (4.7)$$

Surrounding gas temperature:

$$\frac{dT}{dx} = \frac{1}{FC_{pa}} \left[-\pi^2 R^2 d_p^2 N_0 h_s (T - T_s) + 2\pi R h_w (T_w - T) \right] \quad (4.8)$$

Near the surface of the droplet, the solute concentration increased as the droplet shrank, and saturation of the solute occurred. When the solute saturation reached critical saturation, the solute began to precipitate on the surface of the droplet. The solute saturation was calculated with:

$$s = \frac{a_s}{a_c} = \frac{m_s y_s}{m_c y_c} \quad (4.9)$$

Critical saturation was obtained from the following equation:

$$s^* = \exp \left[\frac{16\pi\sigma^3 M_s^2}{3v^2 k T_s^3 \rho_s^2 R_g^2 \ln(A/J)} \right]^{0,5} \quad (4.10)$$

Details of the calculations are given in the Appendix.

A schematic of HAuCl_4 solution droplet evaporation for the DTP mechanism is shown in Figure 4.10, displaying the droplet size, solute concentration, water vapour mass flow, thermal flows, temperature and partial vapour pressure conditions.

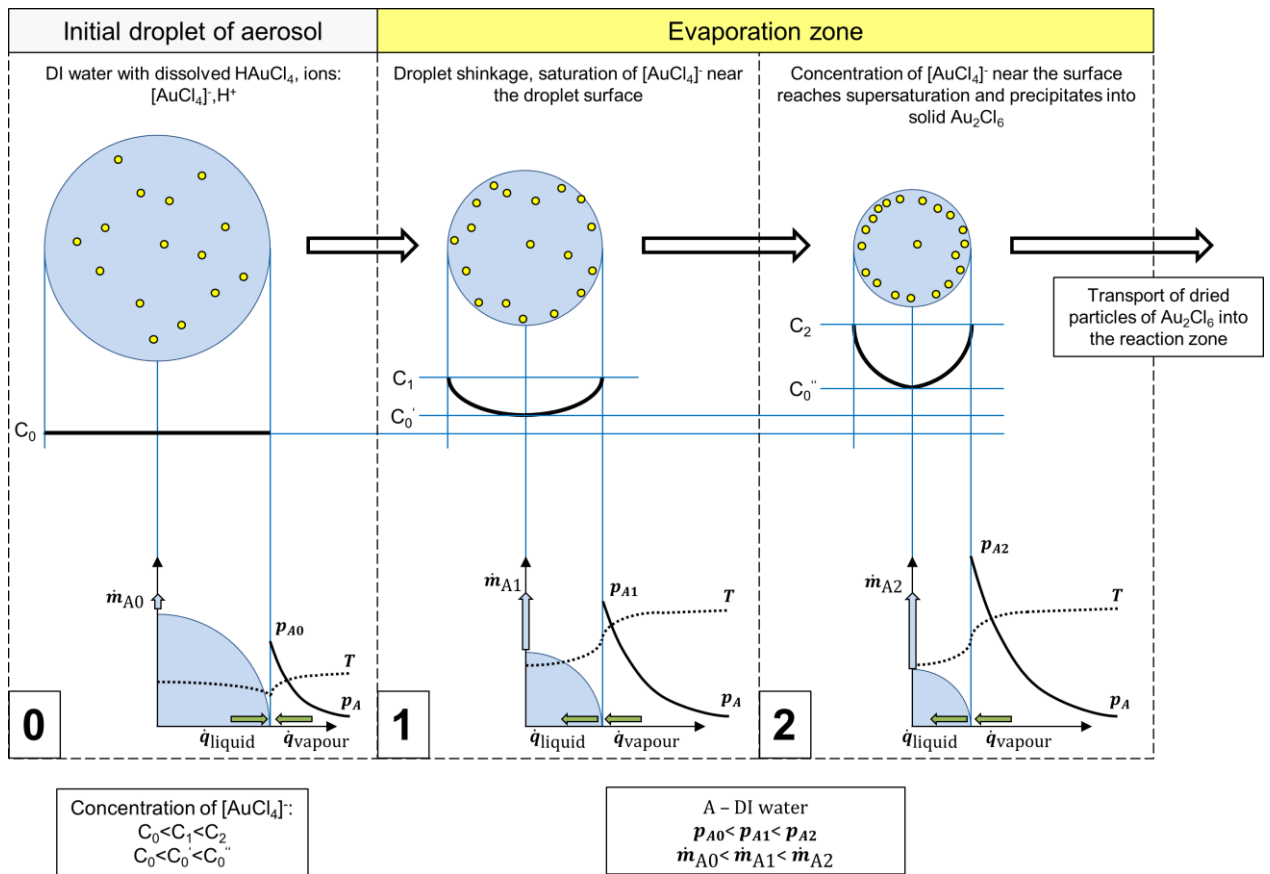


Figure 4.10: Aerosol droplet evaporation and beginning of precipitation of solute with the DTP mechanism

4.4.3 Gas-To-Particle mechanism

The GTP formation mechanism generally follows the supersaturation of a gaseous species of the desired material, which causes nucleation and new particle formation. The particles can be created by chemical reactions of gaseous precursors or by physical processes, such as cooling of a hot vapour.

The average particle diameter, total particle concentration, size distribution and particle morphology evolve along the aerosol reactor in two different modes. One mode is nucleation-condensation, where a monomer (molecule or atom) is formed by a chemical reaction or a decrease in temperature, until nucleation occurs. The saturation ratio increases and growth of the monomer proceeds by condensation of the monomer onto the particles. When no collisions occur, they can remain nearly spherical through the aerosol reactor path. Surface reaction on the particles may also occur, promoting growth. Another mode is nucleation-coagulation, where particles are formed and their high concentration allows collisions and coalescence of particles, resulting in growth of the particles. Both modes can be found in laboratory processes, while nucleation-condensation is usually not found in industrial systems.

In the nucleation-condensation mode, the morphology of the particles depends on collisions and coalescence. Particles coalesce by sintering after collisions in order to become spherical. The ratio of rates of collisions and coalescence (α_c [13], [81], [82]) determines the morphology. In collision-limited growth ($\alpha_c = \infty$), the sintering rate is rapid relative to collisions, allowing for the formation of spherical particles between collisions. In sintering-limited growth ($\alpha_c = 0$) the particles exist as aggregates. Intermediate conditions ($\alpha_c \approx 1$) are in existence in real situations, where the particle morphology is a function of parameters that control the sintering rate – temperature and material properties. The primary particle size is also a function of these parameters (Figure 4.11).

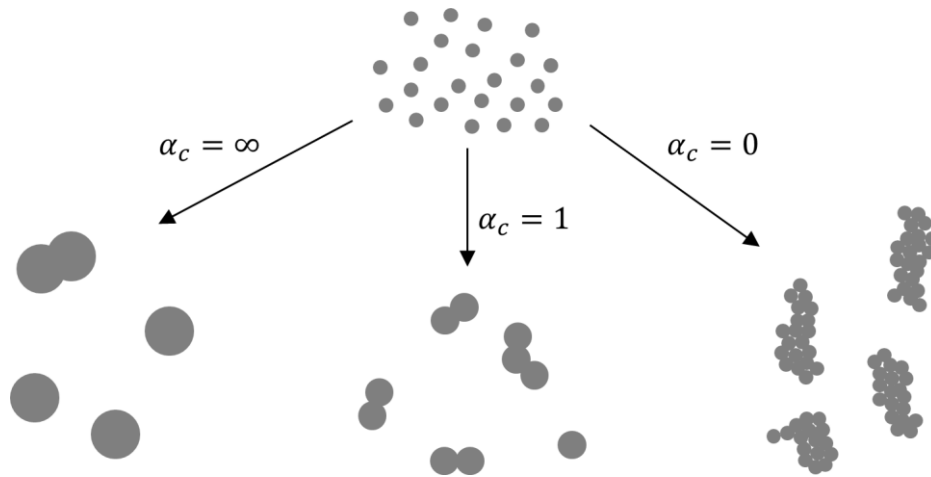


Figure 4.11: The ratios of collisions and coalescence with the GTP mechanism and the resulting nanoparticle morphologies, from [13], [81], [82]

When the aerosol droplet evaporates within the GTP mechanism, the solute is vapourized along with the solvent, resulting in the presence of the solute vapours and its partial vapour pressure (Figure 4.12). When saturation of vapours is reached, nucleation occurs and growth of particles proceeds as described previously.

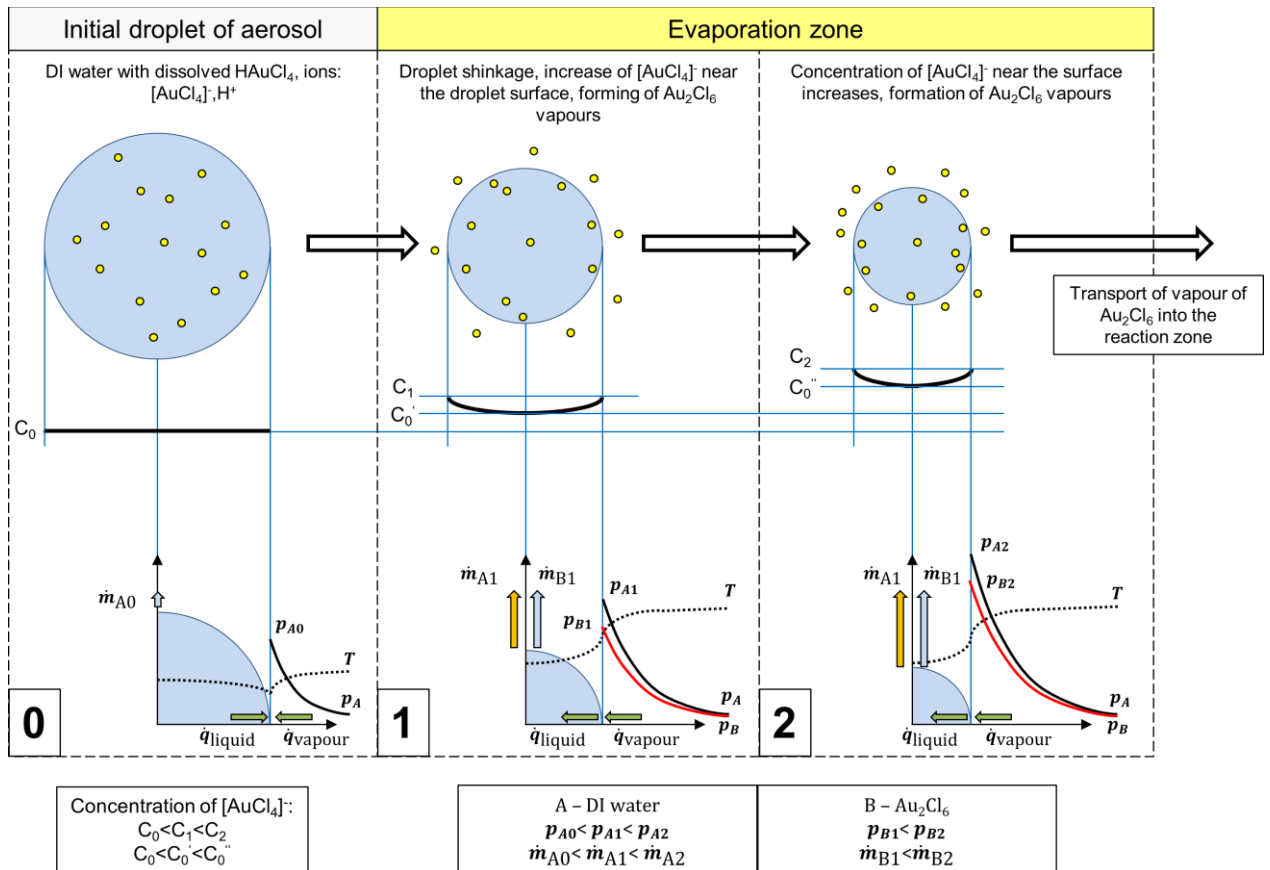


Figure 4.12: Aerosol droplet evaporation and vapourization of solute with the GTP mechanism

5 SYNTHESIS OF AuNPs WITH THE CONVENTIONAL USP

For AuNP synthesis, the equipment developed at the IME Institute of Process Metallurgy and Metal Recycling, RWTH Aachen University was used (Figure 5.1) [83], [84]. The main elements of the device consist of the ultrasonic atomizer (Gapusol 9001, RBI/France), a tubular reactor furnace, quartz tube (SiO_2 , length of 1.0 m, diameter of 20 mm) and quartz connectors, a thermostat, and two bottles with collection medium (DI water and/or alcohol) for nanoparticle collection. These preliminary experiments represent an effort to determine whether AuNPs were possible to synthesize with USP.



CONVENTIONAL USP

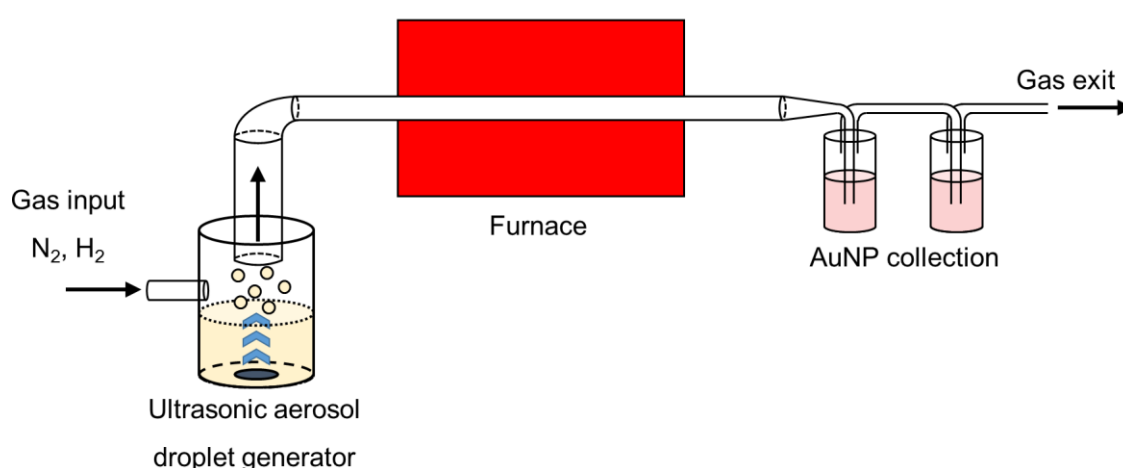


Figure 5.1: USP equipment at the IME Institute of Process Metallurgy and Metal Recycling, RWTH Aachen and a simple schematic of the devices used

5.1 Parameter selection

The size of obtained nanoparticles is related to the droplet diameter and the initial concentration of the precursor solution. Increasing the ultrasonic frequency reduces the droplet diameter of the produced aerosol and also increases the ratio of smaller nanoparticles in the final product. The formation of droplets by ultrasound was first described by R. W. Wood and A. L. Loomis in 1927 [85]. In 1962, Lang formulated an equation to describe the connection between the ultrasonic frequency and the mean droplet diameter [86]. This equation is well known for use in ultrasonic atomization and with the use of one particle-per-droplet mechanism in nanoparticle synthesis.

$$d = 0,34 \cdot \left(\frac{8 \cdot \pi \cdot \gamma}{\rho_{sol} \cdot f^2} \right)^{1/3} \quad (5.1)$$

A theoretical equation for the prediction of sizes of obtained nanoparticles was formed in a previous work [73], combining Kelvin's equation and an equation based on the capillary theory.

$$D_{Au} = 0,34 \cdot \sqrt[3]{\left(\frac{8 \cdot \pi \cdot \gamma \cdot C_{sol} \cdot M_{Au}}{\rho_{sol} \cdot f^2 \cdot \rho_{Au} \cdot M_{sol}} \right)} \quad (5.2)$$

A few assumptions and simplifications were made in the calculations:

- No coalescence of ultrasonically made droplets
- One particle-per droplet mechanism (each droplet is considered as a sort of micro-reactor for the formation of a single nanoparticle)
- The characteristics of the precursor (surface tension), for the purpose of the calculations, were comparable to the characteristics of water, since the solution was a diluted tetrachloroauric acid – HAuCl_4

Because of the one particle-per droplet mechanism, the size of the particle depends mainly on the diameter of the droplet (frequency of the ultrasonic atomizer) and on the Au concentration of the precursor solution. Unfortunately, coalescence of the droplets is difficult to prevent, and the calculated mean droplet diameter was expected to be somewhat smaller than the actual size of the droplets in the performed experiments. In the mentioned equation, there is also no account for the effect of temperature on particle size.

The parameters required for the calculations are well known: Surface tension of water, molar masses of gold and HAuCl_4 , and density of gold. The calculated droplet diameter thus amounted to $d = 4,82 \times 10^{-6}$ m for an ultrasonic frequency of $f = 0,8$ MHz. Increasing the ultrasound frequency to $f = 2,5$ MHz decreased the size of the droplets to $d = 2,25 \times 10^{-6}$ m.

For the calculations, a concentration of Au between 1 and 20 g/l was selected. Hence, for an ultrasonic frequency of 0,8 MHz, the calculated mean AuNP diameter ranged from 150 to 407 nm. Increasing the frequency up to $f = 2,5$ MHz, the calculated mean particle diameter was between 70 and 190 nm (Figure 5.2). The increase in frequency resulted in smaller droplet diameter and smaller particle size.

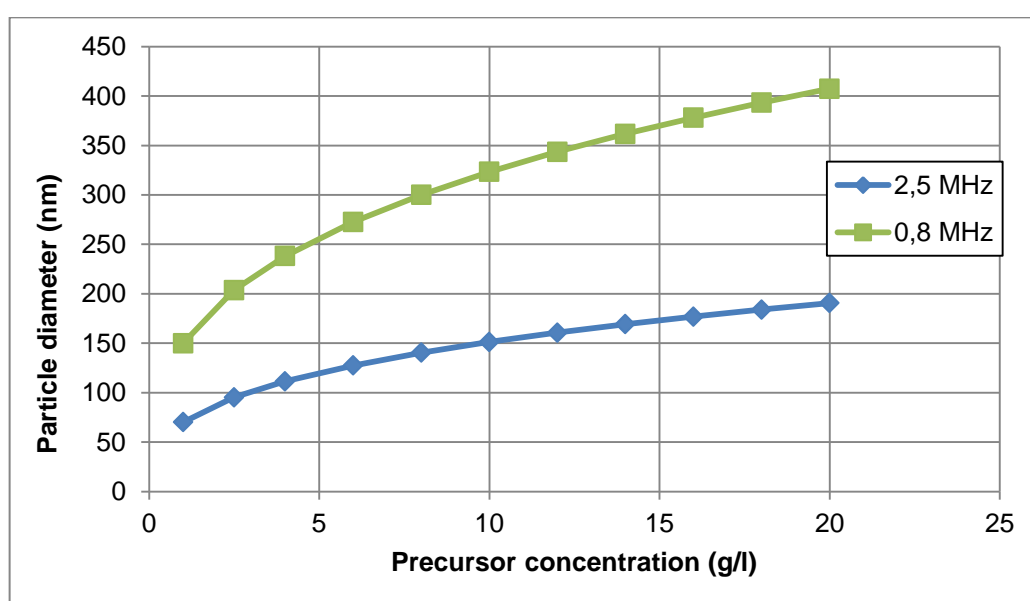


Figure 5.2: Theoretically calculated diameter of AuNPs, concentration of gold in solution: 1 – 20 g/l

5.2 Experiments with conventional USP

The parameters for the experiments were selected from the theoretical calculations from the previous Chapter. For the precursor solution, tetrachloroauric acid HAuCl_4 from Johnson Matthey Company, Germany, was dissolved in DI water, with a concentration of 2.5 g/l Au. The atomizer was set to a frequency of 0,8 MHz and 2,5 MHz and produced aerosol droplets, which were transported by nitrogen gas into the reactor, at a rate of 1.5 l/min. Hydrogen gas was added for reduction at a rate of 1.0 l/min. The reactor was running at a temperature from 260°C to 500°C. When transported to the reactor, the droplets were exposed to drying, droplet

shrinkage, solute precipitation, thermal decomposition, hydrogen reduction and densification, before collection in two bottles with collection medium. For the collection medium, DI water (prepared with a deionizer system³) or alcohol was selected to prevent possible agglomeration of the synthesized AuNPs. The Table 5.1 shows the parameters selected for experiments with an ultrasound frequency of 0.8 MHz, while Table 5.2 shows the parameters selected for experiments with an ultrasound frequency of 2,5 MHz [18]. These are the parameters for the preliminary experiments, where the aim was to determine whether it was possible to synthesize AuNPs with USP.

Table 5.1: Synthesis parameters for AuNPs, ultrasound frequency of 0,8 MHz

Experiment⁴	Conc. of Au in precursor solution	Temperature	Gas flow	Collection medium
CAu1	2.5 g/l	260°C	1.5 l/min N ₂ , 1.0 l/min H ₂	DI water
CAu2	2.5 g/l	280°C	1.5 l/min N ₂ , 1.0 l/min H ₂	Ethanol
CAu3	2.5 g/l	300°C	1.5 l/min N ₂ , 1.0 l/min H ₂	Ethanol
CAu4	2.5 g/l	400°C	1.5 l/min N ₂ , 1.0 l/min H ₂	DI water
CAu5	2.5 g/l	500°C	1.5 l/min N ₂ , 1.0 l/min H ₂	Ethanol

³ Inside the deionizer, tap water was passed through a cartridge containing cationic and anionic resins which removed impurities electrostatically. The result was very pure, deionized water with low conductivity.

⁴ Experiments performed with the conventional USP were designated CAu(x), where (x) denotes the number of the experiment

Table 5.2: Synthesis parameters for AuNPs, ultrasound frequency of 2,5 MHz

Experiment	Conc. of Au in precursor solution	Temperature	Gas flow	Collection medium
CAu6	2.5 g/l	260°C	1.5 l/min N ₂ , 1.0 l/min H ₂	DI water
CAu7	2.5 g/l	260°C	1.5 l/min N ₂ , 1.0 l/min H ₂	Ethanol
CAu8	2.5 g/l	280°C	1.5 l/min N ₂ , 1.0 l/min H ₂	Ethanol
CAu9	2.5 g/l	300°C	1.5 l/min N ₂ , 1.0 l/min H ₂	Ethanol

6 SYNTHESIS OF AuNPs WITH THE MODIFIED USP

Based on AuNP synthesis with the conventional USP, a modification to the USP device was made, in which we have separated the droplet evaporation from the rest of the synthesis stages (thermal decomposition, hydrogen reduction and densification). In this way, higher control would be achieved over the synthesis stages in order to obtain the desired sizes and shapes of the AuNPs. We presumed, that a separate evaporation stage would allow for a more optimal material diffusion inside the droplet ($[AuCl_4]^-$ in H^+) and would result in the synthesis of desired shapes of the AuNPs. This modification also prevented formation of AuNPs in the ultrasonic generator, as the reduction gas would be introduced directly into the reaction zone (Figure 6.1). The approach of modification of the USP and the identification of AuNP synthesis mechanisms from $HAuCl_4$ has not yet been described in literature.

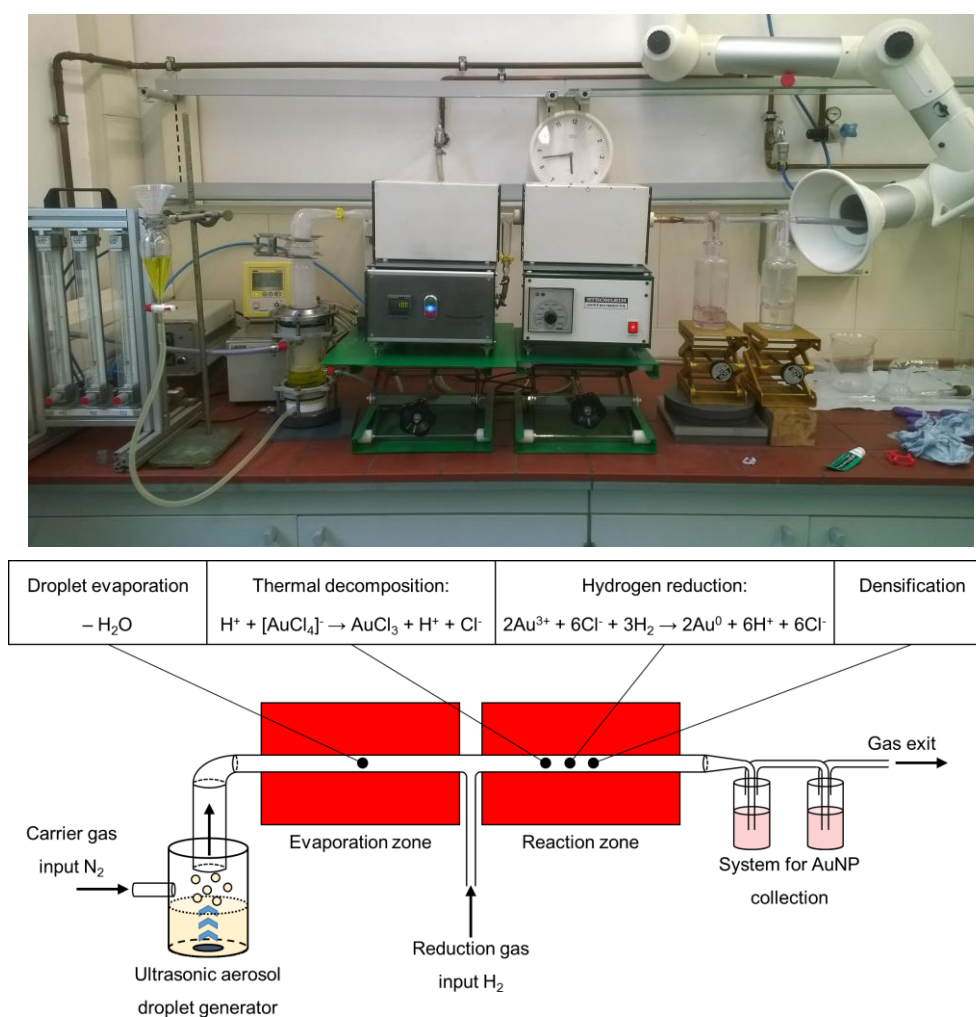


Figure 6.1: Modification of the conventional USP with a separate evaporation zone and reduction gas input directly into the reaction zone

The separate evaporation stage would ensure the formation of spherical dried particles of gold chloride before the reaction stage with hydrogen – this would be accomplished by using the low temperatures required for slow evaporation of the solvent. Theoretically, this would enable more stable conditions for evaporation. When the solvent (DI water) evaporation is slow enough, the solute (gold chloride) will diffuse into the centre of the droplet, forming a spherical dried particle (Figure 6.2) [22] and without the reaction gas present at this stage, the particles cannot form on the surfaces of the droplets from gold chloride.

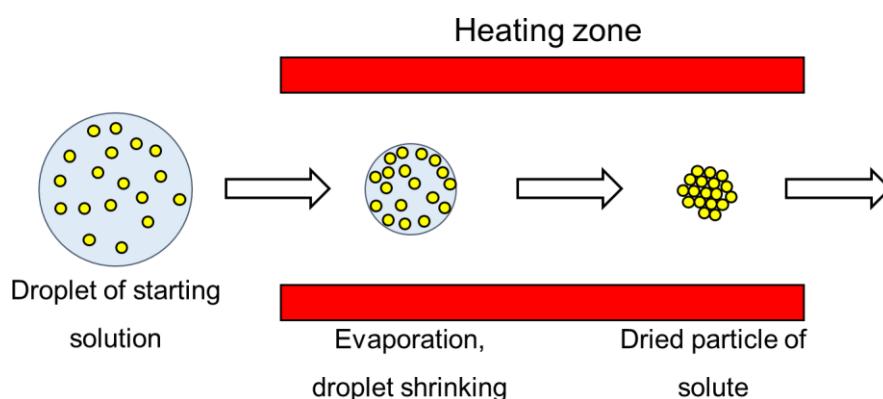


Figure 6.2: Simple presentation of the evaporation of an aerosol droplet with solute precipitation

After evaporation, in the reaction zone, hydrogen gas was introduced and the dried particles were decomposed, reduced from gold chloride to gold and densified into AuNPs. The AuNPs were then collected for analysis.

6.1 Parameter selection

6.1.1 Concentration of Au in the starting solution

The sizes of AuNPs obtained with the conventional USP were ranging from a few 10 nm to a few 100 nm with 2.5 g/l Au concentration in the precursor solution. For use in biomedicine, it was shown that 50 nm is the most optimal size for AuNPs (Chapter 2, [26]). From a theoretical standpoint, this means that low concentrations of gold should be used in the precursor solution. Low concentrations of the material in the precursor solution for nanoparticle production also provide better conditions for solid, spherical nanoparticle formation [13]. Somewhat higher concentrations should also be considered, in order to determine their effect on the final AuNPs' properties. As such, concentrations of 0.5, 1.25, 2.5

and 5 g/l Au were selected. A summary of selected parameters is presented in Tables from Table 6.1 to Table 6.6.

6.1.2 Ultrasound frequency

From the results obtained from conventional USP and from literature [18], [69], low frequencies of ultrasound generate larger aerosol droplets and, subsequently, larger final nanoparticles. Laser diffraction measurements (Malvern Spraytec) were conducted on the aerosol generators with ultrasound frequencies of 0.8 and 2.5 MHz of solutions with dissolved $\text{Al}(\text{NO}_3)_3$, $\text{C}_{16}\text{H}_{36}\text{O}_4\text{Ti}$ with RuCl_3 and H_3PO_4 with FeCl_2 and Li_2SO_4 [21], [87]. Some conclusions can be drawn from the measurements. It was shown that the concentration of the dissolved material in diluted solutions had no considerable effect on the aerosol droplet size distribution, while higher gas flows varied the droplet size distribution slightly, by increasing the number of larger droplets. A frequency of 2.5 MHz with diluted solutions yielded droplet sizes ranging from 1 to 15 μm , with the highest probability of droplet diameter from 4 to 6 μm . When using a frequency of 0.8 MHz, 30% larger droplets were generated than with 2.5 MHz. From this data, and with the aim of producing AuNPs of a mean diameter of 50 nm, the ultrasound frequency was selected to be 2.5 MHz. The estimated size distribution from the laser diffraction results of diluted solutions is presented in Figure 6.3.

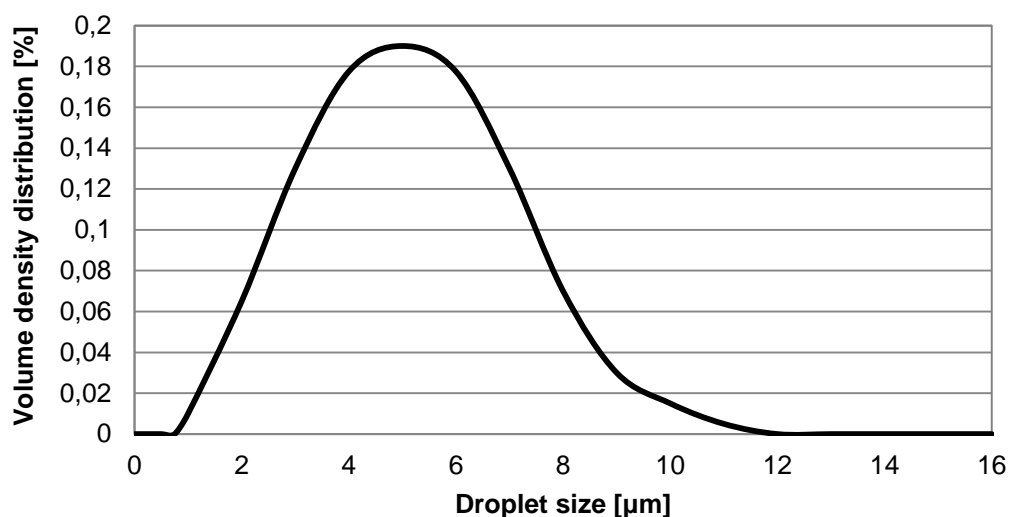


Figure 6.3: Aerosol droplet size distribution for diluted starting solutions with HAuCl_4 , estimated from [21], [87]

6.1.3 Evaporation zone temperature

The evaporation temperatures were selected to be from 50 to 100°C, in order to prevent any unwanted reactions of the dissolved HAuCl_4 in the evaporation zone. The heating zone had a length of 28 cm and, ideally, the aerosol droplets should evaporate at the end of this zone. The evaporation of droplets with HAuCl_4 was calculated with the calculations presented in chapter 4.4.2. The calculations for an aerosol droplet of 5 μm (most numerous droplet size) is shown in Figure 6.4. In order to ensure that the aerosol droplets are dried into particles before entering the reaction zone, somewhat higher temperatures should be selected. In this way, the larger droplets are evaporated before entering the reaction zone, preventing very fast rates of uncontrollable evaporation of these droplets in the reaction zone with elevated temperatures. For experimentally determining the effects of different evaporation temperatures on the final AuNP sizes and morphologies, a few of them were selected, as shown in Tables from Table 6.1 to Table 6.6.

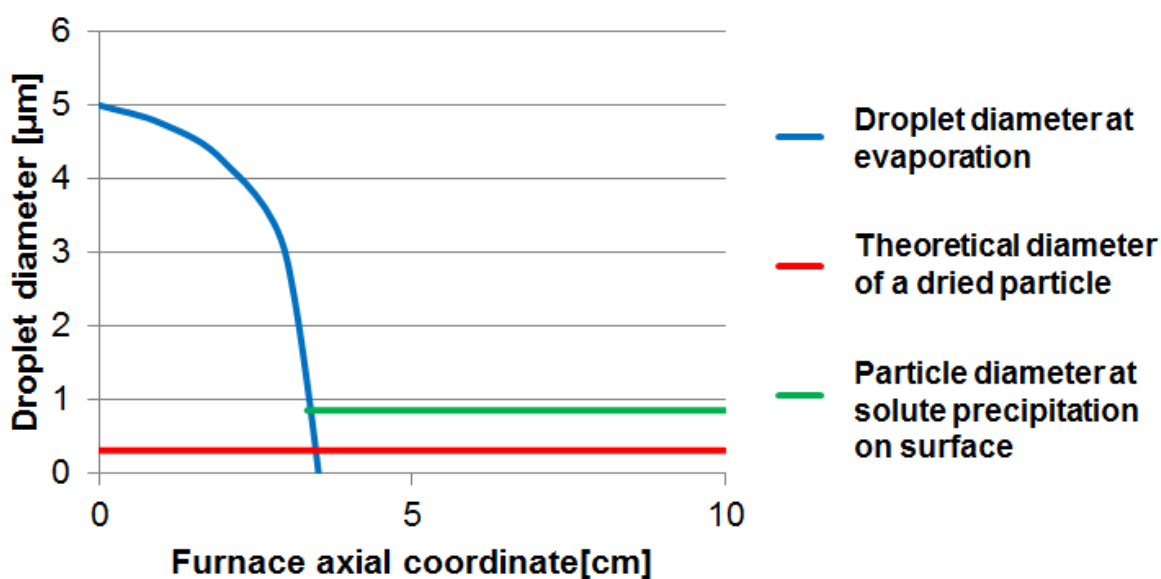


Figure 6.4: Calculated droplet size during evaporation. Initial droplet size 5 μm , Au concentration 2.5 g/l, evaporation zone temperature 100°C, gas flow 1.5 l/min N_2 , density of droplets in the evaporation zone 1000 droplets/ cm^3

6.1.4 Reaction zone temperature

Temperatures above the decomposition temperature of HAuCl_4 (258°C) should be selected for the reaction zone. When a temperature of 260°C is selected, the residence time – the amount of time the particles are in the reaction zone, where the temperature reaches 258°C, is very short because of the gas flow (from 0.60 to 0.23 s for gas flows of both N_2 and H_2 from 2.5 to 6.5 l/min). For this reason, somewhat higher temperatures should be selected, so that

the particles can be reacted and that no un-reacted particles exit the second furnace. When using high temperatures (up to 500°C) in conventional USP, more agglomeration was observed in the synthesized nanoparticles. To avoid this, the temperatures should be kept somewhat lower. As such, the optimal reaction temperatures are between 300 and 400°C. This allows for the reactions to be carried out completely, while it is still low enough to avoid unwanted agglomeration.

Since the temperature inside the tubes depends on the gas flow, a number of temperature measurements were performed to ensure the best possible conditions for particle formation (Figure 6.5). The temperatures measured were from 50 to 100°C for the first furnace and from 250 to 400°C for the second furnace. At very low temperature settings (50°C) for the first furnace, more condensation was observed in the tubes, which resulted in aerosol droplet loss with synthesis. To avoid needless condensation, the temperature at which the condensation at the first furnace exit was not observed was selected for synthesis experiments. Condensation of aerosol droplets reduces the nanoparticle output.

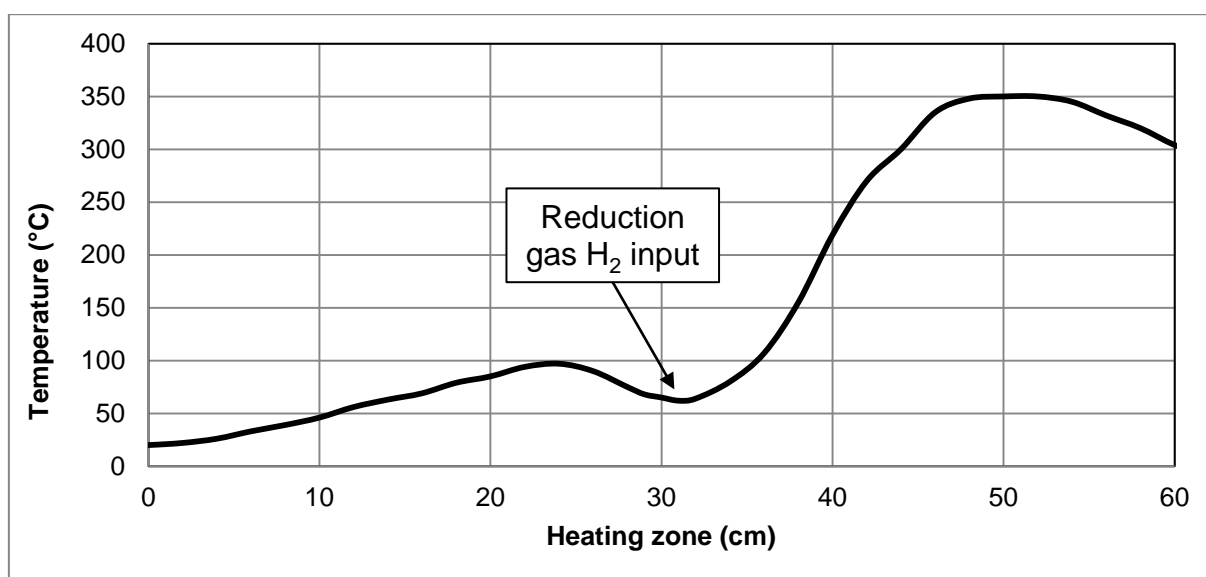


Figure 6.5: Temperature profile of the heating zone in the modified USP, evaporation zone temperature: 100°C, reaction zone temperature: 350°C, gas flow: 1.5 l/min N₂ + 1.0 l/min H₂

6.1.5 Gas flow

The gas flow was selected from previous experience with the use of an aerosol generator with an ultrasound frequency of 2.5 MHz. It was observed, that a gas flow of 1.5 l/min of the carrier gas N₂ allowed for an optimal transport of the generated aerosol droplets into the furnaces. When using lower gas flows, the aerosol mist was not transported into the tubes fast

enough, lowering the effectiveness of the aerosol generator, as the droplets re-dissolved into the precursor solution in the generator chamber. This also meant longer synthesis times for the synthesis of reasonable AuNP quantities. When using higher carrier gas flows, the aerosol mist was transported rapidly into the tubes, raising the effectiveness of the aerosol generator. The gas flow for the reduction gas H_2 was selected in relation to the carrier gas flow. There should always be enough of the reduction gas present in the system, to allow for reactions of the particles. When raising the carrier gas flow in the experiments, the reduction gas flow was raised accordingly. The used gas flows are presented in Tables from Table 6.1 to Table 6.6.

6.1.6 Collection medium

When synthesizing AuNPs with USP, a side product of the chemical reactions is Hydrochloric Acid HCl, in gaseous form. When the gas flow reaches the collection bottles, the HCl (a polar compound) redissolves in the polar medium, lowering the pH value of the medium. The synthesized AuNPs have a negative surface charge and are considered to be relatively stable in low pH mediums. However, using DI water or alcohol for collection, small particles were visible at the bottom of the collection bottles during and after synthesis. The presence of visible particles indicated agglomeration of the AuNPs. In order to prevent agglomeration of the collected AuNPs, some stabilizing compounds were selected from literature, and their influence was observed. The most widely used stabilizing agents are listed in Chapter 2.3. For our experiments, these collection mediums were used: DI water, DI water with trisodium citrate and DI water with PEG (with a molecular weight of 6000 g/mol).

6.1.7 Summary of selected parameters

By setting up a modified USP device with a separate evaporation stage, the influence of different conditions needed to be analysed (Au concentration in precursor solution, gas flow, temperatures) on AuNP synthesis and the changes in their sizes and shapes. Previous USP models of prediction of dried particle formation, Au nuclei formation and growth to final AuNP do not predict the synthesis of different sizes and shapes. A new model of AuNP prediction with USP synthesis was derived from a study of the influential parameters during synthesis, in connection with characterization of the synthesized Au nanoparticles. During characterization we examined the sizes, shapes, microstructure, chemical composition, level of agglomeration and the concentration of the synthesized AuNPs. From these, the influence of synthesis parameters on the formation and growth of AuNPs with USP were explained and we identified the optimal parameters.

For determining the effects of different parameters on AuNP sizes and shapes, the following experimental scheme was used:

Table 6.1: Experiments performed with the modified USP, variable parameter: Au concentration in precursor solution

Experiment⁵	Conc. of Au in precursor solution	Temperature 1 (evaporation zone)	Temperature 2 (reaction zone)	Gas flow	Collection medium
MAu1	0.5 g/l	100°C	300°C	1.5 l/min N ₂ , 1.0 l/min H ₂	DI water
MAu2	1.25 g/l	100°C	300°C	1.5 l/min N ₂ , 1.0 l/min H ₂	DI water
MAu3	2.5 g/l	100°C	300°C	1.5 l/min N ₂ , 1.0 l/min H ₂	DI water
MAu4	5 g/l	100°C	300°C	1.5 l/min N ₂ , 1.0 l/min H ₂	DI water

Table 6.2: Experiments performed with the modified USP, variable parameter: Temperature 1 (evaporation zone)

Experiment	Conc. of Au	Temp. 1	Temp. 2	Gas flow	Col. medium
MAu5	2.5 g/l	50°C	350°C	1.5 l/min N ₂ , 1.0 l/min H ₂	DI water
MAu6	2.5 g/l	75°C	350°C	1.5 l/min N ₂ , 1.0 l/min H ₂	DI water
MAu7	2.5 g/l	100°C	350°C	1.5 l/min N ₂ , 1.0 l/min H ₂	DI water

Table 6.3: Experiments performed with the modified USP, variable parameter: Temperature 2 (reaction zone)

Experiment	Conc. of Au	Temp. 1	Temp. 2	Gas flow	Col. medium
MAu3	2.5 g/l	100°C	300°C	1.5 l/min N ₂ , 1.0 l/min H ₂	DI water
MAu7	2.5 g/l	100°C	350°C	1.5 l/min N ₂ , 1.0 l/min H ₂	DI water
MAu8	2.5 g/l	100°C	400°C	1.5 l/min N ₂ , 1.0 l/min H ₂	0,1% NaCitrate

⁵ Experiments performed with the modified USP were designated MAu(x), where (x) denotes the number of experiment

Table 6.4: Experiments performed with the modified USP, variable parameter: Au concentration in precursor solution and Temperature 1 (evaporation zone) – values for optimal evaporation, obtained from calculations

Experiment	Conc. of Au	Temp. 1	Temp. 2	Gas flow	Col. medium
MAu6	2.5 g/l	75°C	350°C	1.5 l/min N ₂ , 1.0 l/min H ₂	DI water
MAu9	1.25 g/l	80°C	350°C	1.5 l/min N ₂ , 1.0 l/min H ₂	DI water
MAu10	0.5 g/l	85°C	350°C	1.5 l/min N ₂ , 1.0 l/min H ₂	DI water

Table 6.5: Experiments performed with the modified USP, variable parameter: Collection medium

Experiment	Conc. of Au	Temp. 1	Temp. 2	Gas flow	Col. medium
MAu11	2.5 g/l	100°C	300°C	1.5 l/min N ₂ , 1.0 l/min H ₂	DI water
MAu12	2.5 g/l	100°C	300°C	1.5 l/min N ₂ , 1.0 l/min H ₂	0.1% PEG
MAu8	2.5 g/l	100°C	400°C	1.5 l/min N ₂ , 1.0 l/min H ₂	0,1% NaCitrate

Table 6.6: Experiments performed with the modified USP, variable parameter: Gas flow

Experiment	Conc. of Au	Temp. 1	Temp. 2	Gas flow	Col. medium
MAu8	2.5 g/l	100°C	400°C	1.5 l/min N ₂ , 1.0 l/min H ₂	0,1% NaCitrate
MAu13	2.5 g/l	100°C	400°C	3.0 l/min N ₂ , 1.5 l/min H ₂	0,1% NaCitrate
MAu14	2.5 g/l	100°C	400°C	4.5 l/min N ₂ , 2.0 l/min H ₂	0,1% NaCitrate
MAu15	0.5 g/l	100°C	400°C	1.5 l/min N ₂ , 1.0 l/min H ₂	0,1% NaCitrate
MAu16	0.5 g/l	100°C	400°C	3.0 l/min N ₂ , 1.5 l/min H ₂	0,1% NaCitrate
MAu17	0.5 g/l	100°C	400°C	4.5 l/min N ₂ , 2.0 l/min H ₂	0,1% NaCitrate

6.2 Characterization of AuNPs

6.2.1 TEM

Conventional Transmission Electron Microscopy (CTEM; JEOL 2100), High-Resolution Transmission Electron Microscopy (HRTEM; JEOL 2100), Electron Diffraction (ED/TEM; JEOL 2100) and Energy Dispersive Spectroscopy (EDS/TEM; JED-2300) investigations were conducted on the prepared AuNPs. A drop of colloidal suspension of AuNPs was pipetted onto a formvar film coated with a layer of carbon or a lacey formvar film enforced by a heavy coating of carbon TEM copper grid of 200 mesh and dried at room temperature. The grid was then observed directly in a TEM once the medium had evaporated.

The AuNPs` size distributions were measured from 10-15 TEM micrographs of each sample. Measurement of sizes and shape determination were done with ImageJ software [88]. The number of nanoparticles for size measurements ranged from 10 to 600 nanoparticles for each particle size distribution. A few TEM micrographs were selected for sample representation purposes. Measurements were performed following the measurement protocols in [89]. Size distributions have been quoted as the mean nanoparticle diameter \pm the Standard Deviation. Two means are quoted in samples where bimodal distributions were found.

6.2.2 DLS, zeta potential and ICP-OES

DLS size measurements and zeta potential measurements (Malvern ZetaSizer Nano ZS) were performed on some samples, for comparison with manually measured sizes from TEM micrographs and stability examination of the synthesized AuNPs. Only a few selected synthesized AuNPs were measured, because DLS measurements give the hydrodynamic diameter of AuNPs and thus, the results are only accurate if the particles are spherical [90]. 1 ml of AuNP suspensions was pipetted into the measurement dip cell, the measurement parameters were: Material properties: Absorption – 0.010, refractive index – 1.59, dispersant properties – water, temperature – 25°C, measurement angle: 173° back scatter.

Optical Emission Spectrometry with Inductively Coupled Plasma (ICP-OES; Agilent 720) investigations were conducted on the samples prepared for determining the concentrations of synthesized AuNPs.

7 RESULTS AND DISCUSSION

7.1 AuNPs obtained with conventional USP

The effects of temperature and Au concentration in the precursor solution were examined after AuNP synthesis with the parameters from Table 5.1 and Table 5.2. Some smaller nanoparticles were spherical in shape, others were also hexagonal and of irregular polygonal shapes. The average sizes of the smaller AuNPs ranged from 20 nm to about 70 nm. The presence of bigger particles was also confirmed, in the range of about a couple of hundred nanometers. The chemical composition of the obtained nanoparticles was checked by EDS and scanning TEM analyses.

Particles of round, triangular and irregular shapes were obtained at a temperature of 260°C and an ultrasonic frequency of 0,8 MHz. Particles of similar morphology were reported with the synthesis of silver nanoparticles at 300°C, with silver nitrate as the precursor [83]. Increasing the temperature to 280°C resulted in the presence of cylindrical particles (Figure 7.1). At this temperature there also seemed to be more rounded particles than at 260°C.

EDS analyses showed the presence of impurities in the AuNPs. Traces of Co, Cr, Fe, Si, Ni and Ca were analysed, in amounts of up to 1.5 mass% each. This indicated that the USP process needed to be improved also in relation to obtaining higher purity. It was also observed, that the impurities of Co, Cr and Fe came from unwanted reactions of some USP construction elements with the precursor solution with the dissolved HAuCl_4 . In order to obtain high purity, the USP device should be positioned in a clean environment and set up with construction elements that do not react with the precursor (Teflon and quartz glass). Special cleaning protocols should also be used on the device to remove any impurities with acids (HNO_3 and HCl) from the USP construction elements, before experiments are performed to ensure the synthesis of AuNPs with the highest possible purity. This presents a technological improvement, which was also implemented in experiments with the modified USP.

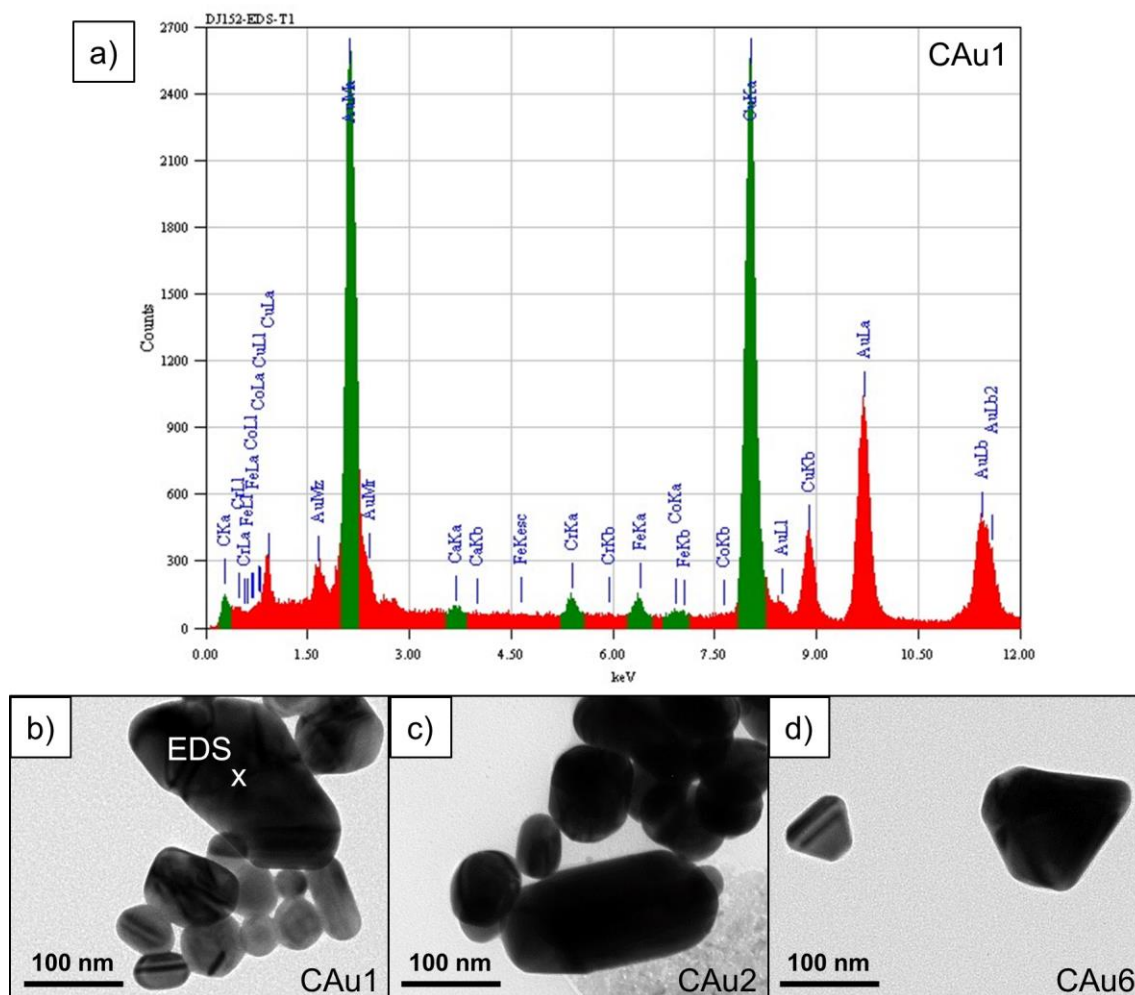


Figure 7.1: a) EDS analysis of AuNPs obtained with conventional USP; b) TEM image of spherical and irregular AuNPs at synthesis temperatures from 260°C-500°C; c) Presence of cylindrical AuNPs at synthesis temperatures from 280°C-500°C; d) Presence of triangular AuNPs at synthesis temperatures of 260°C. The C and Cu content in the EDS analyses comes from the TEM formvar grid, on which the AuNPs were examined

Triangular, rounded and particles of irregular shape suggest that ideally spherical AuNPs are more difficult to synthesize with USP in comparison to some other metallic nanoparticles (silver, nickel) [91], [92]. The experiments have shown the different particle shapes obtained by increasing the reaction temperature up to 500°C, with a constant ultrasound frequency (Figure 7.2). An increase in AuNP agglomeration was also observed with the use of higher temperatures.

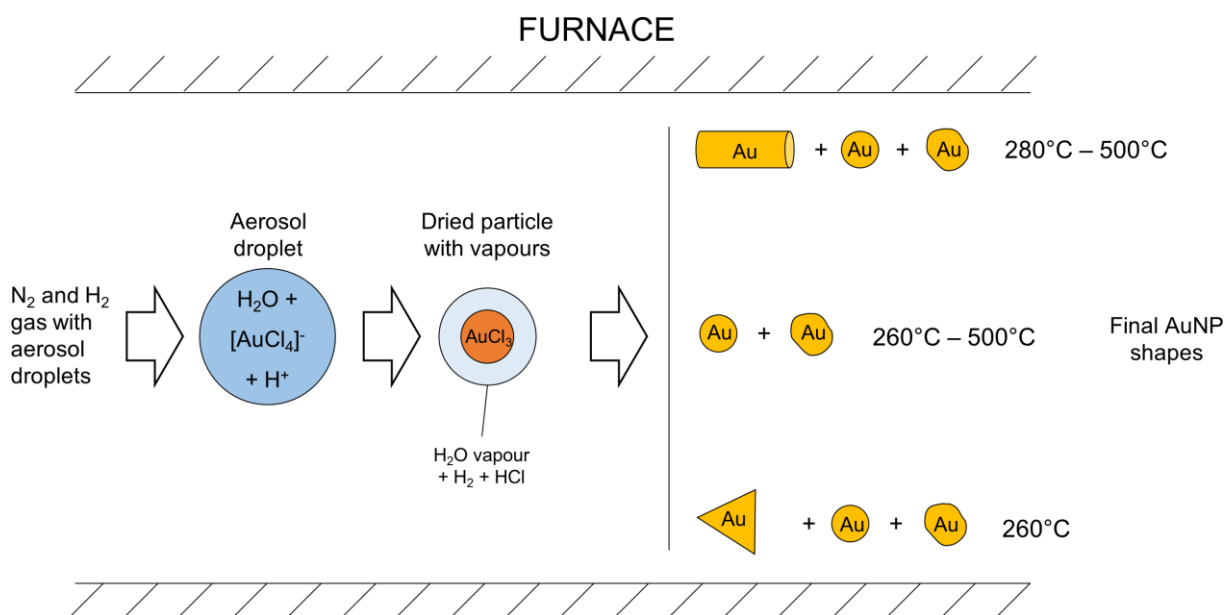


Figure 7.2: Different shapes of AuNPs obtained at different temperatures (spherical, irregular, cylindrical, triangular)

There was a difference between the theoretically calculated and experimentally obtained sizes of AuNPs (Table 7.1). The obtained nanoparticles had a mixture of different morphologies, which was not taken into account in the theoretical calculations. The aerosol droplets were also generated in a size distribution, rather than a single droplet size. The coalescence of aerosol droplets was also not considered, which is difficult to prevent, as the gas flows in an enclosed system, where turbulence effects are to be expected. The microporosity of the nanoparticles was also not seen after synthesis, the result of which perhaps would have been an even greater discrepancy between the experimental and theoretical values. However, we obtained not only spherical shapes as in the synthesis of other metallic nanoparticles (Co, NiTi, Ni and Cu) [84], [92], [93], but also rods and discs with different optical properties. Preparing ideal shapes in this manner is difficult by only changing the synthesis parameters in the conventional USP. With the conventional USP, the synthesis stages occur simultaneously, which are then difficult to control due to the very fast kinetics of thermal decomposition and hydrogen reduction. The aerosol size distribution, collisions, fast particle formation and growth of AuNPs further increased the difficulty of preparing one ideal shape of AuNPs (Figure 7.3). Measuring sizes of a mixture of AuNP shapes also presents difficulties, meaning only a general average size with SD can be declared. For this purpose, the system has to be modified or redesigned, allowing for better control over the synthesis stages.

Table 7.1: Experimentally measured mean AuNP sized compared to theoretically calculated values

Ultrasonic frequency 0,8 MHz, precursor concentration 2.5 g/l	
Experimentally obtained	Theoretically calculated
125 ± 45 nm	190 nm
Ultrasonic frequency 2,5 MHz, precursor concentration 2.5 g/l	
Experimentally obtained	Theoretically calculated
135 ± 80 nm	90 nm

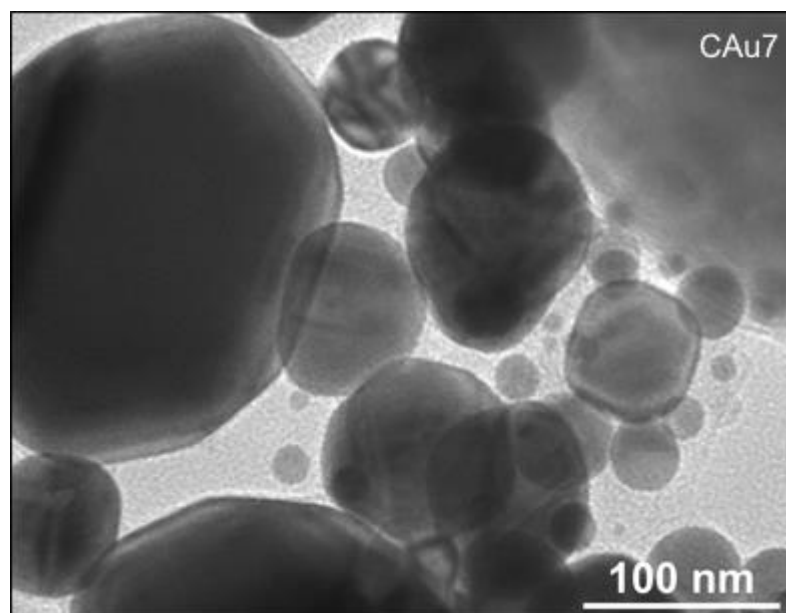


Figure 7.3: TEM image of AuNPs (CAu7, from Table 5.2)

7.1.1 AuNPs appearing in the ultrasonic generator chamber

While the aerosol was produced, an unexpected formation of AuNPs took place in the ultrasonic generator. These particles were round and agglomerated. The AuNPs were collected by filtration and were analysed with TEM and EDS (Figure 7.4).

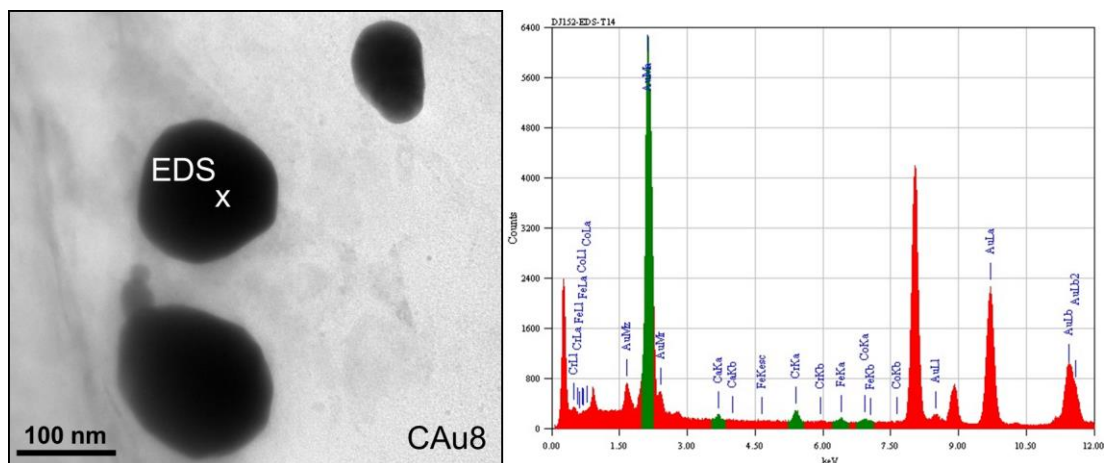


Figure 7.4: TEM picture of AuNPs obtained in the ultrasonic generator with accompanying EDS

The formation of AuNPs occurs at relatively low temperatures (theoretically, decomposition of HAuCl_4 begins at 258°C [73]). This means that the conditions of aerosol formation by ultrasound and the presence of the reduction gas hydrogen inside the generator can allow AuNPs to start forming inside the generator (Figure 7.4). This perhaps introduces the possibility of AuNPs' formation at room temperature. However, this also means the gold chloride is being used up from the solution to form AuNPs, effectively lowering the Au concentration in the solution, from which the aerosol droplets are generated. Control of AuNP formation with USP is, thus, hindered further, as we then have an inconsistent Au concentration in the precursor solution, making the sizes and forms of the AuNPs unpredictable. We can postulate, that these AuNPs only appear in the presence of the reduction gas hydrogen and, as such, a modification is also needed to remove the presence of hydrogen from the ultrasound generator chamber. This will prevent formation of AuNPs in this part of the USP and improve control over the AuNP synthesis.

The conventional USP was proven to be able produce AuNPs, but with several issues that needed to be addressed in order to be able to synthesize AuNPs with desired forms, such as 50 nm spherical AuNPs in a narrow size distribution. We have synthesized AuNPs in a size distribution from 10 to 300 nm, with different shapes, from spherical, irregular, triangular and cylindrical [18], [94]. Such a mixture of nanoparticles is hard to use in further stabilization and functionalization. In addition, the formation of AuNPs in the ultrasonic generator, means there is little control over the synthesis, and a modification of the process needs to be carried out in order to achieve the desired results. This was the starting point for the required improvements in the USP technology, in order to synthesize more uniform sizes and shapes of AuNPs.

7.2 AuNPs obtained with modified USP

7.2.1 Influence of Au concentration in precursor solution

In previous experiments of AuNP synthesis with conventional USP, nanoparticles of different shapes were obtained (spherical, irregular, triangular and cylindrical). In comparison, separating the evaporation stage from the reaction and densification stages has yielded mostly non-ideally spherical nanoparticles with some irregularly shaped nanoparticles. Lower concentrations of Au in the precursor have yielded less irregular shapes of AuNPs.

The parameters used for identifying the influence of Au concentration in the precursor solution with the modified USP are shown in Table 6.1. Using a precursor solution with 2,5 g/l Au and an ultrasound frequency of 2,5 MHz, sizes ranging from 15-300 nm have been obtained (Figure 7.5). It seems there is less agglomeration present when AuNPs are synthesized with a separate evaporation zone.

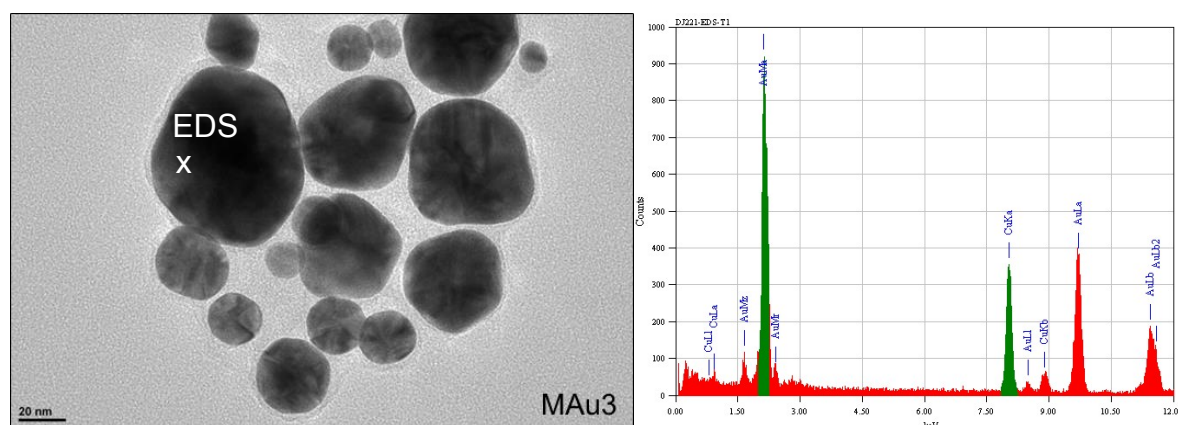


Figure 7.5: TEM picture and EDS of AuNPs obtained with the modified USP with a separate evaporation zone, Au concentration in precursor solution: 2,5 g/l

The sizes of the AuNPs are generally accepted to be mainly dependent upon the Au concentration in the precursor and the droplet size. In our experiments, the droplet sizes are considered to be the same in each experiment, while the precursor concentration was changed for each experiment. With an Au concentration of 5 g/l in the precursor solution we have obtained AuNPs in the size range from around 40 nm up to 360 nm. While there are small AuNPs present, the bulk of the AuNPs have a diameter of about 200 nm. There are also a bigger number of irregularly shaped AuNPs, with less spherical AuNPs present. More agglomeration was also observed when using a high Au concentration in the precursor solution. The separate evaporation zone seemed to be beneficial for the production of more uniformly shaped AuNPs, as the irregularly shaped AuNPs had round edges, even though

they were not spherical. When not using a separate evaporation zone, AuNPs have appeared with sharper edges, in the form of triangles and discs and irregular shapes with sharp edges [18]. Such shapes have not appeared with a separate evaporation zone. A separate evaporation zone is therefore favourable in order to achieve the goal to produce only spherical shapes of AuNPs with USP.

With an Au concentration of 2,5 g/l in the precursor solution, we obtained sizes ranging from 15 to 300 nm. The average size of the AuNPs with such a concentration was 55 nm. The shapes of the AuNPs were still not ideally spherical, as there were still particles with irregular shapes present. However, even though they were not ideally spherical, their shapes appeared to have a high order of sphericity, while the smaller AuNPs were more spherical than the bigger ones.

An Au concentration of 1,25 g/l in the precursor solution has yielded AuNPs in the range from 10 to 170 nm. The bulk of the AuNPs sizes were about 30 nm (Figure 7.6). With a precursor concentration of 0,5 g/l of Au in the precursor solution, the AuNPs sizes obtained were from 10 to 130 nm, with the average size being somewhat smaller, around 15 nm (Figure 7.7).

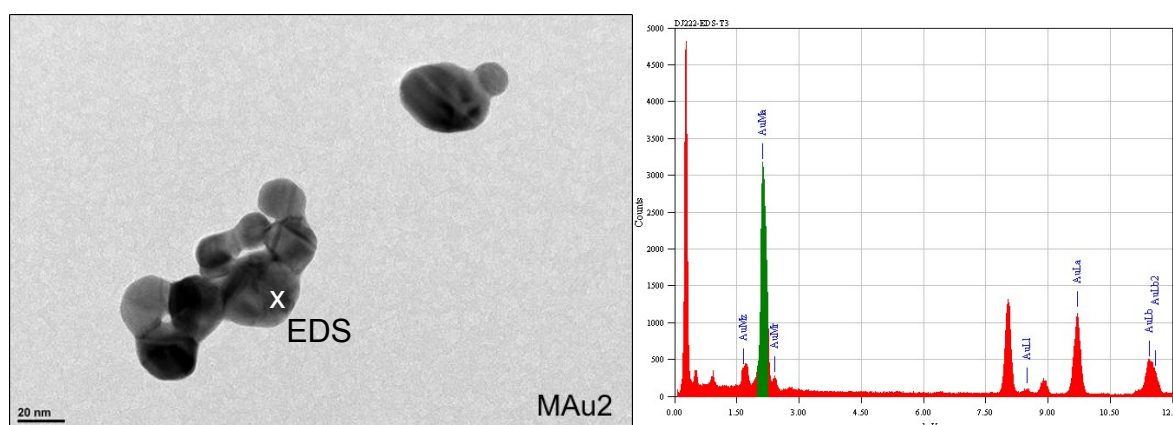


Figure 7.6: TEM picture and EDS of AuNPs obtained with the modified USP with a separate evaporation zone, Au concentration in precursor solution: 1,25 g/l

The shapes of nanoparticles with gold concentrations of 2,5; 1,25 and 0.5 g/l in the precursor solution are very similar. With all three concentrations we obtained a mixture of spherical and irregularly shaped nanoparticles.

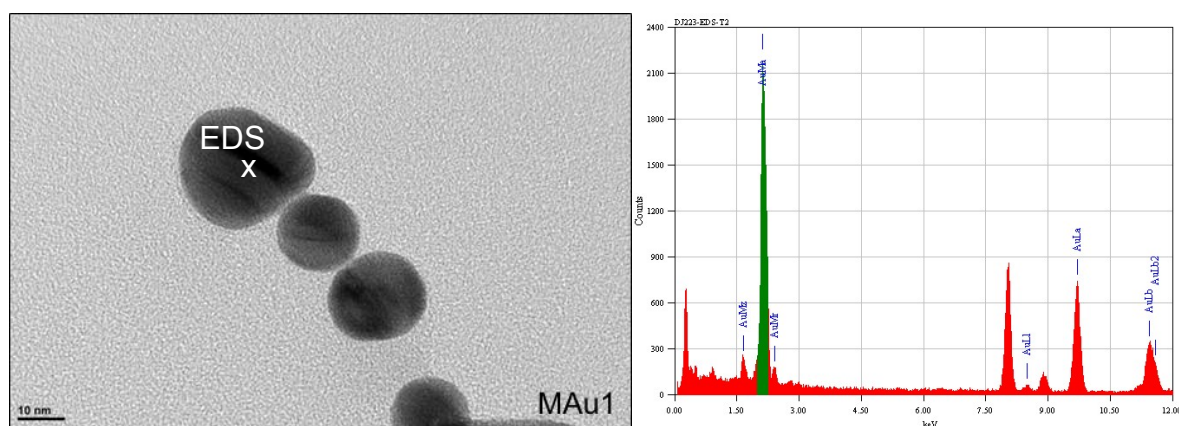


Figure 7.7: TEM picture and EDS of AuNPs obtained with the modified USP with a separate evaporation zone, Au concentration in precursor solution: 0,5 g/l

The separate evaporation zone has yielded better results regarding the uniformity of shapes and sizes with lower Au concentrations (0,5 and 1.25 g/l) in the precursor. Even though the shapes were still not ideally uniform, less diverse shapes were produced while using a separate evaporation zone in the USP process. In this regard, the separated evaporation zone was useful for producing AuNPs of more similar shapes and sizes with USP. This was not apparent when using higher Au concentrations (2,5 and 5 g/l, Figure 7.8). With lower concentrations, solid, spherical shapes were formed more readily also with the conventional USP, and the benefits of a separate evaporation zone were not seen so easily. From a theoretical standpoint, using a low concentration in the precursor solution is effective for producing solid and more uniform nanoparticles with a standard USP process. Even though spherical shapes of AuNPs were formed in our experiments with the modified USP process, irregular shapes were also present.

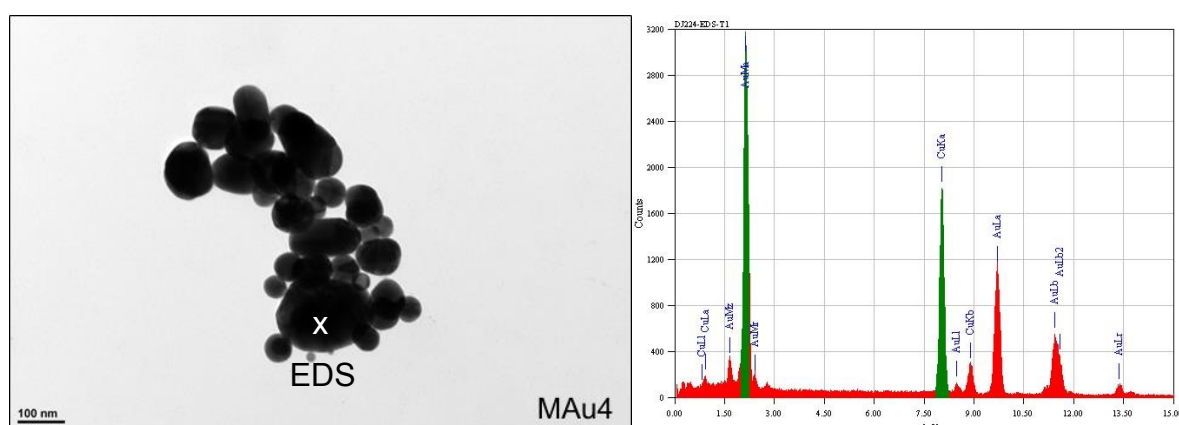


Figure 7.8: TEM picture and EDS of AuNPs obtained with the modified USP with a separate evaporation zone, Au concentration in precursor solution: 5 g/l

As such, it was difficult to determine the effectiveness of a separate evaporation zone when using lower concentrations of Au in the precursor solution. Other synthesis parameters

needed to be changed in order to determine their optimal values for spherical AuNP synthesis. However, from a technological point of view, the separate evaporation zone has eliminated the reactions with hydrogen and particle formation inside the ultrasound generator. The precursor solution remained the same before and after AuNP synthesis, which is a good indicator of this technical issue being resolved, compared to the conventional USP setup, where AuNPs are formed inside the precursor solution in the aerosol generator chamber.

Varying the Au concentration in the precursor solution yielded larger AuNPs for higher concentrations and smaller AuNPs for lower concentrations, which was expected. The effects of the separate evaporation zone on the final AuNP sizes and shapes have been demonstrated. When using lower concentrations of Au in the precursor solution, the experiments showed more uniformly shaped AuNPs when using the modified USP with a separate evaporation zone, compared to the conventional USP setup. When using higher Au concentrations in the precursor solution, similar advantages are not as apparent as the shapes of the synthesized AuNPs are not as uniform. As the separate evaporation zone has not removed the presence of irregularly shaped AuNPs entirely, it is apparent that the modification has improved the process, in accordance with producing more AuNPs of spherical shapes.

7.2.2 Influence of evaporation zone temperature

The experiments shown in Table 6.2 were carried out for determining the shapes of AuNPs when using different evaporation zone temperatures. From Figure 7.9 it can be seen, that the best sphericity of AuNPs with given parameters was obtained with an evaporation zone temperature of 75°C. With 50°C, somewhat less ideal AuNPs were synthesized than with 75°C. With 100°C, the shapes of AuNPs had more sharper edges and were even more irregular than with 50 and 75°C. Evaporation of droplet and diffusion of solute inside the droplet depends on a number of factors (temperature, gas flow, number of droplets, pressure), while for the final AuNP shapes, the temperature of reactions also needs to be taken into account. For the given set of experiments in Table 6.2, the constant parameters were gas flows of 1.5 l/min N₂ and 1.0 l/min H₂ with a reaction temperature of 350°C. For these parameters, an evaporation temperature of 75°C yielded the most spherical AuNPs, while in other experiments, this was not the case. The results of these experiments suggest, that the parameter selection is very interdependent, meaning all of them have to be taken into account at the same time to produce favourable results. As such, the optimal values of parameters for AuNP synthesis have to be selected on a case-by-case basis, for desired final AuNP sizes and shapes.

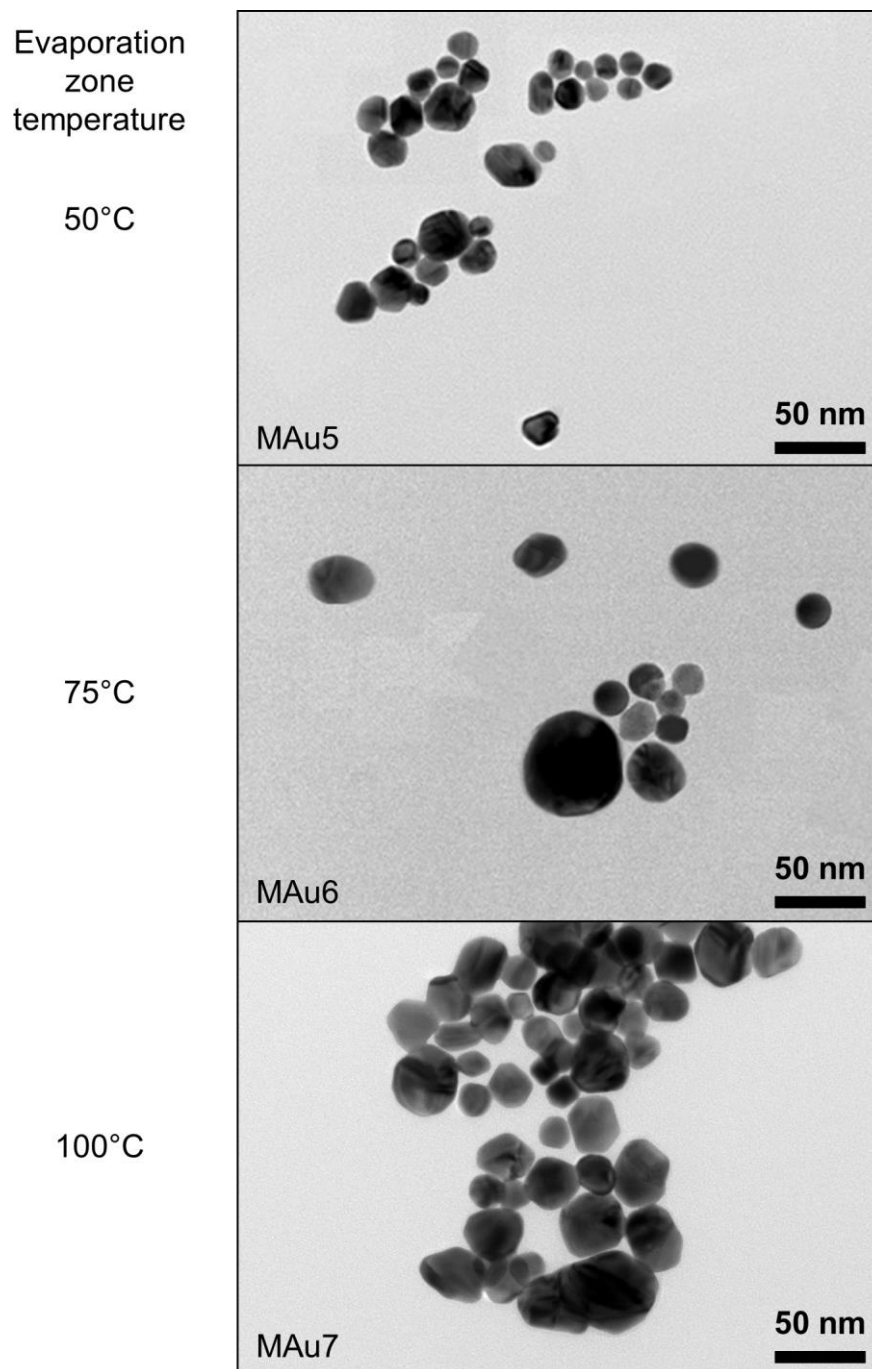


Figure 7.9: Comparison of synthesized AuNPs shapes with increasing evaporation zone temperatures

7.2.3 Influence of reaction zone temperature

Table 6.3 shows the parameters used for determining the reaction zone temperature effects. The thermal decomposition and hydrogen reduction temperatures were exceeded in the experiments, ensuring no unreacted particles were left the reaction zone to be collected in the collection bottles. Figure 7.10 shows the comparison of the agglomeration degree of the synthesized AuNPs, when using 300, 350 and 400°C. As the Au concentration used were the same, no significant nanoparticle size differences were observed, the sizes ranged from 10 to 300 nm. The shapes seemed to deteriorate from spherical to irregular shapes when using increasingly higher temperatures. The reason for this could be changes in chemical reaction rates, collisions and coagulations of the particles due to the higher temperature and influence of the higher temperature on the evaporation zone. The higher temperature in the reaction zone changed the temperature in the evaporation zone somewhat by raising it in the last third of the evaporation zone.

It can be seen that the agglomeration increased by a small degree when using higher temperatures for reactions. This was expected and is in agreement with previous experiments with the conventional USP. When synthesizing AuNPs, an optimal temperature should be used, where favourable conditions for reactions are met (preventing unreacted particles) and agglomeration is kept to a minimum. When using higher gas flows, the optimal temperature increases. Before synthesis is carried out, temperature measurements should be done for the given synthesis parameters, in order to choose the optimal temperatures for both the evaporation and reaction zones.

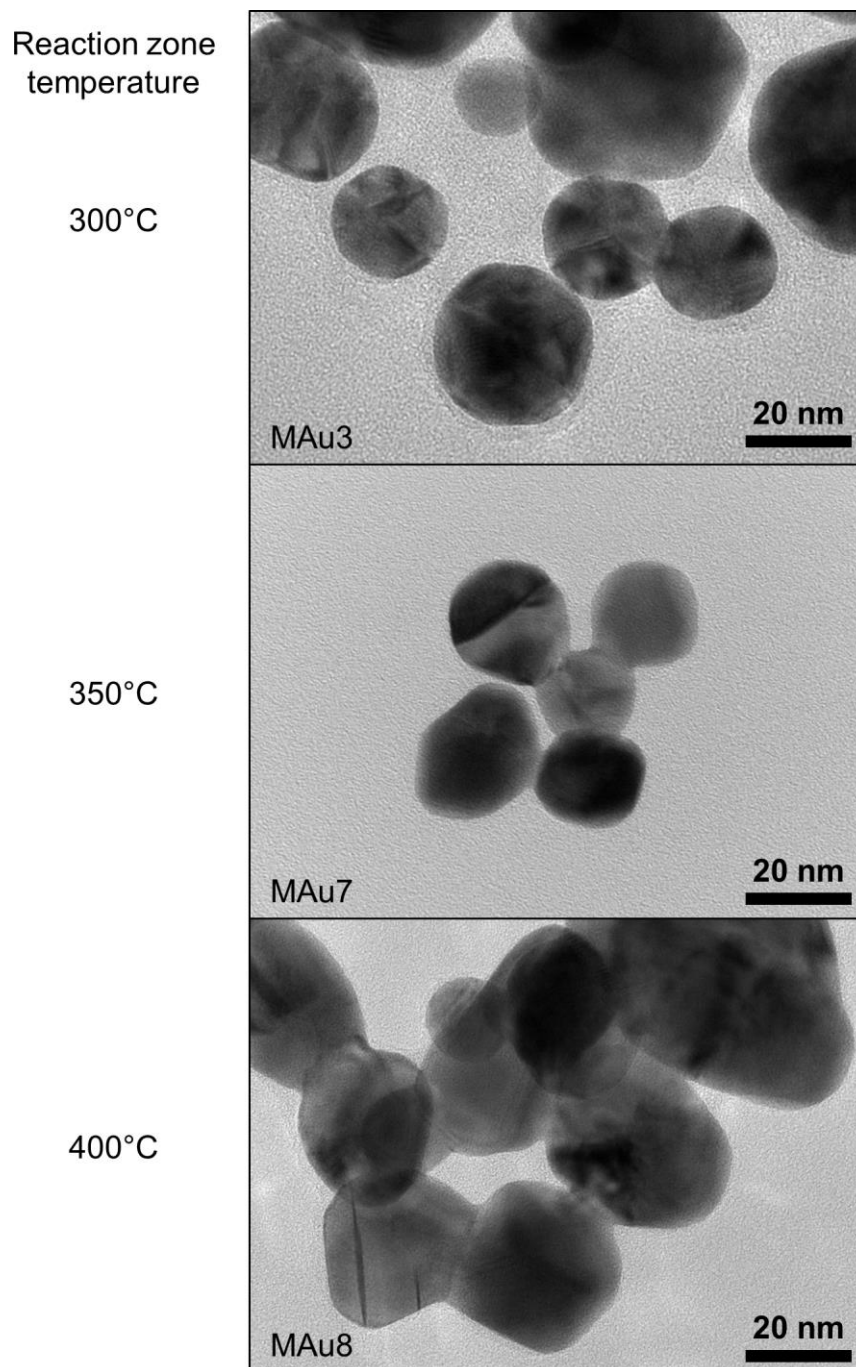


Figure 7.10: Comparison of synthesized AuNPs agglomeration degree with increasing reaction zone temperatures

7.2.4 Influence of Au concentration in precursor solution and temperature of evaporation zone – evaporation parameters obtained from calculations

The calculations for evaporation of solution droplet presented in Chapter 4.4.2 were used for calculating the evaporation for synthesis in the modified USP device at the IME Institute of Recycling and Processes at RWTH University in Aachen (Germany). The resulting chosen parameters are presented in Table 6.4. The geometries of the device: Transport tube diameter of 20 mm, two tube furnaces both 28 cm in length. The precursor solution Au concentrations were selected to be 2.5, 1.25 and 0.5 g/l. The calculation of temperature for evaporation was based on the droplet of the starting solution, of a diameter of 10 μm . The droplet evaporation was to be finished at the end of the evaporation zone (28 cm, residence time of 3.5 seconds with gas flow of 1.5 l/min N_2). The diffusion of solute into the droplet centre therefore has the highest amount of time for evaporation in the given system, which favours the formation of spherical AuNPs. It was calculated that evaporation of droplets and super saturation of gold chloride was favourable for solid spherical AuNP synthesis with evaporation temperatures of 75, 80 and 85°C for Au concentrations in precursor solutions of 2.5, 1.25 and 0.5 g/l, respectively. The temperature of the first heating zone was varied in the experiments, while the second heating zone remained constant (350°C). The final AuNP properties were thus determined by the temperatures in the first heating zone and starting concentrations of Au in the precursor solution.

It was observed from TEM measurements, that the obtained AuNPs in the experiments had a bimodal size distribution (Figure 7.11 and Figure 7.12). Namely, the AuNPs obtained with 2.5 g/l Au had a number size distribution with 38.5 ± 24.5 nm (14-63 nm, 71% of the total AuNP number) and 211 ± 91 nm (120-302 nm, 29% of the total AuNP number) (Figure 7.11).

With 1.25 g/l Au, the sizes were 11 ± 7 nm (4-18 nm, 81% of the total AuNP number) and 115 ± 65 nm (50-180 nm, 19% of the total AuNP number) (Figure 7.12). With 0.5 g/l Au, a bimodal distribution was not as apparent, as there was no clear gap between the smaller and larger nanoparticle size group (Figure 7.13), sizes of 66.5 ± 53.5 nm (13-120 nm) were obtained. Previously, we had obtained spherical and irregular nanoparticles within a certain size range. The larger, somewhat irregular nanoparticles obtained in the experiments were accompanied by much smaller particles with spherical morphologies (Figure 7.11, Figure 7.12 and Figure 7.13).

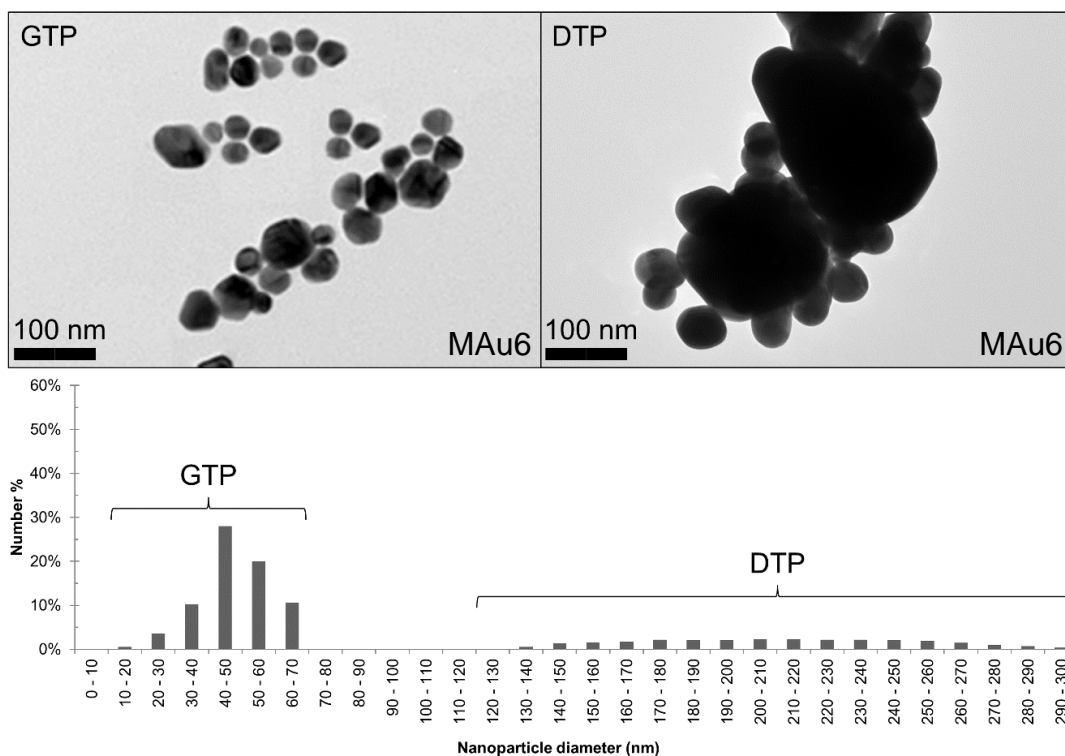


Figure 7.11: Bimodal size distribution of AuNPs obtained with 2.5 g/l Au concentration, experiment MAu6

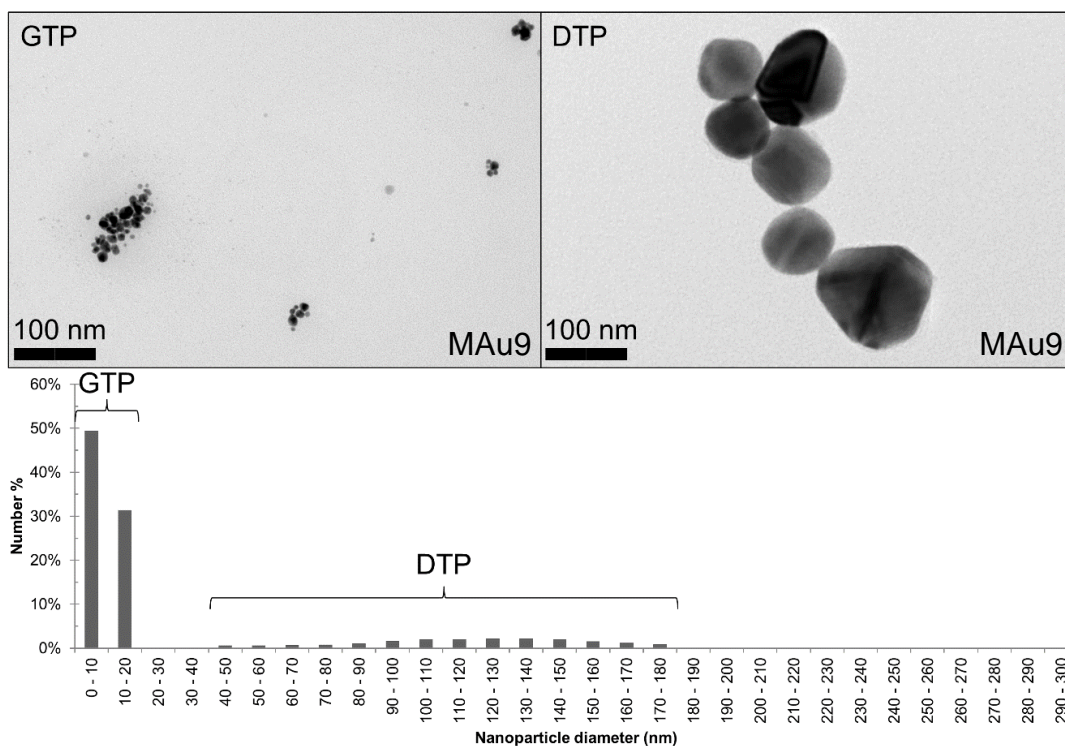


Figure 7.12: Bimodal size distribution of AuNPs obtained with 1.25 g/l Au concentration, experiment MAu9

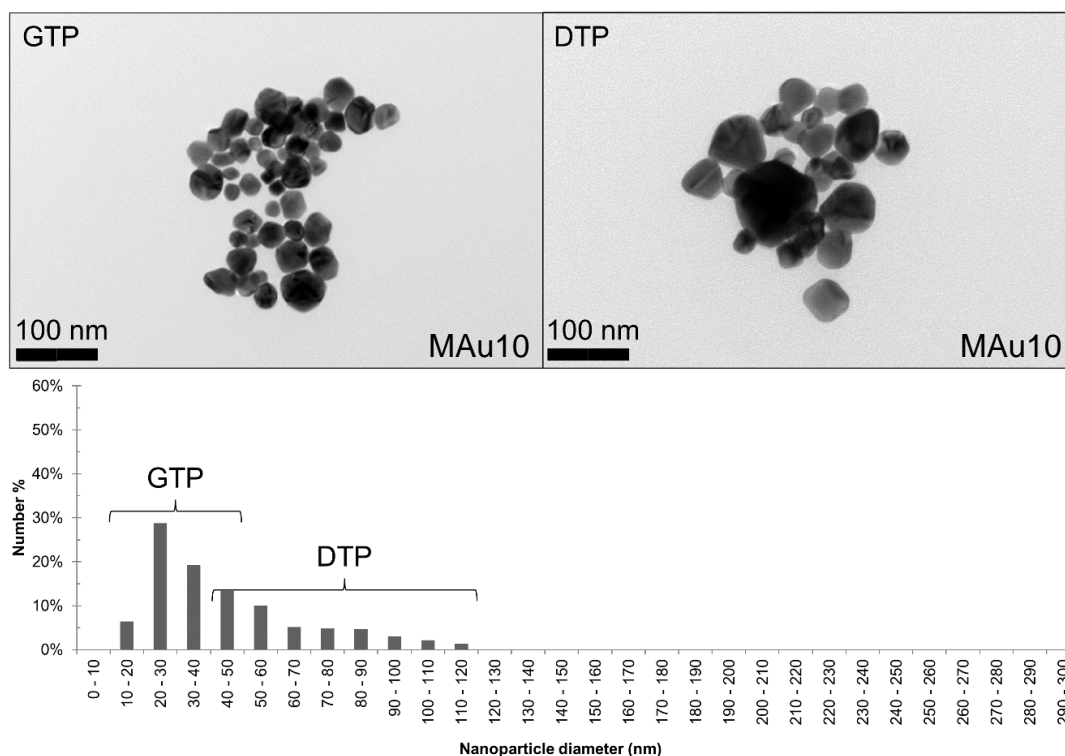


Figure 7.13: Size distribution of AuNPs obtained with 0.5 g/l Au concentration, experiment MAu10

AuNP formation mechanisms

The obtained bimodal particle size distribution was most probably caused by a combination of the DTP and GTP mechanisms. This combination of mechanisms makes controlling the synthesized AuNP sizes and morphologies more difficult. To determine which mechanism (DTP or GTP) used more Au content from the precursor solution in order to produce AuNPs we have compared the volume of AuNPs of smaller sizes versus the volume of larger AuNP sizes. The number size distributions showed a greater number of smaller AuNPs (from 71% to 81% of the total AuNPs, for syntheses with 2.5 and 1.25 g/l Au) than in the volume size distributions in Figure 7.14. In the volume size distributions, a lesser percentage of the smaller AuNPs for 2.5 g/l Au (3.6% of the total volume for sizes 38.5 ± 24.5 nm) is shown than for the larger AuNPs (96.4% of the total volume for sizes 211 ± 91 nm). A lesser percentage of the smaller AuNPs was apparent for 1.25 g/l Au (7.6% of the total volume for sizes from 11 ± 7 nm) and a much greater percentage for the larger AuNPs (92.4% of the total volume for sizes from 115 ± 65 nm). For 0.5 g/l Au the size distribution was more continuous, and the difference between the smaller and larger size groups was not as apparent, as there is no clear gap between the peaks. However, a greater volume of Au was used up for the larger AuNPs ranging from 40-120 nm (Figure 7.13, 83.9% of the total volume). This probably

occurred since the DTP mechanism is more dominant than the GTP mechanism and a greater volume of the dissolved Au from the precursor is used to generate particles from the droplet, instead of generating the particles from the gas phase.

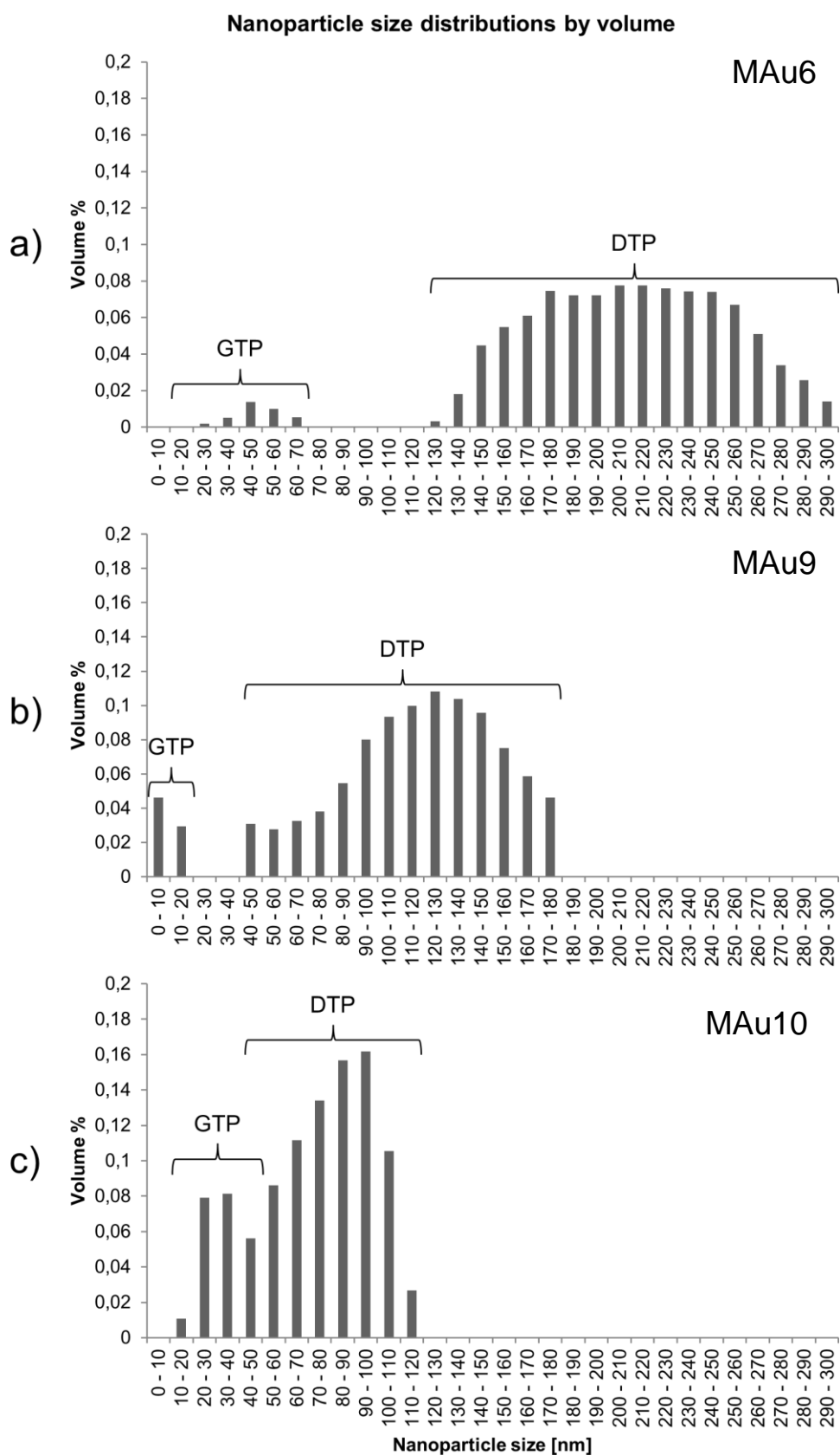


Figure 7.14: AuNP bimodal size distributions by volume, Au concentration in precursor solution: a) MAu6, 2.5 g/l Au; b) MAu9, 1.25 g/l Au; c) MAu10, 0.5 g/l Au

In regard to the formation mechanisms, a higher Au concentration allowed a bigger portion of AuNPs to be formed by the DTP mechanism:

- Conc.: 2.5 g/l Au, 96.4% of the total volume used up for larger AuNPs;
- Conc.: 1.25 g/l Au, 92.4% of the total volume used up for larger AuNPs;
- Conc.: 0.5 g/l Au, 83.9% of the total volume used up for larger AuNPs (from 40 to 120 nm).

The AuNP sizes were bigger for experiments with a higher starting Au precursor solution concentration, which was to be expected. This was apparent for both GTP and DTP mechanisms (Figure 7.11 and Figure 7.12). For 1.25 g/l Au, the smaller AuNPs, produced by GTP, had very small sizes (11 ± 7 nm) in high numbers; this indicated that more seeds were formed from the gas phase, which did not grow into bigger AuNPs due to material depletion. The GTP mechanism presence increased with lower Au precursor concentrations (which was also confirmed by the volume % used up for larger nanoparticles). Due to a more heterogeneous precipitation from the liquid phase during evaporation, more material was then formed into the gas phase and GTP had more influence on the final AuNP sizes.

With 0.5 g/l Au (Figure 7.13) the sizes of the AuNPs, obtained through the GTP mechanism should have been even lower due to the use of the lowest Au precursor solution concentration. However, the AuNPs produced by the GTP mechanism overlapped the ones produced by DTP, and the two size ranges were difficult to distinguish. This suggests that the gas phase from the GTP mechanism had very low vapour pressures and was being used up mainly for growth of the smaller AuNPs, which were produced by DTP.

The occurrence of this combination of formation mechanisms suggests unfavourable conditions for a controlled synthesis of AuNPs. This indicates that during the evaporation in the first heating zone of the synthesis, partially dried droplets of the starting solution were produced. These were then evaporated rapidly in the second heating zone, producing unfavourable results (bimodal size distribution). The use of higher evaporation temperatures produced an unfavourable rapid evaporation of droplets in the length of the given evaporation zone (28 cm).

After the initial precursor solution droplets (HAuCl_4 with water) were created, they were transported inside the first heating zone. In this zone, the water was evaporated, raising the mass fraction of water vapour in the system. When more water vapour was present, the droplets evaporated more slowly. This resulted in droplets not evaporating fully, forming partially dried droplets in the evaporation zone. These partially dried droplets then entered the

second heating zone, where the reactions took place. Inside the reaction zone, the droplets entered an environment of relatively high temperatures, increasing the droplet temperature rapidly. The remaining water then evaporated fast, not giving time for diffusion of the solute into the center of the droplet. This produced a combination of a particle and vapour of gold chloride from the droplet. From this point, there were several further occurrences that formed the final nanoparticles (Figure 7.15):

1. AuNPs formed from a droplet were collected in the washing bottles (DTP mechanism)
2. AuNPs formed from a droplet collided with other AuNPs formed from a droplet, coalescing into large AuNPs, and these larger AuNPs were then collected in the washing bottles (DTP mechanism)
3. AuNPs formed from a droplet collided with vapour, promoting growth, and were then collected in the washing bottles (DTP and GTP mechanisms)
4. Vapour molecules collided with other vapour molecules resulting in the nucleation of a new AuNPs, to be collected in the washing bottles (GTP mechanism)

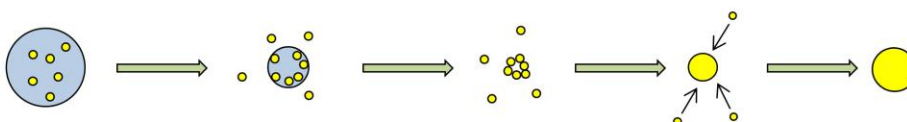
1.) AuNPs formed only by DTP



2.) AuNPs formed by DTP collided with other AuNPs, causing coalescence



3.) AuNPs formed by DTP are grown larger by condensation with vapour formed by GTP mechanism



4.) Vapour molecules formed by GTP saturated to form a nucleus, which is then grown into a new AuNP

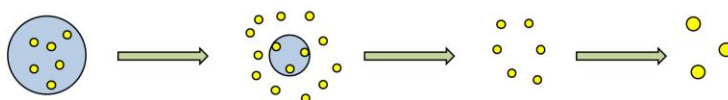


Figure 7.15: AuNP formation modes with a combination of DTP and GTP mechanisms in USP

7.2.5 Influence of gas flow

With changing the gas flows of the AuNP synthesis the bimodal sizes from the two formation mechanisms were investigated further. This time, the evaporation zone was set at a temperature of 100°C, while the reaction zone was set at a temperature of 400°C to ensure conditions for reactions to take place with higher gas flows (and thus lower residence times). The parameters are shown in Table 6.6. To determine the gas effects on the synthesized nanoparticles' sizes, three gas flows were used (low: 1.5 l/min N₂ + 1.0 l/min H₂, medium: 3.0 l/min N₂ + 1.5 l/min H₂ and high: 4.5 l/min N₂ + 2.0 l/min H₂). The residence times are shown in Table 7.2.

Table 7.2: Residence times for aerosol droplets and AuNPs in the modified USP device

Experiment	Gas flow	Evaporation zone residence time (length: 28 cm)	Reaction zone residence time (length: 28 cm)	Total residence time
MAu8, MAu15	Low: 1.5 l/min N ₂ + 1.0 l/min H ₂	3.52 s	2.11 s	5.62 s
MAu13, MAu16	Medium: 3.0 l/min N ₂ + 1.5 l/min H ₂	1.76 s	1.17 s	2.93 s
MAu14, MAu17	High: 4.5 l/min N ₂ + 2.0 l/min H ₂	1.17 s	0.81 s	1.98 s

Although bimodal size distributions of the AuNPs were still present, the number of larger AuNPs was decreased dramatically with the use of higher gas flows in the USP system. Figure 7.16 shows TEM micrographs with visible sizes and morphology of obtained AuNPs. It can be seen, that higher gas flows produced more uniform, spherical shapes of AuNPs, while there were more irregular shapes present when using lower gas flows. AuNP sizes were measured as shown in Table 7.3.

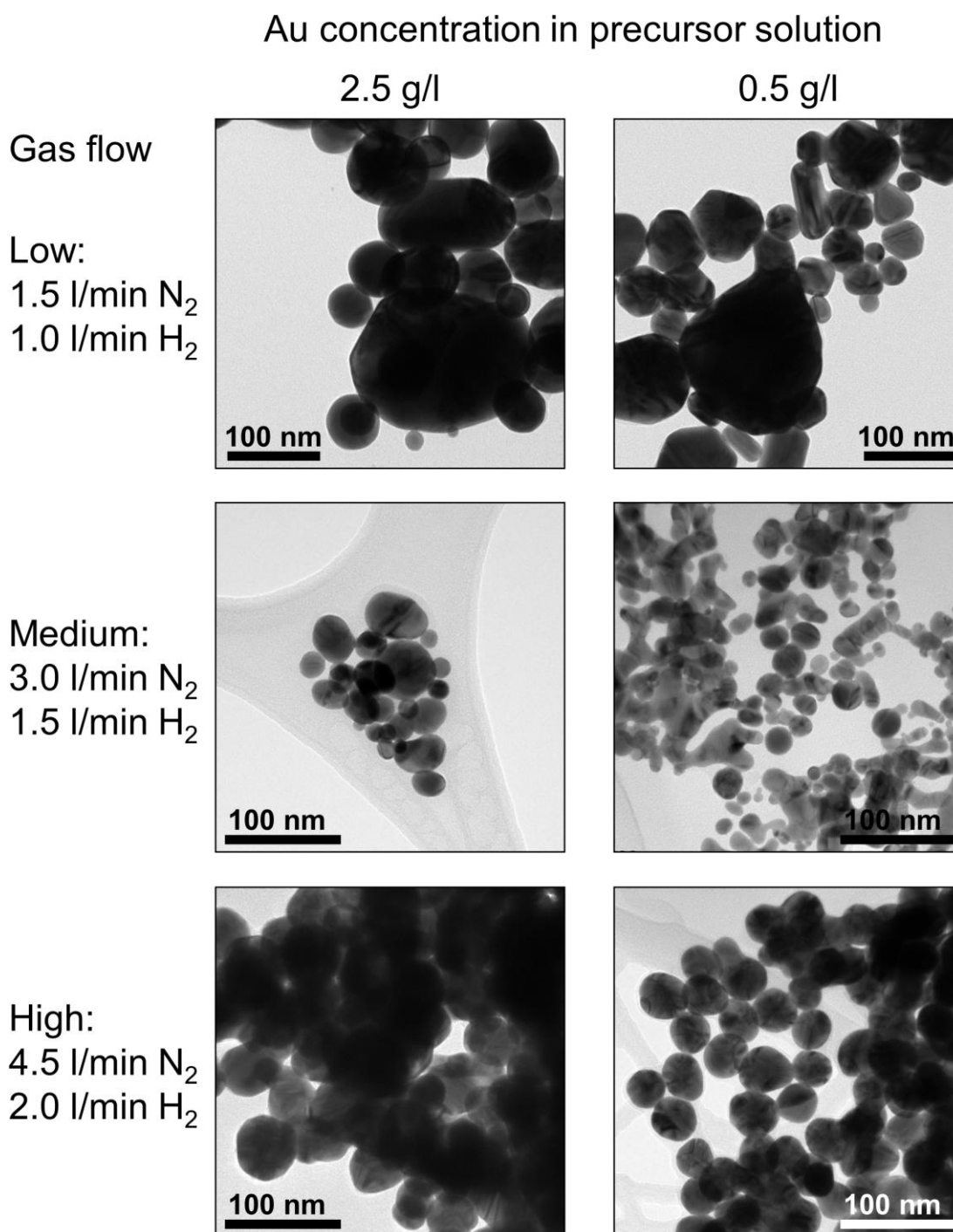


Figure 7.16: Representative TEM micrographs of AuNPs obtained with the modified USP and increasing gas flows, experiments MAu8 and MAu13-MAu17

Table 7.3: Sizes of AuNPs synthesized with variable gas flow, measured from TEM images

Gas flow	AuNP mean sizes \pm SD, at 2.5 g/l Au	AuNP mean sizes \pm SD, at 0.5 g/l Au
Low: 1.5 l/min N ₂ + 1.0 l/min H ₂	39.4 \pm 20.6 nm 207.9 \pm 38.3 nm	38.9 \pm 15.1 nm 91.3 \pm 15.2 nm
Medium: 3.0 l/min N ₂ + 1.5 l/min H ₂	26.7 \pm 13.1 nm	17.7 \pm 6.9 nm
High: 4.5 l/min N ₂ + 2.0 l/min H ₂	45.5 \pm 12.5 nm	37.0 \pm 5.5 nm

Low gas flow

With a precursor solution concentration of 2.5 g/l Au, the obtained AuNPs had a bimodal size distribution with smaller AuNPs (a mean size of 39.4 nm, 66.0% of total AuNPs), formed by the GTP mechanism and larger AuNPs (a mean size of 207.9 nm, 34.0% of AuNPs) formed by the DTP mechanism (Table 7.3, Figure 7.17). When using a concentration of 0.5 g/l Au, the bimodal distribution was not as apparent. However, in the distribution, two peaks were visible (Figure 7.16), indicating two size ranges, from which we can assume that the two formation mechanisms were present in the synthesis (a mean size of 38.9 nm for GTP, 63.3% of AuNPs and a mean size of 91.3 nm for DTP, 36.7%, Table 7.3). As such, both DTP and GTP mechanisms were present in the USP synthesis of AuNPs when using low gas flows. (Reynolds number in evaporation zone, $Re = 87.5$).

Medium gas flow

When using medium gas flows ($Re = 174.9$) the obtained AuNPs had a mean size of 26.7 nm for 2.5 g/l Au and 17.7 nm for 0.5 g/l Au in the precursor solution. Larger particles were characterized as agglomerates of these AuNPs. This indicated that the GTP mechanism was more dominant with these parameters. Even though the possibility of the presence of the DTP mechanism was not excluded entirely, GTP was prevalent in these experiments. It is possible that AuNPs formed by DTP have sizes similar to those formed by GTP, making them difficult to isolate and identify. For higher Au concentrations in the precursor solution, bigger AuNPs were obtained than for lower concentrations, which were to be expected, according to literature and previous results. A large number of AuNPs were in the narrow size range from 10 to 30 nm (69.0%) for 2.5 g/l Au and in the size range from 10 to 20 nm (55.6%) for 0.5 g/l Au in the precursor solution.

High gas flow

With higher gas flows ($Re = 262.4$) the AuNPs sizes were increased somewhat in comparison to medium gas flows, with a mean size of 45.5 nm for 2.5 g/l Au and 37.0 nm for 0.5 g/l Au in the precursor solution. When using higher gas flows there was more turbulence in the USP system compared with medium gas flow, causing more collisions of aerosol droplets, precursor vapours and AuNPs. The increased number of eddies (local rotations and swirls) in the gas flow, especially due to the inlet of the reduction gas H_2 between the furnaces, may also have been the cause of the increase in nanoparticle sizes. High gas flow thus caused the formation of larger AuNPs than medium gas flow, as is visible when comparing the histograms from medium and high gas flows in Figure 7.17. A large number of AuNPs were in the narrow size range from 40 to 60 nm (64.2%) for 2.5 g/l Au and in the size range from 30 to 40 nm (69.1%) for 0.5 g/l Au in the precursor solution.

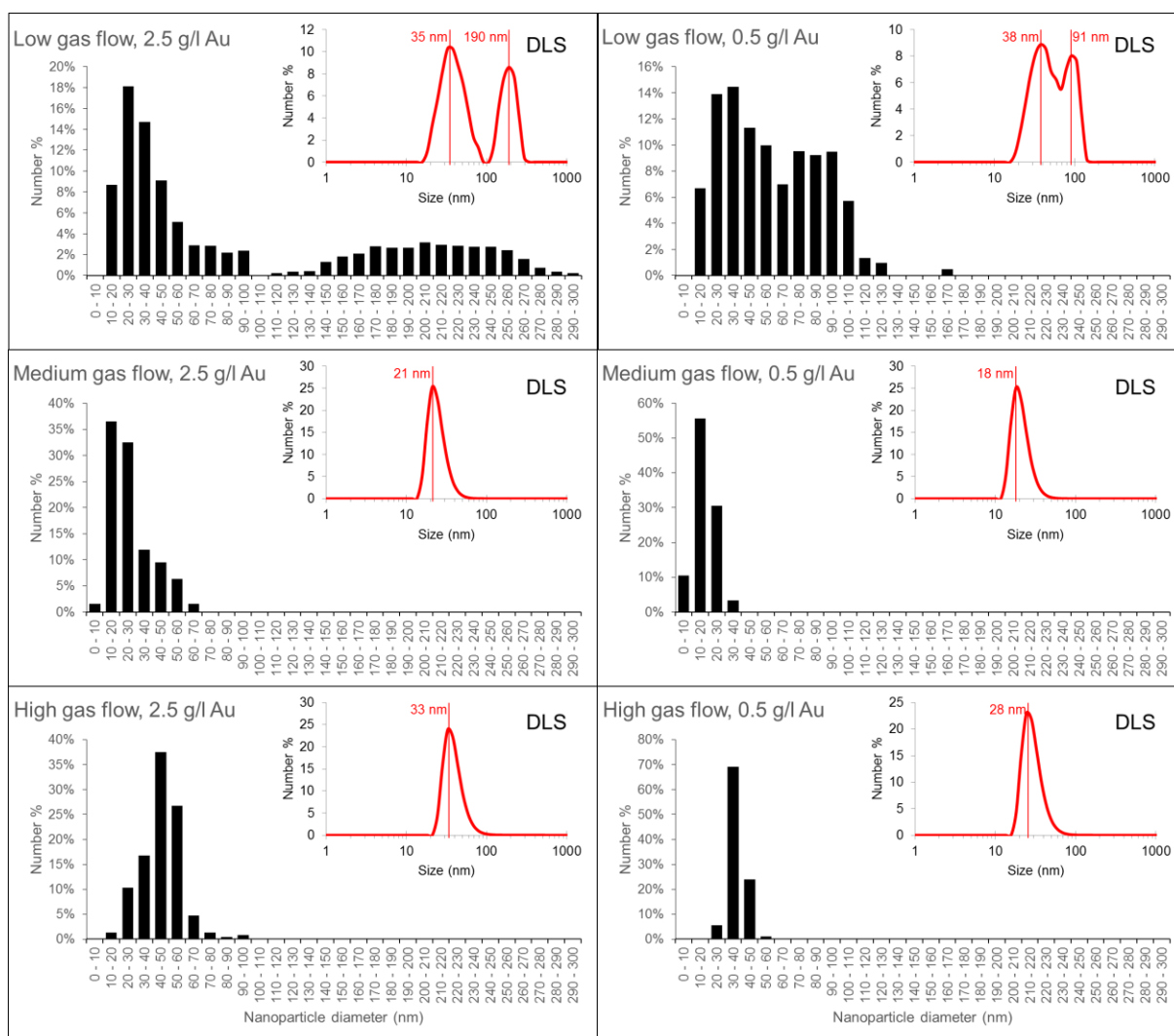


Figure 7.17: Size distributions of AuNPs measured from TEM micrographs (experiments MAu8 and MAu13-MAu17) with accompanying DLS size measurements for comparison, accuracy of measured AuNP sizes from TEM images is estimated at ± 2 nm

Medium and high gas flows provided a narrower AuNP size distribution compared to a low gas flow, as is apparent from the lower SDs in Table 7.3 and narrower size distributions from the histograms in Figure 7.17. The bimodal distribution of AuNPs is also not as apparent with medium and high gas flows, while the AuNP diameters are only a few 10 nm in size. This indicates that the GTP mechanism was the prevailing formation mechanism and DTP formation was diminished. The rapid heating up of aerosol droplets with high gas flows caused them to burst, not allowing time for the precursor in the droplet to form a dried nanoparticle. The vapours from the droplet then formed new nuclei, which grew into AuNPs of a few 10 nm in diameter. Depending on the gas flow stability, more or less uniform AuNPs were formed from the vapours (Figure 7.18). The Au concentration in the precursor

determined the sizes of the final AuNPs. When using 2.5 g/l Au, larger AuNPs were present in the system than with 0.5 g/l Au, which was expected.

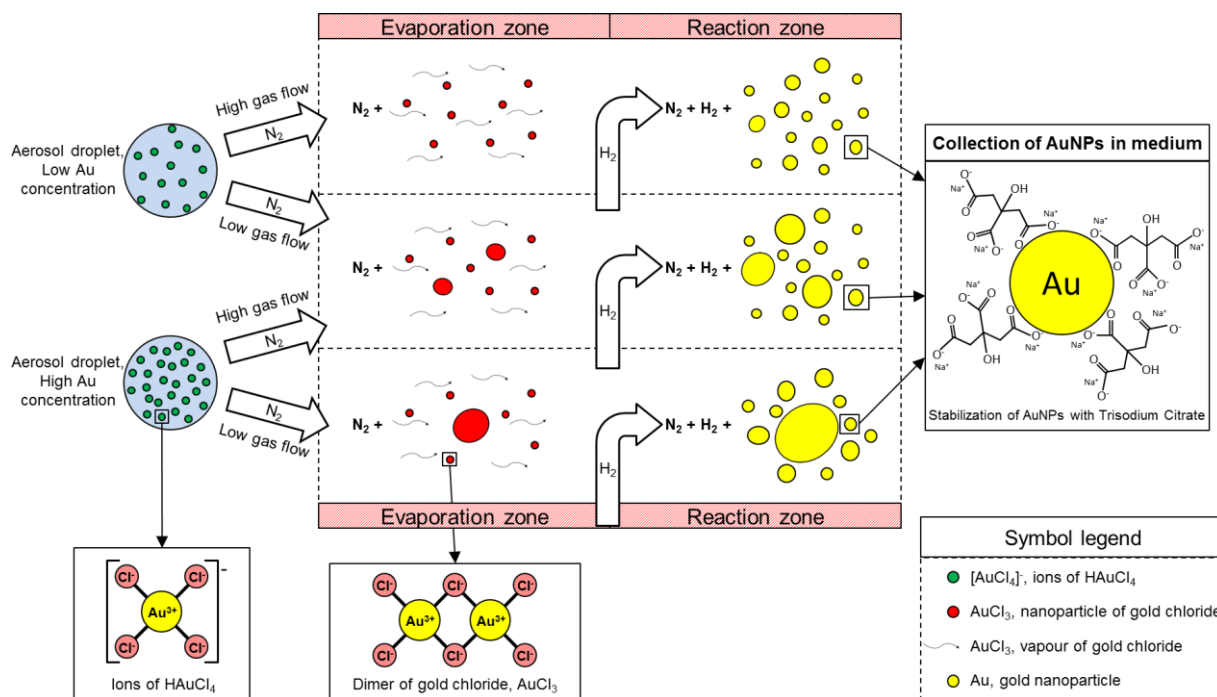


Figure 7.18: Schematic illustration of proposed AuNP formation mechanisms DTP and GTP, depending on 2 parameters: Au concentration in the precursor solutions and gas flows.

The differences of nanoparticle sizes when using different gas flows in connection with the formation mechanisms are also dependent on the gas mean free path (average distance of particles/molecules travelled between collisions – λ). Theoretically, the most influential parameters for λ are the density (affected by temperature, pressure and other factors) and particle size [13]:

$$\lambda = \frac{k_B T}{\sqrt{2} \pi p \sigma_d^2}$$

Where k_B – Boltzmann constant, T – temperature, p – pressure and σ_d – hard-sphere molecular diameter. However, in our case, we have two types of USP nanoparticle formations and particle sizes (with and without bimodal size distribution), which set different physical conditions that govern collisions. We can assume that λ is longest when using medium gas flows. When a low gas flow is used the particle mean free path is shorter, which results in growth of the larger particles present in the system, due to a larger influence of the DTP mechanism. The presence of DTP is diminished when using high gas flows. However, increased AuNP growth could be observed, indicating that the mean free path λ was shorter than with medium gas flows. We can assume that medium gas flows (with the longest mean

free path) provided the most optimal conditions for controlling final AuNP formation. Lower precursor Au concentrations extended the mean free path even more, as less particles and vapour were present in the system.

7.3 Electron diffraction

Electron diffraction was conducted on the samples for explaining the crystal structure and AuNP growth with the DTP and GTP mechanisms. The electron diffraction showed a space group Fm-3m in the typical samples, which corresponded to the face centered cubic lattice structure present in Au (Figure 7.19) [95].

The surface energies of the Au face centered cubic lattice were as follows [96]: $a_{\{111\}} < a_{\{100\}} < a_{\{110\}}$. No apparent grain orientation was present (some possible growth directions are presented in Figure 7.19a and Figure 7.20 of singular AuNPs). There was a high concentration of grain boundaries and twins present in the AuNPs, while there appeared to be no visible vacancies or porosity. There was also no distinct concentration gradient from the AuNP centre to its surface (Figure 7.20). This is in agreement with the AuNP formation mechanisms from aerosol droplets, as the smaller AuNPs formed from the gas phase by GTP grow from nuclei in several directions. The larger AuNPs formed by DTP, show heterogeneous growth due to several nucleation sites within the aerosol droplet. AuNPs formed initially by DTP and later enlarged by GTP also do not exhibit homogeneous growth, which is in compliance with this type of AuNP. Some ED patterns are presented in Figure 7.21 and a simulation of the crystal lattice is also presented in Figure 7.19.

Some possible growth directions and their final AuNP morphologies are presented in Figure 7.22. The AuNPs grow anisotropically on the surfaces with the lowest energy. When a low concentration of defects (twins) is present, the AuNPs grow into unwanted irregular or triangular shapes. When the number of twins is high, there are more growth directions on their surfaces and the AuNPs grow into more spherically shaped nanoparticles. In this regard, for spherical AuNPs, it is more favourable to ensure USP conditions where the kinetics are fast (fast flow rates, high temperatures), producing a higher concentration of twins in the particles and causing growth of spherical AuNPs.

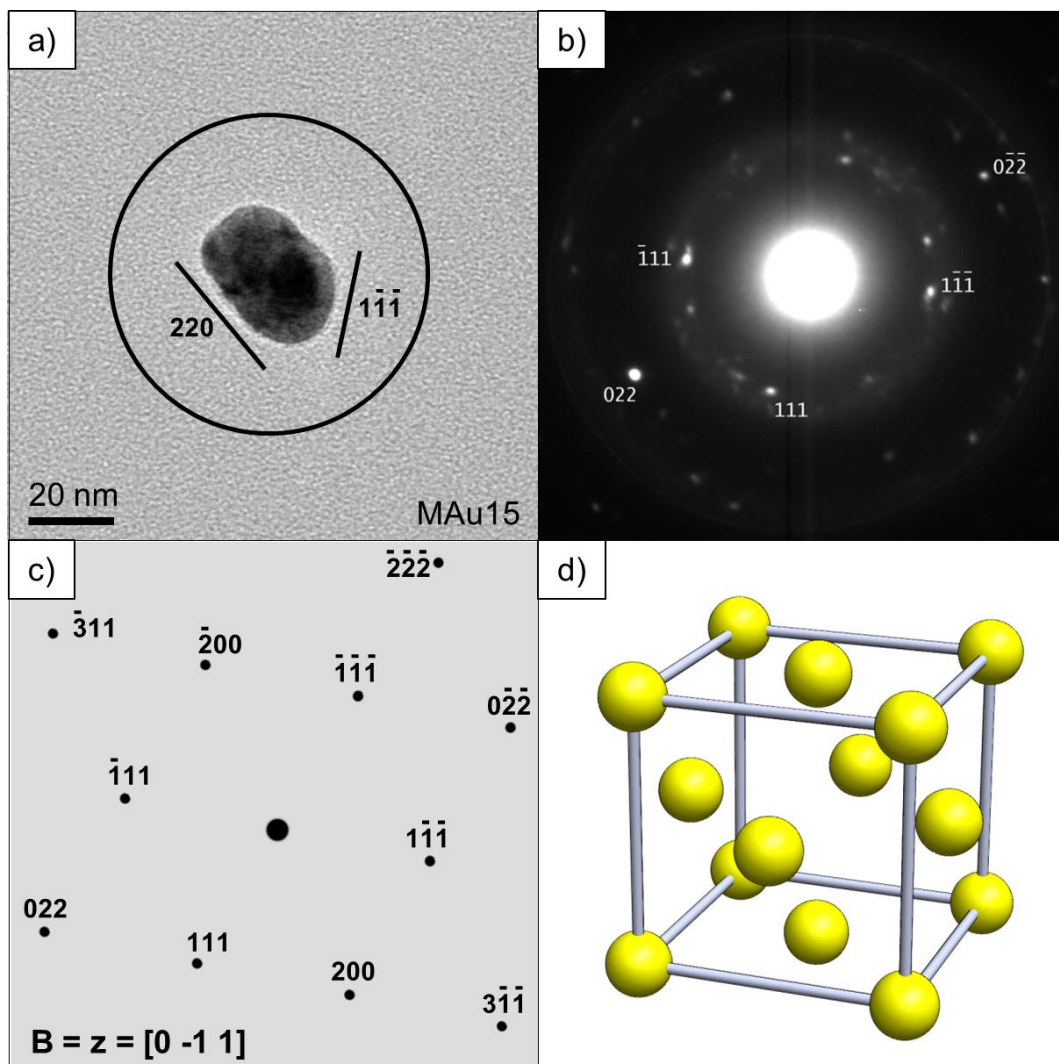


Figure 7.19: Electron diffraction on the synthesized singular AuNP with a crystal lattice simulation; a) TEM micrograph of a single AuNP with visible selected site of electron diffraction; b) Electron diffraction of a single AuNP; c) Crystal lattice simulation, space group Fm-3m; d) Representation of a face centered cubic lattice structure [95]

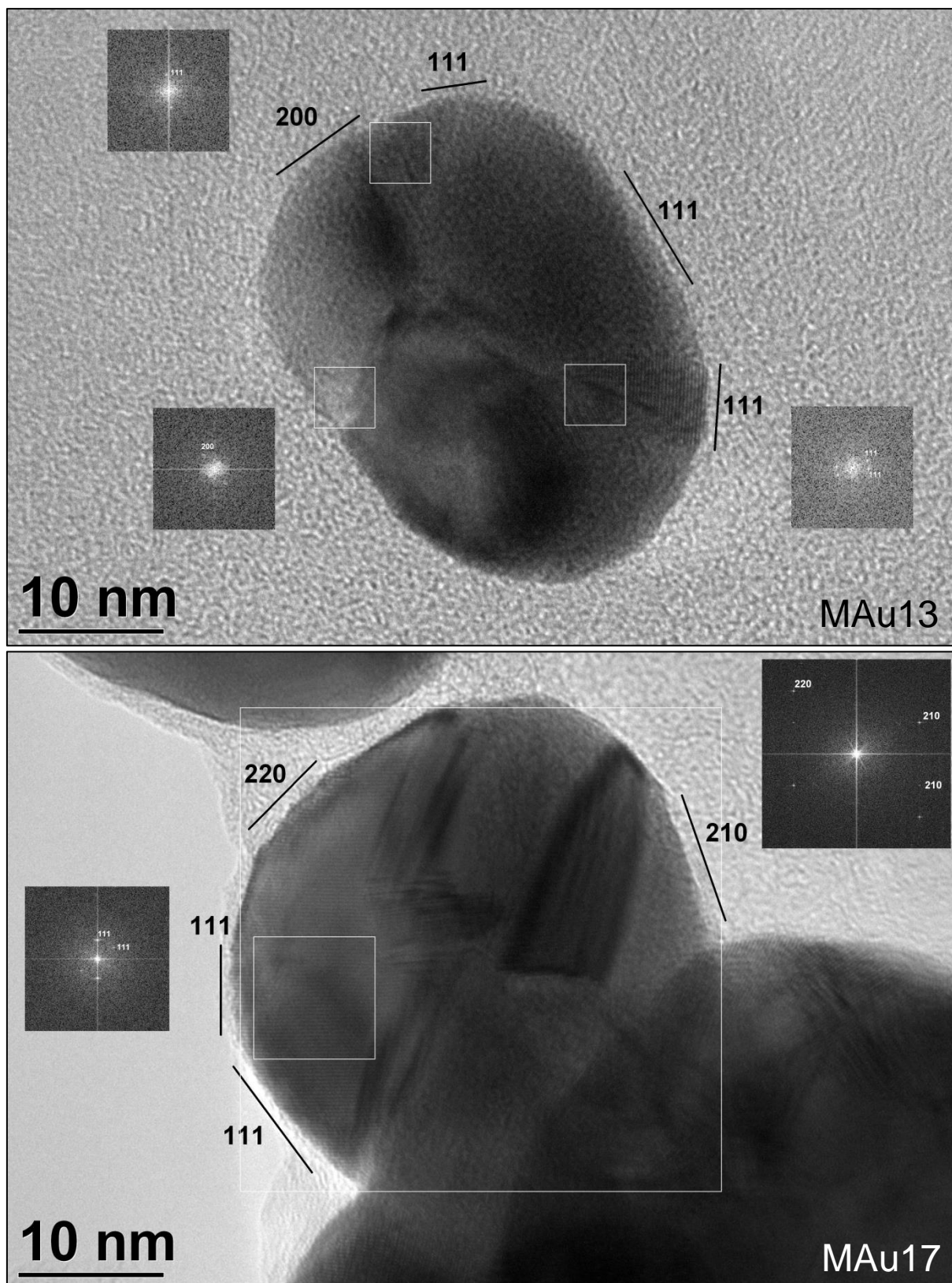


Figure 7.20: Visible defects and possible growth directions of AuNPs

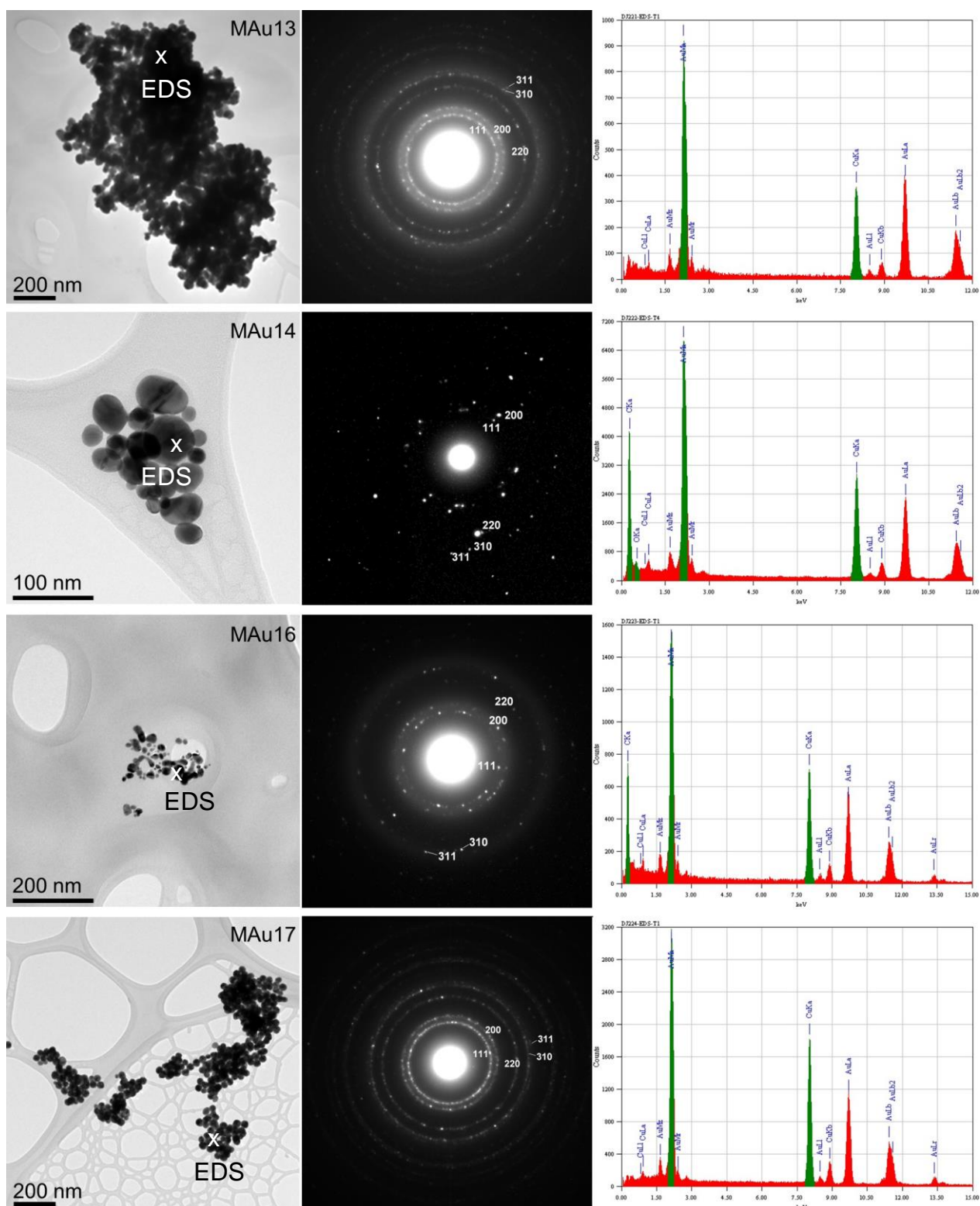


Figure 7.21: ED analyses of synthesized AuNPs with accompanying representative EDS. The C and Cu content in the EDS analyses come from the TEM formvar grid, on which the AuNPs were examined

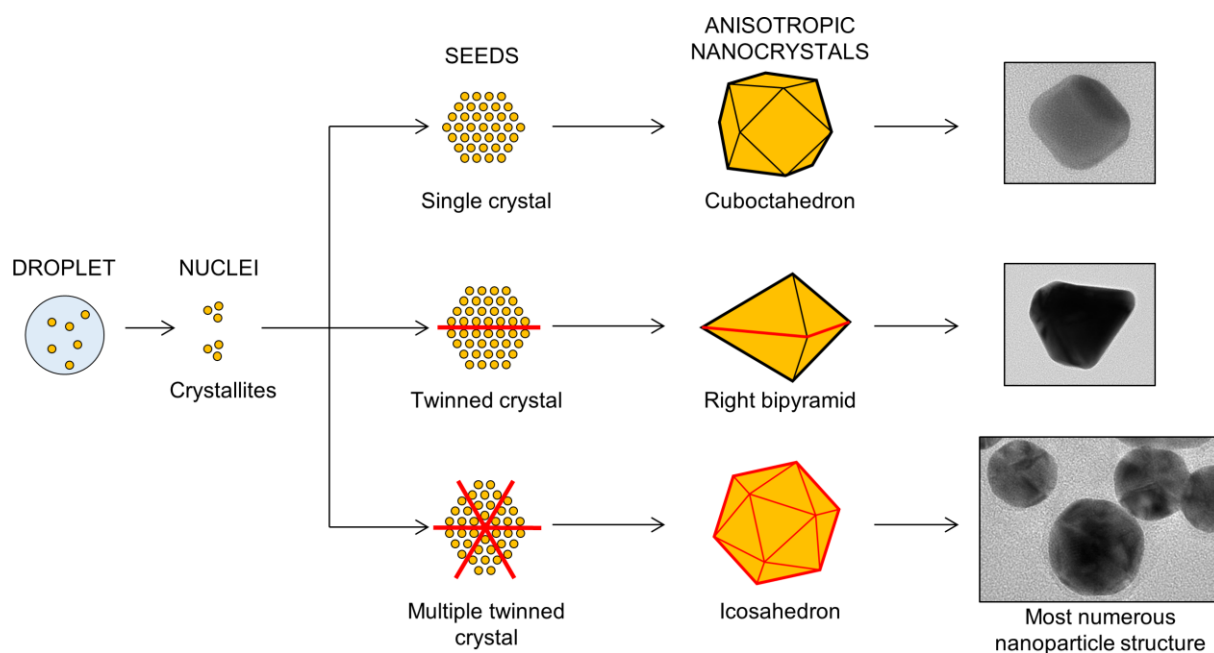


Figure 7.22: Possible growth of AuNPs, adapted from [97]

7.4 Concentrations of synthesized AuNPs

The concentration of AuNPs in suspensions is an important criterion for stabilization, functionalization and use of the synthesized AuNPs in further applications. Measurements were also carried out in order to determine the efficiency of the laboratory USP for AuNP production. As USP is a method with a continuous material flow, the quantities of the AuNPs in the collection bottles depend on the duration of the synthesis and the volume of the precursor solution used for aerosol generation. With higher gas flows, more aerosol droplets are transported into the furnaces, increasing the efficiency of the synthesis. With lower gas flows, a portion of the aerosol droplets redissolve in the precursor solution, decreasing the efficiency, as they need to be converted into droplets again. Concentrations of Au and the main parameters for some of the synthesized AuNPs are shown in Table 7.4.

Table 7.4: Parameters of experiments with measured Au concentration in the final suspensions

Experiment	Conc. of Au in starting solution	Gas flow	Volume of solution used for synthesis	Time of synthesis	Conc. of Au in suspension, measured by ICP-OES	Mass of AuNPs
MAu6	2.5 g/l	Low	40 ml	3 h	20 ppm	10 mg
MAu9	1.25 g/l	Low	110 ml	7 h	21 ppm	10.5 mg
MAu10	0.5 g/l	Low	95 ml	6 h	8 ppm	4 mg
MAu13	2.5 g/l	Medium	50 ml	3 h	14 ppm	7 mg
MAu14	2.5 g/l	High	60 ml	3 h	13.5 ppm	6.8 mg
MAu16	0.5 g/l	Medium	50 ml	3 h	3.3 ppm	1.7 mg
MAu17	0.5 g/l	High	60 ml	3 h	4.1 ppm	2.1 mg
MAu18	2.5 g/l	Low	170 ml	12 h	61 ppm	30.5 mg
MAu19	2.5 g/l	Low	95 ml	6 h	46 ppm	23 mg

Commercially obtained AuNPs are available in small quantities (1 – 50 mg for 50 nm spherical AuNPs [28], [39]), which are comparable to the quantities synthesized by USP. The synthesized AuNPs were collected in a suspension volume of 500 ml. This suspension volume needs to be reduced with low pressure evaporation or centrifugation and removal of the supernatant, in order to raise the concentration for further application testing.

7.4.1 AuNP deposition on tube walls during synthesis and USP efficiency

The efficiency of the USP device can be calculated by dividing the measured mass of AuNPs in suspensions with the mass of the used up dissolved Au during synthesis from

$$\eta = \frac{\text{Conc. of Au in suspension} \left[\frac{\text{mg}}{\text{l}} \right] \cdot \text{Suspension volume} [0.5 \text{ l}]}{\text{Conc. of Au in solution} \left[\frac{\text{mg}}{\text{l}} \right] \cdot \text{Volume of solution used} [\text{l}]} \cdot 100\% \quad (1)$$

The average efficiency of the experiments was calculated to be $\eta = 7.4 \pm 1.7\%$. The low efficiency of the synthesis was due to aerosol condensation and particle deposition on the tube walls. As the USP device used for synthesis was for laboratory purposes, it was not optimized

for efficiency. However, fundamental laboratory research of the AuNP formation is important for up-scaling the process onto an industrial level for AuNP manufacturing, where the process would be optimized for maximum efficiency.

The AuNP deposition onto the transport tube walls is presented in Figure 7.23. As the AuNPs are formed, they can bind to the tube walls with physisorption on the oxygen atoms of the quartz tubes (SiO_2). This principle is also used in stabilization of the AuNPs, where the weak van der Waals bonds are created between the oxygen atoms and the surface of Au. When synthesizing AuNPs, other materials need to be considered for the transport tubes, where deposition of the nanoparticles is not inherent. This is important for increasing the efficiency of the USP synthesis, especially if the process production quantities are to be increased from the laboratory scale.

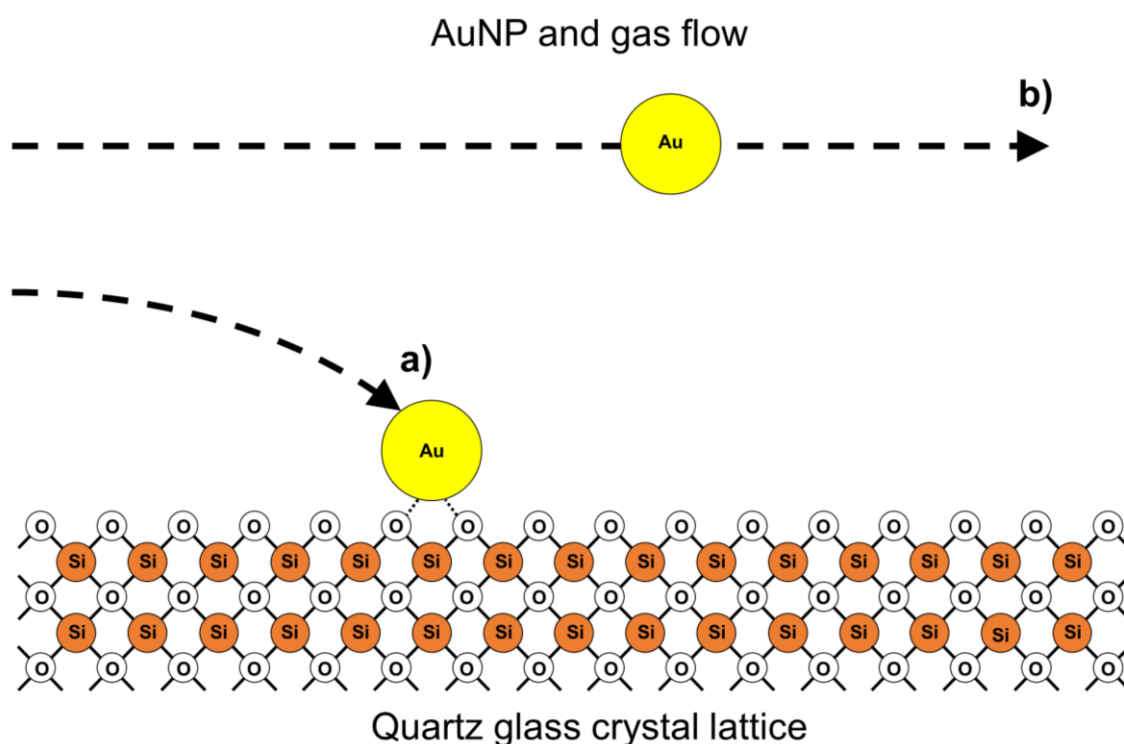


Figure 7.23: Deposition of AuNP on the quartz glass tube wall; a) Physisorption of AuNP with oxygen atoms from the quartz crystal lattice; b) AuNP in the gas flow far away from the tube walls, to be collected in the collection bottles

7.5 Zeta potential of synthesized AuNPs

The synthesis parameters of AuNPs with measured zeta potential are shown in Table 6.5. The zeta potential measurements were performed 3 months after synthesis. With USP synthesis from HAuCl_4 , a side product of the process is Hydrochloric Acid HCl , which is dissolved in the collection medium, lowering its pH value. As such the native pH values of the AuNP suspensions after synthesis were: 2.72, 3.57 and 3.36 for MAu11, MAu12 and MAu8, respectively. The pH level of the AuNP suspensions was raised up to pH7 and pH10 with the addition of NaOH , in order to determine the stability behaviour of the AuNPs. A pH level of around 7 is required for biocompatible testing and applications. The zeta potential was measured 5 times at 3 pH levels for each AuNP suspension (native pH, pH7 and pH10). The mean values of the 5 measurements and their SDs are presented in Table 7.5. Figure 7.24 is a graphical representation of these values for easier identification of stability behaviour at different pH levels.

Table 7.5: Measured zeta potential of synthesized AuNPs, collected in different mediums

	Col. medium	pH native (mean)	pH native (SD)	pH 7 (mean)	pH 7 (SD)	pH 10 (mean)	pH 10 (SD)
MAu11	DI water	-30.5	1,7	-13.0	0,9	-21.0	1.5
MAu12	0.1% PEG	-28.3	1,7	-24.0	0,1	-28.8	0.4
MAu8	0,1% NaCitrate	-23.2	1,3	-29.9	4,1	-32.8	1.1

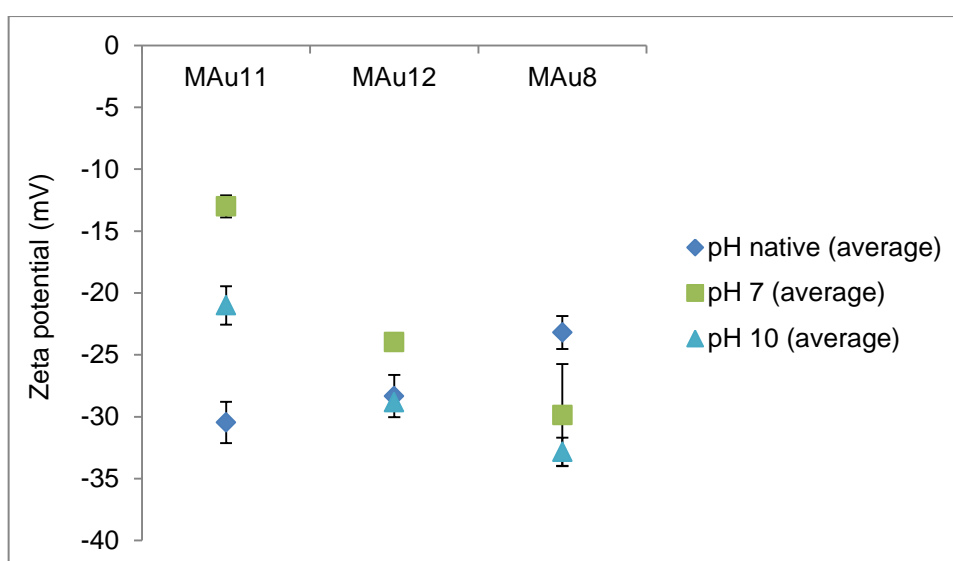
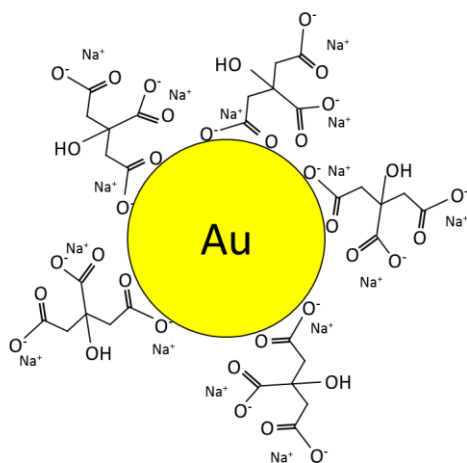


Figure 7.24: Zeta potential of AuNP suspensions at 3 pH levels

From Table 7.5 and Figure 7.24 it can be seen that the AuNP suspensions were relatively stable in their native pH levels after synthesis. When collected in DI water, the AuNPs had a zeta potential value of -30.5 mV with low pH levels (pH 2.72). Increasing the pH level up to 7 destabilized the AuNPs (zeta potential of -13 mV), resulting in agglomeration of the nanoparticles. At a higher level (pH 10), the zeta potential again showed the relative stability of the AuNPs (-21 mV).

When collected in mediums with Na citrate or PEG (Figure 7.25), the synthesized AuNPs were relatively stable at the native pH level and higher pH levels (7 and 10). The weight percentages of Na citrate and PEG from Table 6.5 were chosen depending on previously measured concentrations of AuNPs in DI water. The molar ratio of Trisodium Citrate to AuNPs and PEG to AuNPs was selected to be 4000:1 [98]. When stored properly (as described in Chapter 2.3), the synthesized AuNP suspensions with Sodium Citrate and PEG were stable for 3 months, and no visible agglomeration was observed (the suspension colour had not changed from red to blue, which would indicate agglomeration of the AuNPs).

Stabilization of AuNPs with Trisodium Citrate



Stabilization of AuNPs with PEG

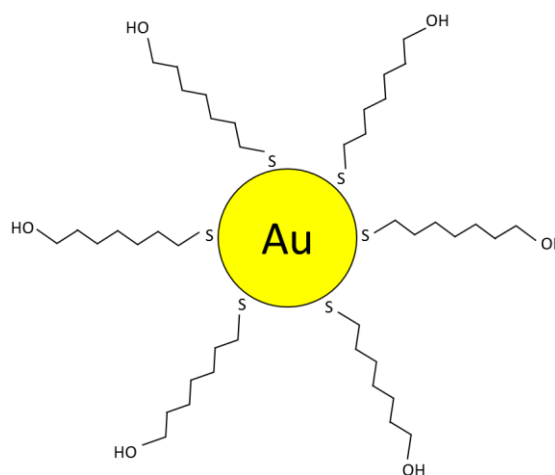


Figure 7.25: Schematic presentation of AuNP stabilized with Trisodium Citrate (adapted from [99]) and PEG (adapted from [98])

8 SETTING UP A MODEL OF AuNP FORMATION

8.1 Formation of AuNPs

In the modified USP system with the precursor HAuCl_4 , a combination of both DTP and GTP are present. The ratio of DTP and GTP mechanisms depends on the evaporation of the aerosol droplet (controlled by parameters: Au concentration in the precursor solution, gas flow, evaporation temperature) (Figure 8.1). Due to solute vapourization, a mass flow and partial vapour pressure of the gaseous gold chloride is also present on the droplet surface.

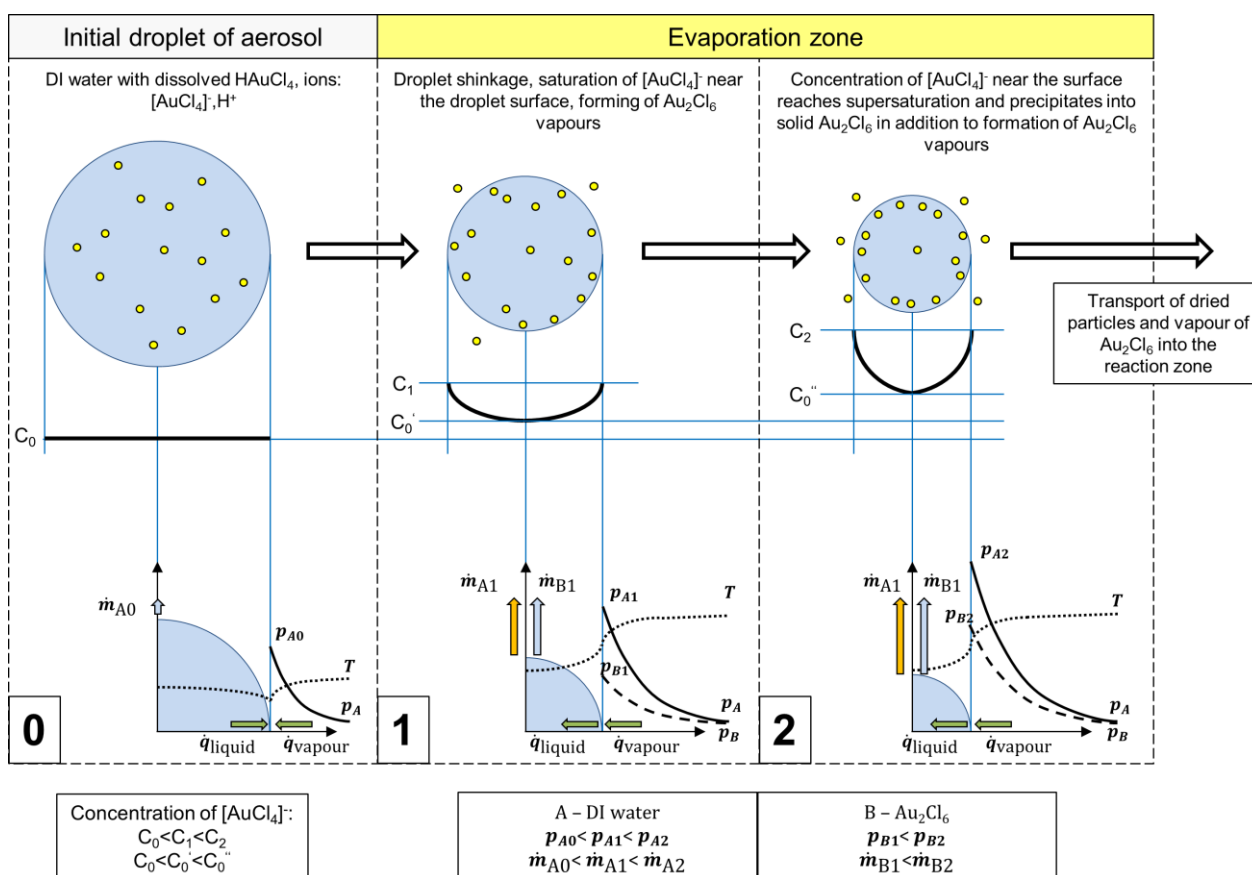


Figure 8.1: Aerosol droplet evaporation and occurrence of the combination of DTP and GTP mechanisms in the synthesis of AuNPs

The main characteristics of the DTP and GTP formation mechanisms are explained in Chapters 4.4.1 and 4.4.3. For DTP formation, the gold chloride dimer of AuCl_3 or, alternatively, Au_2Cl_6 [72] is precipitated from the droplet and then converted thermochemically into pure AuNPs. For GTP formation of AuNPs in the nucleation-condensation

mode, the nucleation and growth proceeds by the condensation of vapours of Au_2Cl_6 . When a low number of collisions occur, the AuNPs can remain nearly spherical through the aerosol reactor path. In the nucleation-coagulation mode, the AuNPs are formed and their high concentration allows collisions and coalescence of AuNPs, resulting in growth of the particles. The AuNP growth rate is inversely proportional to its size – small AuNPs grow faster than larger ones [13], which results in a narrow size distribution of final AuNPs.

While the evaporation rate, solute diffusion, supersaturation and vapourization are important factors for particle morphology, other phenomena need to be considered. When manipulating the rate of evaporation by changing the temperature (higher temperatures – faster evaporation and vice-versa) with a low, steady gas flow used in the experiments, a higher influence of the DTP mechanism is apparent on the AuNP formation. Manipulating the evaporation rate by gas flow achieves different results. In these cases, the GTP mechanism is more influential. It seems that by using high gas flows, the evaporation of droplets and vapourization of the solvent from the droplet is more dispersed in the system, yielding more uniform, smaller AuNPs.

A faster evaporation rate induced by a high gas flow favours the GTP mechanism (rapid evaporation and flow conditions promote precursor vapourization), while a slower evaporation rate by using low gas flows and low temperatures favours the DTP mechanism (diffusion of precursor into the droplet centre and creation of the dried particle). It is important to note that the ratio of the DTP and GTP mechanisms is difficult to determine from TEM or DLS measurements of AuNPs, as the smaller AuNPs can also be formed by the DTP mechanism, although their growth rate is slower. The AuNPs formed by GTP catch up to the AuNPs formed by DTP, due to their higher growth rate. Because of their similar sizes it is then difficult to distinguish which AuNPs have been formed by which mechanism. In theory, GTP produces smaller sizes, matching our results; however, DTP (to a lesser extent) cannot be excluded entirely.

The formation of finer AuNPs may also occur due to the aerosol droplets not being fully evaporated in the evaporation zone. The droplets then superheat in the reaction zone and burst into smaller fragments, from which new, small nanoparticles are formed. These explosions could be the basis of small AuNP formation, as TGA also suggests formation of pure gold without vapors. However, gold chloride is reported to easily sublime [72] and can also be used for aerosol assisted chemical vapor deposition [12], implicating that GTP is present. A fraction of the smaller nanoparticles may be formed by droplet explosions in the reaction

heating zone. However, by using a conventional USP, where the droplets would be naturally superheated, the formation of small, fairly uniform AuNPs was not reported [18]. In those experiments, AuNPs, smaller than 40 nm were not formed.

Upon analysis of the sizes and shapes of the obtained AuNPs by varying the precursor Au concentration and gas flows, it was proposed that these are the influential parameters for controlling the AuNP formation mechanisms, DTP and GTP. Increasing the precursor Au concentration reinforced the presence of DTP, while decreasing it weakened the DTP presence. When using low gas flows, the AuNPs were formed by both mechanisms, indicated by the bimodal size distributions (mean sizes of 39.4 ± 20.6 nm and 207.9 ± 38.3 nm for 2.5 g/l Au and mean sizes of 38.9 ± 15.1 nm and 91.3 ± 15.2 nm for 0.5 g/l Au). After increasing the gas flows, the GTP mechanism became prevalent in the system, producing AuNPs a few 10 nm in size, with a narrower size distribution (mean sizes for medium gas flow: 26.7 ± 13.1 nm, 17.7 ± 6.9 nm, for high gas flow: 45.5 ± 12.5 nm, 37.0 ± 5.5 nm; for both Au concentrations). Favourable control of AuNP formation was achieved by using a low Au concentration (0.5 g/l) with high gas flows (4.5 l/min N₂ and 2.0 l/min H₂). This has led to GTP being the dominant mechanism, with which more uniform, spherical AuNPs in a narrow size range (37.0 ± 5.5 nm) were synthesized, reaching our desired sizes.

8.2 Model of AuNP formation with the modified USP

The USP modification has shown that both DTP and GTP mechanisms are present in the formation of AuNPs with HAuCl₄ as the precursor. The influential parameters for changing the ratio between the formation mechanisms are Au concentration in the precursor solution and gas flows. These parameters determine the evaporation of aerosol droplets and vapourization of the solute inside the droplet. When the evaporation is controlled with changing the evaporation temperature, the change in combinations of the two formation mechanisms is not as apparent.

Increasing the gas flow reduces the DTP presence in the synthesis, producing more uniform, smaller sizes of AuNPs, formed by the GTP mechanism. Using a very high gas flow produces somewhat larger AuNPs, due to their different growth. With low gas flows, the influence of the DTP mechanism increases, producing AuNPs in a bimodal size distribution.

When the Au concentration in the precursor solution is raised, there is a greater presence of the DTP mechanism in the AuNP formation.

The parameter conditions for producing more uniform shapes of AuNPs in a narrower size range were identified, achieving the goal of controlling the synthesis on the modified USP.

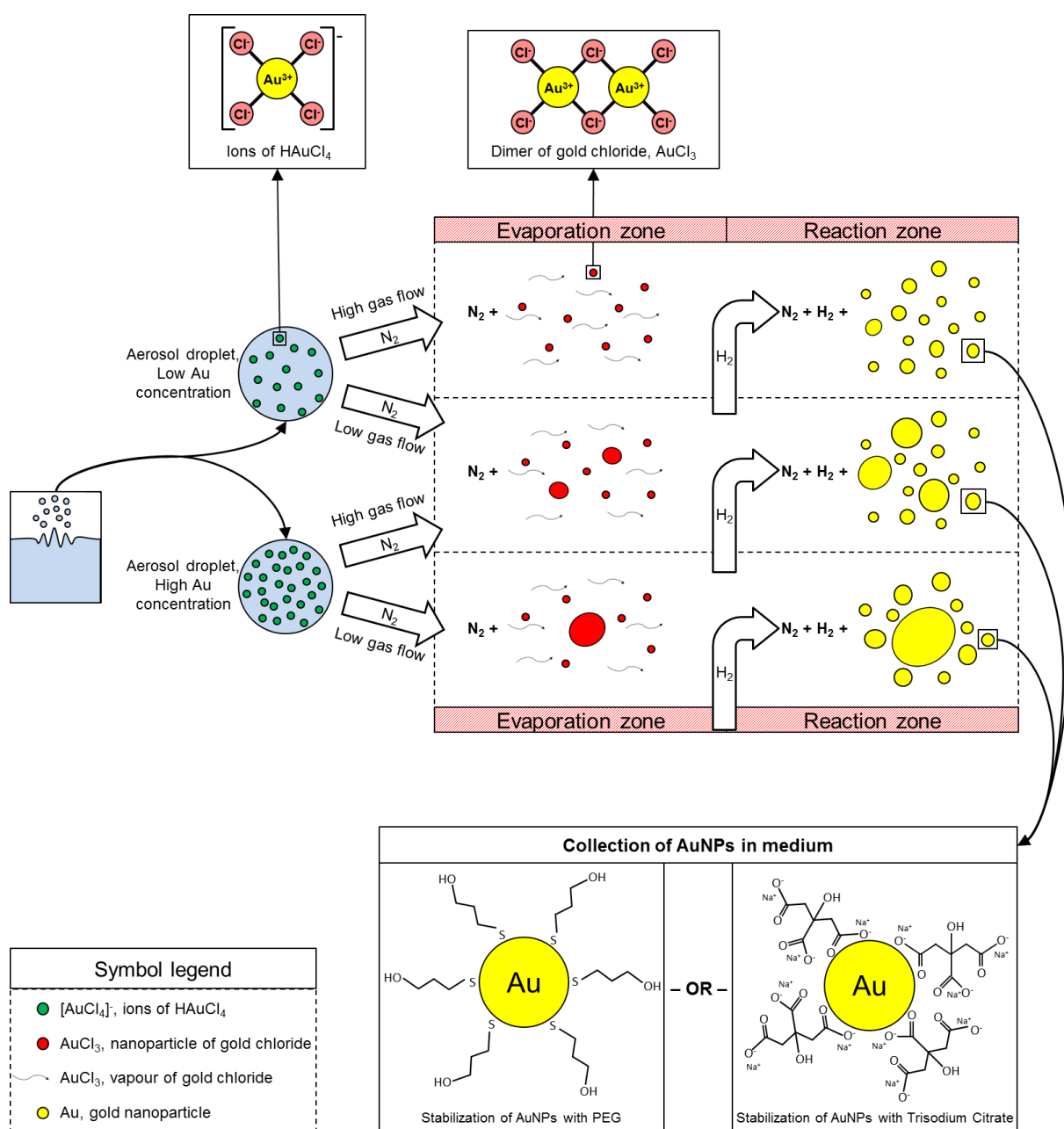


Figure 8.2: Schematic illustration of proposed AuNP formation mechanisms with the modified USP

9 CONCLUSIONS

The aim of the Doctoral Dissertation was to: (i) Modify the conventional USP synthesis and (ii) Synthesize spherical, pure (with a content of at least 99.99 wt.% Au), AuNPs with sizes of 50 nm. The following conclusions can be summarized from the obtained results:

1. AuNPs can be synthesized with the conventional USP, with different shapes in sizes from 10 to 300 nm. Unsuitable AuNPs were the result of all the processes occurring simultaneously (droplet evaporation, thermal decomposition, reduction and densification), which could not be controlled. The synthesized AuNPs also did not have the required chemical composition, as they contained impurities (Co, Cr, Fe, Si,...).
2. Two formation mechanisms, DTP and GTP take place in the USP system. With DTP, larger AuNPs are formed ($2 r < 300$ nm), while with GTP smaller are formed ($10 \text{ nm} < 2 r < 50$ nm). With the conventional USP, these mechanisms cannot be controlled.
3. The modified USP has an evaporation zone separated from the reaction furnace and the reduction gas introduced directly into the reaction furnace. With such a modification, controlling the droplet evaporation and the reactions was possible.
4. Experiments have confirmed, that the Au concentration in the precursor solution and gas flows have the highest influence on the AuNP formation. For lower Au concentrations and higher gas flows, there is a greater probability of formation of spherical, small AuNPs (up to 50 nm).
5. Increasing the Au concentration in the precursor solution (from 0.5 to 5.0 g/l) leads to domination of the DTP mechanism and formation of AuNPs of larger sizes (<300 nm).
6. High gas flows ($\text{N}_2 \geq 3.0$ l/min, $\text{H}_2 \geq 1.5$ l/min) establish conditions, where the GTP mechanism is dominant, forming smaller AuNPs (10 – 50 nm).
7. With the modified USP, using optimal parameters (0.5 g/l Au in precursor solution, 4.5 l/min N_2 and 2.0 l/min H_2), it was possible to synthesize spherical AuNPs of the desired mean sizes up to 50 nm in a narrow size range (68% of AuNPs of sizes 37.0 ± 5.5 nm).
8. The microstructure and ED simulations of AuNPs have shown that they have a polycrystal structure with no distinguishably oriented grains. The AuNPs have a face centered cubic crystal structure, space group Fm-3m, typical for gold. The AuNPs grow anisotropically on surfaces with the lowest energy ($a_{\{111\}} < a_{\{100\}} < a_{\{110\}}$) and

- due to their fast growth kinetics they have a high concentration of grain boundaries and twins. There appear to be no visible vacancies.
9. The modified USP enables synthesis of AuNPs with high purity (99.99 wt.% Au). Achieving high purity is the result of setting up the USP in a suitably clean environment (at the IME Institute, RWTH Aachen), cleaning the USP construction elements with acids (HNO_3 and HCl) and using materials for the construction elements, that do not react with HAuCl_4 (Teflon and quartz glass).
 10. AuNPs in solution with Na citrate were stable after 3 months, confirmed by DLS and zeta potential measurements. The measured sizes of AuNPs have shown a low level of agglomeration.
 11. The efficiency of the laboratory USP is estimated at $\eta = 7.4 \pm 1.7\%$. AuNPs are deposited onto the walls of the quartz SiO_2 transport tubes with physisorption, due to weak van der Waals bonds between the Au and oxygen atoms from the quartz crystal structure.

9.1 Future work

For further work, an optimized assembly of the modified USP should be designed, where the AuNP deposition would be prevented. This should be done by constructing the individual USP elements with suitable materials for deposition prevention. USP element dimensions should also be optimized, by taking into account the interdependent technological parameters. In order to up scale the USP synthesis of AuNPs to an industrial level, the efficiency should be raised and the following components of the USP should be revised and developed anew, based on the findings in this research work: Aerosol generation and droplet transport, transport tube dimensions and gas flow conditions, evaporation/drying and heating elements (diffusion driers, electroresistance or induction furnaces, microwaves), collection system (collection in suspensions or electrostatic precipitators, based on final application).

For further studies regarding AuNP formation mechanisms and applications of AuNPs, the synthesis should be examined using precursors other than HAuCl_4 . Additional stabilization agents should also be used for synthesis of AuNPs in the range of 10 – 50 nm, more suited for biocompatibility testing and potential use in biomedical applications [26], which is currently the primary application of AuNPs.

10 LITERATURE

- [1] V. V. Mody, R. Siwale, A. Singh, and H. R. Mody, "Introduction to metallic nanoparticles," *J. Pharm. Bioallied Sci.*, vol. 2, no. 4, pp. 282–289, 2010.
- [2] P. Pattnaik, "Surface plasmon resonance," *Appl. Biochem. Biotechnol.*, vol. 126, no. 2, pp. 79–92, Aug. 2005.
- [3] P. K. Jain, K. S. Lee, I. H. El-Sayed, and M. A. El-Sayed, "Calculated absorption and scattering properties of gold nanoparticles of different size, shape, and composition: applications in biological imaging and biomedicine," *J. Phys. Chem. B*, vol. 110, no. 14, pp. 7238–7248, Apr. 2006.
- [4] G. Mie, "Beiträge zur Optik trüber Medien, speziell kolloidaler Metallösungen," *Ann. Phys.*, vol. 330, no. 3, pp. 377–445, 1908.
- [5] M. A. Mahmoud and M. A. El-Sayed, "Different Plasmon Sensing Behavior of Silver and Gold Nanorods," *J. Phys. Chem. Lett.*, vol. 4, no. 9, pp. 1541–1545, May 2013.
- [6] D. A. Giljohann, D. S. Seferos, W. L. Daniel, M. D. Massich, P. C. Patel, and C. A. Mirkin, "Gold Nanoparticles for Biology and Medicine," *Angew. Chem. Int. Ed.*, vol. 49, no. 19, pp. 3280–3294, 2010.
- [7] X. Huang and M. A. El-Sayed, "Gold nanoparticles: Optical properties and implementations in cancer diagnosis and photothermal therapy," *J. Adv. Res.*, vol. 1, no. 1, pp. 13–28, Jan. 2010.
- [8] A. Kumar, B. Mazinder Boruah, and X.-J. Liang, "Gold Nanoparticles: Promising Nanomaterials for the Diagnosis of Cancer and HIV/AIDS," *J. Nanomater.*, vol. 2011, p. e202187, Oct. 2011.
- [9] A. J. Mieszawska, W. J. M. Mulder, Z. A. Fayad, and D. P. Cormode, "Multifunctional Gold Nanoparticles for Diagnosis and Therapy of Disease," *Mol. Pharm.*, vol. 10, no. 3, pp. 831–847, 2013.
- [10] S. Das, N. Debnath, S. Mitra, A. Datta, and A. Goswami, "Comparative analysis of stability and toxicity profile of three differently capped gold nanoparticles for biomedical usage," *Biometals*, vol. 25, no. 5, pp. 1009–22, Oct. 2012.
- [11] Y.-C. Wang and S. Gunasekaran, "Spectroscopic and microscopic investigation of gold nanoparticle nucleation and growth mechanisms using gelatin as a stabilizer," *J. Nanoparticle Res.*, vol. 14, no. 10, pp. 1–11, Sep. 2012.
- [12] R. G. Palgrave and I. P. Parkin, "Aerosol Assisted Chemical Vapor Deposition of Gold and Nanocomposite Thin Films from Hydrogen Tetrachloroaurate(III)," *Chem. Mater.*, vol. 19, no. 19, pp. 4639–4647, Sep. 2007.
- [13] T. T. Kodas and M. J. Hampden-Smith, *Aerosol Processing of Materials*, 1 edition. New York: Wiley-VCH, 1998.
- [14] J. Kimling, M. Maier, B. Okenve, V. Kotaidis, H. Ballot, and A. Plech, "Turkevich Method for Gold Nanoparticle Synthesis Revisited," *J. Phys. Chem. B*, vol. 110, no. 32, pp. 15700–15707, Aug. 2006.
- [15] N. G. Bastús, J. Comenge, and V. Puntes, "Kinetically Controlled Seeded Growth Synthesis of Citrate-Stabilized Gold Nanoparticles of up to 200 nm: Size Focusing versus Ostwald Ripening," *Langmuir*, vol. 27, no. 17, pp. 11098–11105, Sep. 2011.
- [16] G. Schmid and B. Corain, "Nanoparticulated Gold: Syntheses, Structures, Electronics, and Reactivities," *Eur. J. Inorg. Chem.*, vol. 2003, no. 17, pp. 3081–3098, 2003.
- [17] G. L. Messing, S.-C. Zhang, and G. V. Jayanthi, "Ceramic Powder Synthesis by Spray Pyrolysis," *J. Am. Ceram. Soc.*, vol. 76, no. 11, pp. 2707–2726, Nov. 1993.

- [18] S. Stopic, R. Rudolf, J. Bogovic, P. Majerič, M. Čolić, and S. Tomić, “Synthesis of Au nanoparticles prepared by ultrasonic spray pyrolysis and hydrogen reduction,” *Mater. Tehnol.*, vol. 47, no. 5, pp. 577–583, 2013.
- [19] R. Rudolf, B. Friedrich, S. Stopić, I. Anžel, S. Tomić, and M. Čolić, “Cytotoxicity of Gold Nanoparticles Prepared by Ultrasonic Spray Pyrolysis,” *J. Biomater. Appl.*, vol. 26, no. 5, pp. 595–612, Jan. 2012.
- [20] Y. Xiong and T. T. Kodas, “Droplet evaporation and solute precipitation during spray pyrolysis,” *J. Aerosol Sci.*, vol. 24, no. 7, pp. 893–908, Oct. 1993.
- [21] J. Bogović, A. Schwinger, S. Stopic, J. Schröder, V. Gaukel, H. P. Schuchmann, and B. Friedrich, “Controlled droplet size distribution in ultrasonic spray pyrolysis,” *Metall*, vol. 65, no. 10, pp. 455–459, 2011.
- [22] G. V. Jayanthi, S. C. Zhang, and G. L. Messing, “Modeling of Solid Particle Formation During Solution Aerosol Thermolysis: The Evaporation Stage,” *Aerosol Sci. Technol.*, vol. 19, no. 4, pp. 478–490, 1993.
- [23] S. Ruben, *Handbook of the Elements*. La Salle, Ill: Open Court, 1999.
- [24] C. Freese, C. Uboldi, M. I. Gibson, R. E. Unger, B. B. Weksler, I. A. Romero, P.-O. Couraud, and C. J. Kirkpatrick, “Uptake and cytotoxicity of citrate-coated gold nanospheres: Comparative studies on human endothelial and epithelial cells,” *Part. Fibre Toxicol.*, vol. 9, no. 1, p. 23, Jul. 2012.
- [25] Z. J. Lim, J. J. Li, C. Ng, L. L. Yung, and B. Bay, “Gold nanoparticles in cancer therapy,” *Acta Pharmacol. Sin.*, vol. 32, no. 8, pp. 983–90, Aug. 2011.
- [26] S. Tomić, J. Đokić, S. Vasilijić, N. Ogrinc, R. Rudolf, P. Pelicon, D. Vučević, P. Milosavljević, S. Janković, I. Anžel, J. Rajković, M. S. Rupnik, B. Friedrich, and M. Čolić, “Size-Dependent Effects of Gold Nanoparticles Uptake on Maturation and Antitumor Functions of Human Dendritic Cells In Vitro,” *PLoS ONE*, vol. 9, no. 5, p. e96584, May 2014.
- [27] J. Dokić, R. Rudolf, S. Tomić, S. Stopić, B. Friedrich, B. Budic, I. Anzel, and M. Colić, “Immunomodulatory properties of nanoparticles obtained by ultrasonic spray pyrolysis from gold scrap,” *J. Biomed. Nanotechnol.*, vol. 8, no. 3, pp. 528–538, Jun. 2012.
- [28] Future Markets, “The Global Market for Gold Nanoparticles, 2010-2025,” *Future Markets, Inc.*, 06-Mar-2015. .
- [29] E. Boisselier and D. Astruc, “Gold nanoparticles in nanomedicine: preparations, imaging, diagnostics, therapies and toxicity,” *Chem. Soc. Rev.*, vol. 38, no. 6, pp. 1759–1782, May 2009.
- [30] H. Jans, X. Liu, L. Austin, G. Maes, and Q. Huo, “Dynamic Light Scattering as a Powerful Tool for Gold Nanoparticle Bioconjugation and Biomolecular Binding Studies,” *Anal. Chem.*, vol. 81, no. 22, pp. 9425–9432, Nov. 2009.
- [31] J. A. Ryan, K. W. Overton, M. E. Speight, C. N. Oldenburg, L. Loo, W. Robarge, S. Franzen, and D. L. Feldheim, “Cellular uptake of gold nanoparticles passivated with BSA-SV40 large T antigen conjugates,” *Anal. Chem.*, vol. 79, no. 23, pp. 9150–9159, Dec. 2007.
- [32] M. Shah, V. D. Badwaik, and R. Dakshinamurthy, “Biological Applications of Gold Nanoparticles,” *J. Nanosci. Nanotechnol.*, vol. 14, no. 1, pp. 344–362, Jan. 2014.
- [33] L. Sun, D. Liu, and Z. Wang, “Functional Gold Nanoparticle–Peptide Complexes as Cell-Targeting Agents,” *Langmuir*, vol. 24, no. 18, pp. 10293–10297, Sep. 2008.
- [34] L. Xu, Y. Zhu, W. Ma, W. Chen, L. Liu, H. Kuang, L. Wang, and C. Xu, “New Synthesis Strategy for DNA Functional Gold Nanoparticles,” *J. Phys. Chem. C*, vol. 115, no. 8, pp. 3243–3249, Mar. 2011.

- [35] D. Pissuwan, C. H. Cortie, S. M. Valenzuela, and M. B. Cortie, “Functionalised gold nanoparticles for controlling pathogenic bacteria,” *Trends Biotechnol.*, vol. 28, no. 4, pp. 207–213, Apr. 2010.
- [36] A. Y. Lin, J. P. Mattos Almeida, A. Bear, N. Liu, L. Luo, A. E. Foster, and R. A. Drezek, “Gold Nanoparticle Delivery of Modified CpG Stimulates Macrophages and Inhibits Tumor Growth for Enhanced Immunotherapy,” *PLoS ONE*, vol. 8, no. 5, p. e63550, May 2013.
- [37] K. Otto, I. Oja Acik, M. Krunks, K. Tõnsuaadu, and A. Mere, “Thermal decomposition study of $\text{HAuCl}_4 \cdot 3\text{H}_2\text{O}$ and AgNO_3 as precursors for plasmonic metal nanoparticles,” *J. Therm. Anal. Calorim.*, vol. 118, no. 2, pp. 1065–1072, Nov. 2014.
- [38] K. L. Kelly, E. Coronado, L. L. Zhao, and G. C. Schatz, “The Optical Properties of Metal Nanoparticles: The Influence of Size, Shape, and Dielectric Environment,” *J. Phys. Chem. B*, vol. 107, no. 3, pp. 668–677, Jan. 2003.
- [39] “nanoComposix,” May-2013. [Online]. Available: <http://nanocomposix.com/>.
- [40] S. Eustis and M. A. El-Sayed, “Why gold nanoparticles are more precious than pretty gold: Noble metal surface plasmon resonance and its enhancement of the radiative and nonradiative properties of nanocrystals of different shapes,” *Chem Soc Rev*, vol. 35, no. 3, pp. 209–217, 2006.
- [41] “Gold Nanoparticles: Physical Properties.” [Online]. Available: <http://nanocomposix.eu/pages/gold-nanoparticles-physical-properties#stability>. [Accessed: 10-Feb-2016].
- [42] P. Tiwari, K. Vig, V. Dennis, and S. Singh, “Functionalized Gold Nanoparticles and Their Biomedical Applications,” *Nanomaterials*, vol. 1, no. 1, pp. 31–63, Jun. 2011.
- [43] J. Turkevich, P. C. Stevenson, and J. Hillier, “A study of the nucleation and growth processes in the synthesis of colloidal gold,” *Discuss. Faraday Soc.*, vol. 11, no. 0, pp. 55–75, Jan. 1951.
- [44] A. Lähde, I. Koshevoy, T. Karhunen, T. Torvela, T. A. Pakkanen, and J. Jokiniemi, “Aerosol-assisted synthesis of gold nanoparticles,” *J. Nanoparticle Res.*, vol. 16, no. 11, pp. 1–8, Nov. 2014.
- [45] B. Janković, S. Stopić, J. Bogović, and B. Friedrich, “Kinetic and thermodynamic investigations of non-isothermal decomposition process of a commercial silver nitrate in an argon atmosphere used as the precursors for ultrasonic spray pyrolysis (USP): The mechanistic approach,” *Chem. Eng. Process. Process Intensif.*, vol. 82, pp. 71–87, Aug. 2014.
- [46] J. Bogovic, R. Rudolf, and B. Friedrich, “The Controlled Single-Step Synthesis of Ag/TiO_2 and Au/TiO_2 by Ultrasonic Spray Pyrolysis (USP),” *JOM J. Miner. Met. Amp Mater. Soc.*, 2015.
- [47] K. Okuyama and I. Wuled Lenggoro, “Preparation of nanoparticles via spray route,” *Chem. Eng. Sci.*, vol. 58, no. 3–6, pp. 537–547, Feb. 2003.
- [48] W. H. Suh, A. R. Jang, Y.-H. Suh, and K. S. Suslick, “Porous, Hollow, and Ball-in-Ball Metal Oxide Microspheres: Preparation, Endocytosis, and Cytotoxicity,” *Adv. Mater.*, vol. 18, no. 14, pp. 1832–1837, Jul. 2006.
- [49] P. S. Patil, “Versatility of chemical spray pyrolysis technique,” *Mater. Chem. Phys.*, vol. 59, no. 3, pp. 185–198, Jun. 1999.
- [50] F. Iskandar, Mikrajuddin, and K. Okuyama, “In Situ Production of Spherical Silica Particles Containing Self-Organized Mesopores,” *Nano Lett.*, vol. 1, no. 5, pp. 231–234, May 2001.
- [51] Y. Shang, C. Min, J. Hu, T. Wang, H. Liu, and Y. Hu, “Synthesis of gold nanoparticles by reduction of HAuCl_4 under UV irradiation,” *Solid State Sci.*, vol. 15, pp. 17–23, Jan. 2013.

- [52] A. K. Khan, R. Rashid, G. Murtaza, and A. Zahra, “Gold nanoparticles: Synthesis and applications in drug delivery,” *Trop. J. Pharm. Res.*, vol. 13, no. 7, pp. 1169–1177, Jul. 2014.
- [53] S. Mohammadnejad, J. L. Provis, and J. S. J. van Deventer, “Reduction of gold(III) chloride to gold(0) on silicate surfaces,” *J. Colloid Interface Sci.*, vol. 389, no. 1, pp. 252–259, Jan. 2013.
- [54] A. S. Barnard and Y. Chen, “Kinetic modelling of the shape-dependent evolution of faceted gold nanoparticles,” *J. Mater. Chem.*, vol. 21, no. 33, p. 12239, 2011.
- [55] M. Rai and N. Duran, Eds., *Metal Nanoparticles in Microbiology*. Berlin, Heidelberg: Springer Berlin Heidelberg, 2011.
- [56] O. B. Milosevic, L. Mancic, M. E. Rabanal, L. S. Gomez, and K. Marinkovic, “Aerosol route in Processing of Nanostructured Functional Materials,” *KONA Powder Part. J.*, vol. 27, no. 0, pp. 84–106, 2009.
- [57] G. Frens, “Controlled Nucleation for the Regulation of the Particle Size in Monodisperse Gold Suspensions,” *Nature*, vol. 241, no. 105, pp. 20–22, Jan. 1973.
- [58] M. Brust, M. Walker, D. Bethell, D. J. Schiffrin, and R. Whyman, “Synthesis of thiol-derivatised gold nanoparticles in a two-phase Liquid–Liquid system,” *J. Chem. Soc. Chem. Commun.*, no. 7, pp. 801–802, Jan. 1994.
- [59] J.-E. Park, M. Atobe, and T. Fuchigami, “Synthesis of multiple shapes of gold nanoparticles with controlled sizes in aqueous solution using ultrasound,” *Ultrason. Sonochem.*, vol. 13, no. 3, pp. 237–241, Apr. 2006.
- [60] L. L. Hench and J. K. West, “The sol-gel process,” *Chem. Rev.*, vol. 90, no. 1, pp. 33–72, Jan. 1990.
- [61] J. H. Bang and K. S. Suslick, “Applications of Ultrasound to the Synthesis of Nanostructured Materials,” *Adv. Mater.*, vol. 22, no. 10, pp. 1039–1059, Feb. 2010.
- [62] J. J. Ana Menendez-Manjon, “Mobility of Nanoparticles Generated by Femtosecond Laser Ablation in Liquids and Its Application to Surface Patterning,” *JLMN - J. Laser Micro Nanoeng.*, vol. 4, pp. 95–99, 2009.
- [63] M. Gracia-Pinilla, E. Martínez, G. S. Vidaurri, and E. Pérez-Tijerina, “Deposition of Size-Selected Cu Nanoparticles by Inert Gas Condensation,” *Nanoscale Res. Lett.*, vol. 5, no. 1, pp. 180–188, Jan. 2010.
- [64] Y. Hatakeyama, K. Onishi, and K. Nishikawa, “Effects of sputtering conditions on formation of gold nanoparticles in sputter deposition technique,” *RSC Adv.*, vol. 1, no. 9, p. 1815, 2011.
- [65] W. Cao, “High energy ball milling process for nanomaterial synthesis.” [Online]. Available: <http://www.understandingnano.com/nanomaterial-synthesis-ball-milling.html>. [Accessed: 13-Feb-2016].
- [66] “Gold(III) chloride hydrate ~52% Au basis | Sigma-Aldrich.” [Online]. Available: http://www.sigmaaldrich.com/catalog/product/aldrich/50780?lang=en®ion=SI&cm_sp=Insite-_-prodRecCold_xviews-_-prodRecCold10-2. [Accessed: 23-Feb-2016].
- [67] K. S. Suslick, Y. Didenko, M. M. Fang, T. Hyeon, K. J. Kolbeck, W. B. McNamara, M. M. Mdleleni, and M. Wong, “Acoustic cavitation and its chemical consequences,” *Philos. Trans. R. Soc. Lond. Math. Phys. Eng. Sci.*, vol. 357, no. 1751, pp. 335–353, Feb. 1999.
- [68] M. Eslamian, M. Ahmed, and N. Ashgriz, “Modeling of Solution Droplet Evaporation and Particle Evolution in Droplet-to-Particle Spray Methods,” *Dry. Technol.*, vol. 27, no. 1, pp. 3–13, Jan. 2009.
- [69] S. C. Tsai, Y. L. Song, C. S. Tsai, C. C. Yang, W. Y. Chiu, and H. M. Lin, “Ultrasonic spray pyrolysis for nanoparticles synthesis,” *J. Mater. Sci.*, vol. 39, no. 11, pp. 3647–3657, Jun. 2004.

- [70] N. D. Draper, "Investigation of Surface-Potential Controlled Nucleation Using an Acoustic Levitation Apparatus," Thesis, Science: Department of Chemistry, 2012.
- [71] T. Sawada and S. Ando, "Synthesis, Characterization, and Optical Properties of Metal-Containing Fluorinated Polyimide Films," *Chem. Mater.*, vol. 10, no. 11, pp. 3368–3378, Nov. 1998.
- [72] E. S. Clark, D. H. Templeton, and C. H. MacGillavry, "The crystal structure of gold(III) chloride," *Acta Crystallogr.*, vol. 11, no. 4, pp. 284–288, Apr. 1958.
- [73] R. Dittrich, I. S. Stopić, and B. Friedrich, "Mechanism of nanogold formation by ultrasonic spray pyrolysis," Düsseldorf, Germany, 2011, p. 385.
- [74] P. Zeng, S. Zajac, P. C. Clapp, and J. A. Rifkin, "Nanoparticle sintering simulations," *Mater. Sci. Eng. A*, vol. 252, no. 2, pp. 301–306, Sep. 1998.
- [75] R. H. R. Castro and K. van Benthem, *Sintering mechanisms of convention nanodensification and field assisted processes*. Berlin; New York: Springer, 2013.
- [76] P. Majerič, R. Rudolf, and I. Anžel, "Thermodynamics of nanoparticles / Termodinamika nanodelcev," *Anali PAZU*, vol. 4, no. 1, pp. 28–33, 2014.
- [77] P. Buffat and J.-P. Borel, "Size effect on the melting temperature of gold particles," *Phys. Rev. A*, vol. 13, no. 6, pp. 2287–2298, Jun. 1976.
- [78] T. L. Hill, *Thermodynamics of Small Systems*. Courier Dover Publications, 2002.
- [79] M. Mezhericher, A. Levy, and I. Borde, "Heat and mass transfer of single droplet/wet particle drying," *Chem. Eng. Sci.*, vol. 63, no. 1, pp. 12–23, Jan. 2008.
- [80] O. E. Hileman jr., "Precipitation from homogeneous solution applied to the drop technique for the study of nucleation," *Talanta*, vol. 14, no. 1, pp. 139–140, Jan. 1967.
- [81] M. K. Wu, R. S. Windeler, C. K. R. Steiner, T. Börs, and S. K. Friedlander, "Controlled Synthesis of Nanosized Particles by Aerosol Processes," *Aerosol Sci. Technol.*, vol. 19, no. 4, pp. 527–548, Jan. 1993.
- [82] F. E. Kruis, K. A. Kusters, S. E. Pratsinis, and B. Scarlett, "A Simple Model for the Evolution of the Characteristics of Aggregate Particles Undergoing Coagulation and Sintering," *Aerosol Sci. Technol.*, vol. 19, no. 4, pp. 514–526, Jan. 1993.
- [83] S. Stopić, P. Dvorak, and B. Friedrich, "Synthesis of spherical nanosized silver powder by ultrasonic spray pyrolysis," *Metall*, vol. 60, no. 6, pp. 299–304, 2006.
- [84] S. Srečko, G. Sebahattin, and F. Bernd, "Mechanism of synthesis of nanosized spherical cobalt powder by ultrasonic spray pyrolysis," *Metalurgija*, vol. 11, no. 1, pp. 65–73, 2005.
- [85] E. W. Wood and A. L. Loomis, "XXXVIII. The physical and biological effects of high-frequency sound-waves of great intensity," *Philos. Mag. Ser. 7*, vol. 4, no. 22, pp. 417–436, 1927.
- [86] R. J. Lang, "Ultrasonic Atomization of Liquids," *J. Acoust. Soc. Am.*, vol. 34, no. 1, pp. 6–8, 1962.
- [87] J. Bogović, S. Stopić, and B. Friedrich, "Nanosized metallic oxide produced by Ultrasonic Spray Pyrolysis," presented at the Proceedings of European Metallurgical Conference, Düsseldorf/D, 2011.
- [88] C. A. Schneider, W. S. Rasband, and K. W. Eliceiri, "NIH Image to ImageJ: 25 years of image analysis," *Nat. Methods*, vol. 9, no. 7, pp. 671–675, Jul. 2012.
- [89] G. H. Woehrle, J. E. Hutchinson, S. Özkar, and R. G. Finke, "Analysis of nanoparticle transmission electron microscopy data using a public-domain image-processing program, image," *Turk. J. Chem.*, vol. 30, no. 1, pp. 1–13, 2006.
- [90] "Dynamic Light Scattering: An Introduction in 30 Minutes." [Online]. Available: <http://www.malvern.com/en/support/resource-center/technical-notes/TN101104DynamicLightScatteringIntroduction.aspx>. [Accessed: 26-Feb-2016].

- [91] S. Stopic, B. Friedrich, T. Volkov-Husovic, and K. Raic, "Mechanism and kinetics of nanosilver formation by ultrasonic spray pyrolysis - progress report after successful up-scaling (Part 1)," *Metall*, vol. 64, no. 10, pp. 474–477, 2010.
- [92] S. Stopić, I. Ilić, and D. Uskoković, "Structural and morphological transformations during NiO and Ni particles generation from chloride precursor by ultrasonic spray pyrolysis," *Mater. Lett.*, vol. 24, no. 6, pp. 369–376, Sep. 1995.
- [93] P. Majerič, R. Rudolf, I. Anžel, J. Bogović, S. Stopic, and B. Friedrich, "Synthesis of NiTi/Ni-TiO₂ composite nanoparticles via Ultrasonic Spray Pyrolysis," *Mater. Tehnol.*, no. 2, p. To be issued, 2015.
- [94] R. Rudolf, I. Anžel, S. Stopic, M. Čolić, P. Majerič, and B. Friedrich, "Synthesis and characterization of gold nanoparticles," presented at the 13. International Foundrymen Conference, Opatija, Croatia, Maj 16-17.
- [95] P. Majerič, D. Jenko, B. Budič, S. Tomić, M. Čolić, B. Friedrich, and R. Rudolf, "Formation of Non-Toxic Au Nanoparticles with Bimodal Size Distribution by a Modular Redesign of Ultrasonic Spray Pyrolysis," *Nanosci. Nanotechnol. Lett.*, vol. accepted 31.Oct.2015.
- [96] P. Pallavicini, A. Donà, A. Casu, G. Chirico, M. Collini, G. Dacarro, A. Falqui, C. Milanese, L. Sironi, and A. Taglietti, "Triton X-100 for three-plasmon gold nanostars with two photothermally active NIR (near IR) and SWIR (short-wavelength IR) channels," *Chem. Commun.*, vol. 49, no. 56, p. 6265, 2013.
- [97] Y. Xiong and Y. Xia, "Shape-Controlled Synthesis of Metal Nanostructures: The Case of Palladium," *Adv. Mater.*, vol. 19, no. 20, pp. 3385–3391, Sep. 2007.
- [98] W. Qian, M. Murakami, Y. Ichikawa, and Y. Che, "Highly Efficient and Controllable PEGylation of Gold Nanoparticles Prepared by Femtosecond Laser Ablation in Water," *J. Phys. Chem. C*, vol. 115, no. 47, pp. 23293–23298, Dec. 2011.
- [99] S. J. Kim, S. H. Jeong, H. K. Chung, J. T. Nam, and N. Y. Won, "United States Patent US20110269170 A1: pH Sensitive Metal Nanoparticle and Preparation Method," 03-Nov-2011.

APPENDIX: Theoretical calculations for evaporation of solution droplet

Aerosol droplet residence time:

$$\frac{dt}{dx} = \frac{0,06\pi R^2}{Q} \left(\frac{T_0}{T} \right) \frac{(1 - y_w)}{(1 - y_w^0)} \quad (4.4)$$

t [s] – droplet residence time, x [cm] – furnace axis coordinate, R [cm] – transport tube radius, Q [l/min] – gas flow, T [K] – gas temperature, y_w – mole fraction of water vapor in the gas, index 0 indicates initial value. The expression $(1 - y_w)/(1 - y_w^0)$ takes into account the change in the water vapor fraction, which is the result of evaporation of droplets.

Change of droplet diameter d_p :

$$\frac{dd_p}{dx} = \left(\frac{dd_p}{dt} \right) \left(\frac{dt}{dx} \right) = \frac{4D_v m_1}{\rho_p d_p} (n - n_s) \left(\frac{dt}{dx} \right) \quad (4.5)$$

D_v [cm²/s] – coefficient of diffusion of water vapor in the gas at existing temperature, m_1 [g] – mass of a molecule of water, n [molecules/cm³] – concentration of water vapor in the gas at existing temperature, n_s [molecules /cm³] – concentration of water vapor on the droplet surface at existing temperature, ρ_p [g/cm³] – droplet density, dependant on the size of the droplet.

Coefficient of diffusion D_v :

$$D_v = \frac{0,00266T^{3/2}}{pM_{AB}^{0,5}\sigma_{AB}^2\Omega_D} \quad (4.5.1)$$

p [bar] – pressure, M_{AB} [g/mol] – molecular weight of inter-diffusion species, σ_{AB} [Å] – spherical diameter of inter-diffusion species, Ω_D – integration coefficient ($\Omega_D = 1$).

Droplet density ρ_p :

$$\rho_p = \rho_l \left(\frac{d_p}{d_{ps}} \right)^3 (\rho_s - \rho_l) \quad (4.5.2)$$

ρ_l – water density, ρ_s – solute density, d_{ps} – diameter of the spherical, dried particle.

Concentration of water vapor on the surface of the droplet n_s :

$$n_s = \frac{p_s}{kT_s} \quad (4.5.3)$$

k – Boltzmann constant, p_s – water vapor pressure on the droplet surface at droplet temperature T_s :

$$p_s(T_s) = ap_s^0(T_s) \quad (4.5.4)$$

a – activity coefficient of water in the solution droplet, dependant on the molality of the solution m and the osmotic water coefficient ϕ :

$$a = \exp(-0,036m\phi) \quad (4.5.5)$$

$$m = \frac{1000\rho_s}{M_s\rho_l \left[\left(\frac{d_p}{d_{ps}} \right)^3 - 1 \right]} \quad (4.5.6)$$

M_s – molar mass of the solute.

$$\phi = 1 - 0,392 \left(\frac{298}{T} \right)^{\frac{3}{2}} \frac{\sqrt{m}}{1 + 1,2\sqrt{m}} + (0,0765 + 0,2664e^{-2\sqrt{m}})m + 0,00127m^2 \quad (4.5.7)$$

Concentration of water vapor in the furnace n :

$$\frac{dn}{dx} = \left(\frac{dn}{dt} \right) \left(\frac{dt}{dx} \right) = \left[-2\pi d_p D_v N_0 (n - n_s) - \frac{2K_m (n - n_w)}{R} \right] \left(\frac{dt}{dx} \right) \quad (4.6)$$

N_0 [number/cm³] – concentration of droplets, n_w – concentration of water vapor at the furnace wall, K_m – coefficient of mass flow for water vapor in a laminar flow.

Change of droplet temperature:

$$\frac{dT_s}{dx} = \left(\frac{dT_s}{dt}\right) \left(\frac{dt}{dx}\right) = \frac{1}{C_p d_p} \left[3H_L \frac{dd_p}{dt} + \frac{6h_s}{\rho_p} (T - T_s) \right] \left(\frac{dt}{dx}\right) \quad (4.7)$$

C_p – heat capacity of the droplet, H_L [J/mol] – latent heat of water evaporation, h_s – coefficient of heat transfer at the droplet.

Latent heat of water evaporation H_L :

$$\frac{H_L}{R_g T_c} = 7,08(1 - T_r)^{0,354} + 10,95\omega(1 - T_r)^{0,456} \quad (4.7.1)$$

R_g – gas constant, T_c – critical water temperature (647,3 K), $T_r = T/T_c$, ω – Pitzers factor of acentricity ($\omega = 0,344$, for water)

Coefficient of heat transfer at the droplet h_s :

$$\frac{h_s d_p}{\lambda} = 2 \quad (4.7.2)$$

λ – thermal conductivity of the gas.

Gas temperature:

$$\frac{dT}{dx} = \frac{1}{F C_{pa}} \left[-\pi^2 R^2 d_p^2 N_0 h_s (T - T_s) + 2\pi R h_w (T_w - T) \right] \quad (4.8)$$

F [mol/min] – molar gas flow, C_{pa} – heat capacity of wet gas, h_w – coefficient of heat transfer at the furnace wall.

Coefficient of heat transfer at the wall h_w , for a laminar flow:

$$Nu = 3,66 = 2Rh_w/\lambda \quad (4.8.1)$$

Nu – Nusselt number

Solute saturation:

$$s = \frac{a_s}{a_c} = \frac{m_s y_s}{m_c y_c} \quad (4.9)$$

a_s – activity of solute at m_s or c_s (molality or concentration on the droplet surface), a_c – activity of solute at m_c or c_c (equilibrium saturation concentration), y_s – activity coefficient of the solute at m_s , y_c – activity coefficient of the solute at m_c .

Critical ratio of saturation is obtained from:

$$s^* = \exp \left[\frac{16\pi\sigma^3 M_s^2}{3v^2 k T_s^3 \rho_s^2 R_g^2 \ln(A/J)} \right]^{0,5} \quad (4.10)$$

σ – surface energy of the solute, v – number of ions for total dissociation or $v = 1$ for solutes with no dissociation, A – constant dependent on the solute, J – rate of nucleation (1 nuclei/s cm^3).

ŽIVLJENJEPIS

Osebni podatki

Ime in Priimek	Peter Majerič
Naslov	Bukovci 42a, 2281 Markovci
Državljanstvo	slovensko
Datum rojstva	3. 7. 1987
Spol	moški

Šolanje in izobrazba

Obdobje	2002–2006
Naziv	Gimnazijski maturant
Ustanova	Gimnazija Ptuj
Obdobje	2006–2012
Naziv	Univerzitetni diplomirani inženir strojništva
Ustanova	Univerza v Mariboru, Fakulteta za strojništvo

Delovne izkušnje

Obdobje	December 2012–danes
Zaposlitev ali delovno mesto	Mladi raziskovalec
Naziv in naslov delodajalca	Univerza v Mariboru, Fakulteta za strojništvo, Smetanova ulica 17, 2000 Maribor

UNIVERZA V MARIBORU
FAKULTETA ZA STROJNIŠTVO

IZJAVA DOKTORSKEGA KANDIDATA

Podpisani Peter MAJERIČ, vpisna številka S3000757

izjavljam,

da je doktorska disertacija z naslovom: **Sinteza nanodelcev zlata z modificirano ultrazvočno razpršilno pirolizo**

- rezultat lastnega raziskovalnega dela,
- da predložena disertacija v celoti ali v delih ni bila predložena za pridobitev kakršnekoli izobrazbe po študijskem programu druge fakultete ali univerze,
- da so rezultati korektno navedeni in
- da nisem kršil-a avtorskih pravic in intelektualne lastnine drugih.

Maribor, 9.05.2016

Podpis: _____